Functional role of fibroblast-derived MMP-14 in tumor growth and metastasis

Inaugural-Dissertation

zur

Erlangung des Doktorgrades

der Mathematisch-Naturwissenschaftlichen Fakultät

der Universität zu Köln

vorgelegt von

Elke Pach

aus Langenfeld (Rhld.)

Köln 2022

Berichterstatter: Prof. Dr. Matthias Hammerschmidt

Prof. Dr. Raimund Wagener

Vorsitzende: Prof. Dr. Ines Neundorf

Tag der mündlichen Prüfung: 03.05.2022

Contents

List of Figures I
List of Tables II
Abbreviations III
Summary 1
Zusammenfassung 3
1 Introduction 5
1.1 Melanoma 5
1.1.1 Origin of melanoma 5
1.1.2 Growth, development and metastasis of melanoma 6
1.1.3 Tumor microenvironment 9
1.2 Extracellular matrix 12
1.2.1 Collagens 12
1.2.2 ECM in cancer 16
1.3. MMPs 18
1.3.1 Structure 18
1.3.2 Regulation and activity 19
1.3.3 MMPs role in physiology and pathology 20
1.4 MMP14 22
1.4.1 Structure and functions 22
1.4.2 MMP14 knock-out models 23
1.4.2.1 Complete knock-out models 23
1.4.2.2 Tissue-specific knock-out models 24
1.4.3 MMP14 in cancer 26
1.5 Aim of the project 28
2 Material and Methods 30
2.1 Materials 30
2.1.1 Chemicals 30
2.1.2 Cell culture material 30
2.1.3 Consumable materials 30
2.1.4 Buffers and reagents 32
2.1.5 Kits 33
2.1.6 Antibodies 33
2.1.7 Laboratory equipment 34
2.2 Methods 36

2.2.1 Cell Culture 36
2.2.1.1 Isolation of primary fibroblasts 36
2.2.1.2 Preparation of fibroblast deposited matrix and conditioned medium 37
2.2.1.3 Melanoma spheroids 37
2.2.1.4 Colony outgrowth assay 37
2.2.1.5 Proliferation assay 38
2.2.1.6 Cell death assay 38
2.2.1.7 Adhesion assay 39
2.2.1.8 *Ex vivo* invasion assays 39
2.2.2 Protein Analysis 40
2.2.2.1 SDS PAGE and Western Blot 40
2.2.2.2 Proteome analysis 41
2.2.2.3 Mouse XL Cytokine Array Kit 41
2.2.3 Analysis of nucleid acids 42
2.2.3.1 DNA isolation and genotyping 42
2.2.3.2 RNA isolation 42
2.2.3.3 Reverse transcription - polymerase chain reaction (RT-PCR) 43
2.2.3.4 Quantitative real-time PCR 43
2.2.4 *In vivo* experiments 44
2.2.4.1 Animal housing 44
2.2.4.2 Tumor grafting and skin treatment 44
2.2.5 Tissue Analysis 44
2.2.5.1 Hematoxylin and Eosin (H&E) staining 44
2.2.5.2 Immunofluorescence staining 45
2.2.5.3 Picrosirius red staining 45
2.2.5.4 Atomic Force Microscopy (AFM) 45
2.2.5.5 Second Harmonic Generation (SHG) 46
2.2.6 Statistics 46
3 Results 47
3.1 Role of stromal MMP14 in melanoma growth 47
3.1.1 B16F1 tumor growth is reduced in MMP14$^{Sf-/-}$ skin 47
3.1.1.1 Reduced vascularization in MMP14$^{Sf-/-}$ peritumoral tissue 48
3.1.1.2 Decreased amounts of inflammatory cells in MMP14$^{Sf-/-}$ peritumoral tissue 49
3.1.2 B16F1 invasion in *ex vivo* skin composites 51
3.2 Analysis of peritumoral tissue in MMP14$^{Sf-/-}$ mice 53

3.2.1 Analysis of tissue stiffness in the skin and peritumoral tissue 56
3.3 Role for collagen type I on melanoma cell growth 57
3.3.1 Melanoma proliferation in 2D-culture on fibrillar and monomeric collagen type I 57
3.3.2 Melanoma growth in 3D- spheroid culture within fibrillar collagen type I gels 59
3.4 Melanoma growth in a fibrotic microenvironment 60
3.4.1 Melanoma cell proliferation in tumors developed in fibrotic skin 62
3.4.2 Inflammatory cells and CAFs in fibrotic peritumoral tissue 63
3.5 Efficacy of chemotherapeutic treatment of melanoma in MMP14$^{Sf-/-}$ mice..... 64
3.6 Analysis of peritumoral matrix in MMP14$^{Sf-/-}$ mice 65
3.6.1 Proteome analysis of peritumoral matrix proteins 65
3.7 Fibroblast proteome in the absence of MMP14 68
3.7.1 Fibroblast deposited matrix 68
3.7.1.1 Effect of fibroblast matrix on melanoma proliferation and apoptosis ... 68
3.7.1.2 MMP14$^{Sf-/-}$ fibroblast matrix does not support melanoma cells migration 70
3.7.2 Proteome analysis of fibroblast matrix and supernatants 70
3.7.3 Expression of collagens 71
3.7.3.1 Melanoma cell proliferation on collagen type XIV 73
3.7.3.2 Collagen type XIV is not pro-migratory for melanoma..... 75
3.7.3.3 Melanoma cell adhesion is reduced by collagen type XIV 77
3.7.4 Fibroblast secretome..... 78
3.7.4.1 Influence of fibroblast secreted factors on melanoma proliferation and apoptosis 78
3.7.4.2 Analysis of soluble factors in fibroblast conditioned medium 79
3.7.4.2.1 GROα and MMP3 in melanoma apoptosis 80
3.8 Is deletion of MMP14 in fibroblasts negatively affecting the growth of epithelial tumors? 81
3.8.1 BDVII cell invasion in *ex vivo* skin composites 82
3.9 Altered ECM composition of peritumoral tissue due to deletion of ADAM9 84
4 Discussion 86
4.1 Regulation of melanoma growth by fibroblast-derived MMP14 *in vivo* 86
4.2 Melanoma growth is modulated by collagen abundance and tissue stiffness . 88
4.3 Deletion of MMP14 in fibroblast modulates their proteomic profile 91
4.3.1 Alterations in secreted and deposited matrix 91
4.3.2 Role for collagens remodeling in melanoma 91

4.3.3 Soluble factors released by fibroblasts modulate melanoma cell survival . 94
4.4 Therapeutic importance 95
References 97
Erklärung 117
Lebenslauf 118
Acknowledgements 120

List of Figures

Figure 1. Crosstalk of melanocytes and keratinocytes in the basal membrane. 7
Figure 2. Stages of melanoma development. 8
Figure 3. The tumor microenvironment consisting of numerous different cell types and the non-cellular structural extracellular matrix..... 9
Figure 4. Collagen biosynthesis.....15
Figure 5. Pathways of LOX-mediated collagen cross-linking. 16
Figure 6. The family of matrix metalloproteinases.....19
Figure 7. Skin biopsies and *ex vivo* invasion assay. 40
Figure 8. B16F1 melanoma growth in MMP14$^{Sf-/-}$ and control mice.....48
Figure 9. Analysis of vascularization and hypoxia in B16F1 melanoma of MMP14$^{Sf-/-}$ and control mice.....49
Figure 10. Analysis of immune cells in B16F1 tumors.....50
Figure 11. *Ex vivo* DDS assay with B16F1 cells. 52
Figure 12. *Ex vivo* Decellularized skin assay with B16F1 cells. 53
Figure 13. Second Harmonics Generation of skin and peritumoral tissue. 54
Figure 14. Analysis of protein content in skin and peritumoral tissue. 55
Figure 15. Analysis of collagen cross-link formation in the skin and peritumoral tissue. 56
Figure 16. Atomic Force Microscopy of peritumoral tissue and skin.....57
Figure 17. B16F1 cell proliferation on monomeric and fibrillar collagen type I coating. 58
Figure 18. Analysis of B16F1 cell proliferation on stiffness plates coated with collagen type I. 59
Figure 19. Melanoma spheroid growth in fibrillar collagen type I gels. 60
Figure 20. B16F1 melanoma growth in bleomycin-induced fibrotic skin. 61
Figure 21. Ki67 and cleaved Caspase 3 staining in melanoma grown in fibrotic skin. 62
Figure 22. CD45 immunofluorescence staining of melanoma in fibrotic skin. 63
Figure 23. Immunofluorescence staining for PDGFRα and αSMA in peritumoral tissue of melanoma in fibrotic skin. 63
Figure 24. Chemotherapeutic treatment of B16F1 melanoma in MMP14$^{Sf-/-}$ mice. 65
Figure 25. Proteome analysis of B16F1 melanoma peritumoral tissue. 66
Figure 26. Analysis of decellularized B16F1 melanoma peritumoral tissue. 67
Figure 27. Collagen type I and XIV expression in B16F1 peritumoral tissue. 68
Figure 28. Analysis of melanoma cell proliferation on fibroblast matrix. 69
Figure 29. Analysis of B16F1 cell apoptosis on fibroblast matrix. 69
Figure 30. B16F1 migration on fibroblast deposited matrix. 70
Figure 31. Proteome analysis of fibroblast deposited matrix and conditioned medium. 71
Figure 32. Analysis of selected types of collagens in fibroblast matrix and conditioned medium. 72
Figure 33. *In vitro* cleavage analysis of collagen type XIV by MMP14. 73
Figure 34. Analysis of B16F1 melanoma cell proliferation on collagen type XIV. 74
Figure 35. Analysis of melanoma cell proliferation on fibroblast matrix. 74
Figure 36. B16F1 migration on collagen type XIV coating. 75
Figure 37. B16F1 migration on MMP14$^{Sf+/+}$ fibroblast matrix with collagen type XIV. 76
Figure 38. Adhesion assay on collagen type XIV coating and fibroblast-deposited matrix. ...77
Figure 39. Analysis of melanoma cell proliferation and apoptosis in fibroblast conditioned medium. 78
Figure 40. Cytokine antibody array. 80
Figure 41. Apoptosis assays of B16F1 cells grown in MMP14$^{Sf-/-}$ c.m. with MMP3i and α-GROα. 81
Figure 42. *Ex vivo* DDS assay with BDVII cells. 83
Figure 43. *Ex vivo* decellularized skin assay with BDVII cells. 84

List of Tables

Table 1. Kits for cell- and protein analysis. 33
Table 2. Mouse antibodies used for immunofluorescence stainings. 33
Table 3. Mouse antibodies used for immunoblot analysis. 34
Table 4. Primers used for mouse genotyping. 42
Table 5. Primers used for quantitative real-time PCR. 43
Table 6. Identified growth factors in proteome analysis of fibroblast matrix and conditioned medium. 79

Abbreviations

%	percent
°	degree
µg	microgram
µl	microliter
2D	two-dimensional
3D	three-dimensional
3-PH	prolyl 3-hydroxylase
4-PH	prolyl 4-hydroxylase
AA	antibiotic and anti mycotic
ADAMTS	a disintegrin and metalloproteinase with thrombospondin motifs
AFM	atomic force microscopy
AKT/PKB	serine-threonine protein kinase/proteinkinase B
BCA	bicinchoninic acid
Bleo	bleomycin
BM	basement membrane
BMP1	bone morphogenic protein 1
BRAF	B-Raf kinase
BrdU	bromodeoxyuridine
BSA	bovine serum albumin
C	Celcius
c.m.	conditioned medium
CAA	chloroacetamide
$CaCl_2$	calcium chloride
CAF	cancer-associated fibroblast
CAIX	carbonic anhydrase IX
CD31	cluster of differentiation 31
CD45	cluster of differentiation 45 (leukocyte common antigen)
CDKN2a	cyclin dependent kinase inhibitor 2a
cDNA	complementary DNA
Cis	cisplatin
CO_2	carbon dioxide
Coll I	collagen type I
Coll XIV	collagen type XIV

DDS	de-epidermized devitalized skin
deH-DHLNL	dehydro-dihydroxylysinonorleucine
deH-HHMD	dehydro-histidinohydroxymerodesmosine
deH-HLNL	dehydro-hydroxylysinonorleucine
DNA	deoxyribonucleic acid
d-Prl	deoxypyrrole
d-Pyr	deoxypyridinoline
DTT	dithiothreitol
EC	endothelial cell
ECL	enhanced chemiluminescence
ECM	extracellular matrix
EDTA	ethylenediamine tetraacetic acid
EMT	epithelial-to-mesenchymal transition
ERK	extracellular signal-regulated kinase kinase
EtOH	ethanol
FACIT	fibril-associated collagens with interrupted triple helices
FAK	focal adhesion kinase
FAP	fibroblast activation protein
FCS	fetal calf serum
FN	fibronectin
g	gram
(x) g	force of gravity (metres per second square: m/s^2)
GFP	green fluorescent protein
GG-Hyl	glucosylgalactosylhydroxylysine
GGT	galactosylhydroxylysyl glucosyltransferases
G-Hyl	galactosylhydroxylysine
Gly	glycine
GPa / kPa	giga pascal / kilopascal
GROα	growth related oncogene-alpha (or CXCL1)
GSK3β	glycogen synthase kinase 3 beta
GT	hydroxylyl galactosyltransferases
GTP	guanosintriphosphate
h	hour
H&E	hematoxylin and eosin

H_2SO_4	sulfuric acid
HA	hyaluronic acid
HCl	hydrochloric acid
HHL	histidinohydroxylysinonorleucine
HIF	hypoxia-induced factor
HPLC	high performance liquid chromatography
HPRT	hypoxanthine-guanine phosphoribosyltransferase
HRP	horseradish peroxidase
HSP47	heat shock protein 47
HSPG	heparan sulfate proteoglycan
Hyl^{ald}	δ-hydroxy, α-aminoadipic acid-δ-semialdehyde
Hz	hertz
ICAM-1	intercellular adhesion molecule 1
J	joule
kDa	kilodalton
KO	knock-out
l	liter
LH	lysyl hydroxylase
LN	lymph nodes
LN5	laminin 5
LOX	lysyl oxidase
LOXL	LOX-like
LTBP-1	latent TGF-β binding protein
Lys^{ald}	α-aminoadipic acid-δ-semialdehyde
LysM	lysozyme M
LYVE-1	lymphatic vessel endothelial hyaluronan receptor 1
M	molar
MAPK	mitogen-activated protein kinase
MET	mesenchymal-epithelial transition
MetOH	methanol
$MgSO_4$	magnesium sulfate
min	minute
ml	milliliter
mM	millimolar

MMP	matrix metalloproteinase
mRNA	messenger-ribonucleic acid
MT-MMP	membrane-type matrix metalloproteinase
mTOR	mechanistic target of rapamycin
n	sample size
NaCl	natrium chloride
NF-κB	nuclear factor-kappaB
ng	nanogram
NGS	normal goat serum
NH_4OH	ammonium hydroxide
NK	natural killer
nm	nanometre
o/n	overnight
p	p-value (probability value)
P4-H	prolyl 4-hydroxylase
PBS	phosphate buffered saline
PCR	polymerase chain reaction
PDGFα	platelet-derived growth factor alpha
PDI	protein disulfide isomerase
PEX	hemopexin
PFA	paraformaldehyde
Prl	pyrrole
PTM	posttranslational modification
Pyr	pyridinoline
qRT-PCR	quantitative real-time polymerase chain reaction
rER	rough endoplasmatic reticulum
RGP	radial growth phase
RNA	ribonucleic acid
ROS	reactive oxygen species
rpm	rounds per minute
RT	room temperature
RTK	receptor tyrosine kinase
S26	ribosomal protein S26
SD	standard deviation

SDS	sodium dodecylsulphate
SDS-PAGE	sodium dodecylsulfate-polyacrylamid gel electrophoresis
sec	second
SEM	standard error mean
SHG	second harmonic generation
TACS	tumor-associated collagen signature
TBE	tris-borate-EDTA
TCEP	tris(2-carboxyethyl)phosphin
TEAB	triethylammonium bicarbonate
TGF-β	transforming growth factor-β
TIMP2	tissue inhibitor of metalloproteinase 2
TME	tumor microenvironment
TRP	tyrosinase-related protein
U	unit
UV	ultraviolet
VEGF	vascular endothelial growth factor
VGP	vertical growth phase
WT	wildtype
x	multiplication sign
Zn^{2+}	zinc ion
α-SMA	alpha-smooth muscle actin

Summary

Enzymatic remodeling of the extracellular matrix (ECM) by matrix metalloproteinases (MMPs) is crucial for tissue homeostasis and during pathologic conditions, such as tumor growth. MMP14 is expressed in various skin cells, including fibroblasts; specific deletion of this protease ($MMP14^{Sf-/-}$) results in a fibrosis-like skin phenotype with increased collagen accumulation and tissue stiffness due to impaired collagen remodeling.

Tissue stiffness is commonly associated with cancer progression and is reported to have supportive effects for many types of tumors with a mostly epithelial origin. However, its role in melanoma is up to date controversial. To analyze how the stiff and collagen-rich skin of $MMP14^{Sf-/-}$ mice influences melanoma growth, we used *in vivo* grafts of murine melanoma cells.

Melanoma growth and proliferation were reduced in $MMP14^{Sf-/-}$ mice compared to controls, but the number of metastases was comparable. In addition, vascularization by blood vessels was disturbed, along with reduced hypoxia within the tumor. *Ex vivo*, melanoma cell invasion and growth in devitalized and decellularized skin composites from $MMP14^{Sf-/-}$ was significantly reduced compared to control, demonstrating a growth-restraining function of the matrix-dense dermis from $MMP14^{Sf-/-}$ mice. *In vivo*, although the dense peritumoral tissue of $MMP14^{Sf-/-}$ mice displayed higher collagen levels than controls, neither amount nor pattern of cross-links, collagen fiber alignment, and orientation was changed. Peritumoral tissue stiffness of $MMP14^{Sf-/-}$ mice in early melanoma was increased but dissipated later. Since in late melanomas *in vivo* we observed enhanced collagens but reduced stiffness, we hypothesized that enhanced collagens inhibit melanoma growth, and stiffness may synergize with it. Indeed, 2D cultures of melanoma cells showed that high fibrillar collagen type I and enhanced tissue stiffness together inhibit cell proliferation. Furthermore, the growth of melanoma cell spheroids was dose-dependently inhibited by increasing fibrillar collagen concentrations, despite stiffness being low in these cultures. The anti-proliferative effect of a collagen-rich environment was also detected *in vivo* when melanoma cells were grown in a bleomycin-induced fibrotic dermis. Apart from collagen type I, proteome analysis of the $MMP14^{Sf-/-}$ decellularized peritumoral melanoma tissue and the fibroblast deposited/secreted matrix identified numerous altered proteins, including multiple collagens. Among those was collagen type XIV that we identified as a novel substrate of MMP14. Collagen type XIV was not a suitable cell-adhesive substrate for

melanoma cells, and it did not elicit a pro-proliferative or pro-migratory response. Further, collagen type XIV antagonized melanoma cell proliferation, adhesion, and migration induced by contact with matrix from control fibroblasts reducing them to a level observed on MMP14$^{Sf-/-}$ fibroblast matrix. This study indicates that MMP14 expression and activity in stromal fibroblasts regulate melanoma by remodeling collagen. Furthermore, it demonstrates that collagen type I and XIV are critical modulators of melanoma progression, regulating melanoma cell invasion, migration, and proliferation.

Zusammenfassung

Der enzymatische Umbau der extrazellulären Matrix (EZM) durch Matrix-Metalloproteinasen (MMPs) ist für die Gewebehomöostase und unter pathologischen Bedingungen, wie z. B. Tumorwachstum, entscheidend. MMP14 wird in verschiedenen Hautzellen, einschließlich Fibroblasten, exprimiert; eine spezifische Deletion dieser Protease ($MMP14^{Sf-/-}$) führt zu einem Fibrose-ähnlichen Hautphänotyp mit erhöhter Kollagenanreicherung und Gewebesteifigkeit aufgrund eines gestörten Kollagenumbaus.

Die Steifigkeit des Gewebes wird häufig mit dem Fortschreiten einer Krebserkrankung in Verbindung gebracht und soll bei vielen Tumorarten, die meist epithelialen Ursprungs sind, eine unterstützende Wirkung haben. Ihre Rolle beim Melanom ist jedoch bis heute umstritten. Um zu analysieren, wie die steife und kollagenreiche Haut von $MMP14^{Sf-/-}$ Mäusen das Melanomwachstum beeinflusst, haben wir *in vivo* Transplantate von murinen Melanomzellen verwendet.

Melanomwachstum und -proliferation waren bei $MMP14^{Sf-/-}$ Mäusen im Vergleich zu den Kontrollen reduziert, die Anzahl der Metastasen war jedoch vergleichbar. Darüber hinaus war die Vaskularisierung durch Blutgefäße gestört und die Hypoxie im Tumor reduziert. *Ex vivo* war die Invasion und das Wachstum von Melanomzellen in devitalisierten und dezellularisierten Hautkompositen von $MMP14^{Sf-/-}$ Mäusen im Vergleich zur Kontrollgruppe signifikant reduziert, was eine wachstumshemmende Funktion der matrix-dichten Dermis von $MMP14^{Sf-/-}$ Mäusen belegt. *In vivo* wies das dichte peritumorale Gewebe von $MMP14^{Sf-/-}$ Mäusen zwar höhere Kollagenmengen auf als die Kontrollgruppe, aber weder die Menge noch das Muster der Vernetzungen, die Ausrichtung der Kollagenfasern und die Orientierung waren verändert. Die Steifigkeit des peritumoralen Gewebes von $MMP14^{Sf-/-}$ Mäusen war im frühen Melanom erhöht, nahm aber später ab. Da wir bei späten Melanomen *in vivo* erhöhte Kollagene, aber eine verringerte Steifigkeit beobachteten, stellten wir die Hypothese auf, dass erhöhte Kollagene das Melanomwachstum hemmen und die Steifigkeit damit synergistisch wirken könnte. Tatsächlich zeigten 2D-Kulturen von Melanomzellen, dass ein hoher Anteil an fibrillärem Kollagen Typ I und eine erhöhte Gewebesteifigkeit die Zellproliferation hemmen. Außerdem wurde das Wachstum von Melanomzell-Sphäroiden Dosis-abhängig durch steigende Konzentrationen von fibrillärem Kollagen gehemmt, obwohl die Steifigkeit in diesen Kulturen gering war. Die proliferationshemmende Wirkung einer kollagenreichen Umgebung wurde auch *in vivo*

nachgewiesen, als Melanomzellen in einer durch Bleomycin induzierten fibrotischen Dermis wuchsen. Neben Kollagen Typ I wurden bei der Proteomanalyse des dezellularisierten peritumoralen Melanomgewebes von MMP14$^{Sf-/-}$ und der von Fibroblasten abgelagerten/sezernierten Matrix zahlreiche veränderte Proteine, darunter mehrere Kollagene, festgestellt. Darunter befand sich auch Kollagen Typ XIV, das wir als neues Substrat von MMP14 identifizierten. Kollagen Typ XIV war kein geeignetes zelladhäsives Substrat für Melanomzellen und löste keine proproliferative oder pro-migratorische Reaktion aus. Darüber hinaus hemmte Kollagen Typ XIV die Proliferation, Adhäsion und Migration von Melanomzellen, die durch den Kontakt mit der Matrix von Kontrollfibroblasten ausgelöst wurden, und reduzierte sie auf ein Niveau, das bei MMP14$^{Sf-/-}$ Fibroblastenmatrix beobachtet wurde. Diese Studie deutet darauf hin, dass die Expression und Aktivität von MMP14 in stromalen Fibroblasten das Melanom durch den Umbau von Kollagen reguliert. Darüber hinaus zeigt sie, dass Kollagen Typ I und XIV entscheidende Modulatoren der Melanomentwicklung sind und die Invasion, Migration und Proliferation von Melanomzellen regulieren.

1 Introduction

1.1 Melanoma

1.1.1 Origin of melanoma

Melanoma is the most dangerous and deadliest of all skin cancers, whose incidence has grown steadily in recent decades [1, 2]. It accounts for 5.6% of all new cancer cases and 1.2% of all cancer deaths as estimated for the year 2021 in the US [3]. The predisposition and causes for patients to develop melanoma are manifold. A positive family history with at least one parent having suffered from melanoma or being affected with atypical mole syndrome can increase the predisposition for developing melanoma up to 10 % [4]. Moreover, personal characteristics such as blue eyes, light hair and pale skin, as well as excessive sun exposure might further favor this risk [4]. Apart from exposure to UV-light or other external stimuli, most melanoma are sporadic. They arise spontaneously or as result of intrinsic, namely somatic, genetic mutations [5]. The MAPK (mitogen-activated protein kinase) signaling pathway, among others, that has a crucial role in melanoma growth and survival is constitutively activated in melanoma due to specific mutations [6]. About 50-60% of all melanoma cases carry a mutation in the BRAF gene with the $BRAF^{V600E}$ mutation, in which glutamic acid is replaced with valine at codon 600, being the most frequent one [7]. This and other BRAF mutations result in constitutive ERK phosphorylation leading to continuously enhanced tumor cell proliferation and growth [8]. While the $BRAF^{V600E}$ mutation is mostly present in younger melanoma patients (< 40 years) [5], in older patients (> 55 years) mutations in NRAS are more usual [9]. Mutations in the two key MAPK genes, BRAF and NRAS, which are both present at high rates in primary and metastatic melanoma, do not occur together but exclude each other [10-12]. Mutations in the NRAS gene occur preferentially at position 61 involving the reconstitution of glutamine (Q) with either arginine (R), lysine (K) or leucine (L) [13]. Moreover, position 12 and less frequently position 13 are mutated due to change from glycine (G) to aspartic acid (D) in both cases [13]. These mutations lead to inhibition of or insensitivity to GTPase activity, hence sustaining the NRAS proteins in an active state [14]. In melanoma, alterations in the RAS pathway usually occur with abnormalities in the CDKN2a gene [15]. The CDKN2a gene locus encodes two tumor suppressors, p16INK4 and p14ARF, which control the cell cycle and the G1/S checkpoint under normal conditions [15, 16]. In about 13% of melanoma these proteins are mutated leading to disturbed cell cycle control and uncontrolled cell proliferation [17]. Besides the MAPK, another pathway

that is often deregulated in melanoma is the PI3K (phosphoinositide 3-kinase)/Akt pathway [12]. The tumor suppressor PTEN act as a negative regulator of PIP3 causing inhibition of AKT activity. In 50% of melanoma low levels of PTEN were found and 5-15% of tumors exhibit complete loss of PTEN, which results in increased AKT activation [18, 19]. Constitutive activation of AKT occur in more than 60% of melanoma and promotes cell proliferation and survival [20-23].

1.1.2 Growth, development and metastasis of melanoma

Melanoma originates from the malignant transformation of melanin-producing cells, namely melanocytes. Being neural crest-derived cells, melanocytes can arise to melanoma in multiple tissues, however, mostly in the skin [4, 24]. In healthy skin, melanocytes are attached to the basement membrane (BM) where they occur in a ratio of 1:10 with keratinocytes [25]. Both cells express the cell adhesion proteins, E-cadherin, P-cadherin and desmoglein enabling cell-cell communication that allows keratinocytes to regulate melanocyte division, migration and reattachment to the BM to maintain this distribution, even after disruption due to UV-light overexposure or wounding (Figure 1) [6, 26]. Balanced keratinocyte-melanocyte arrangement is important for proper pigmentation of the skin, which can be divided into three processes: (i) synthesis and transport of melanin within the melanocytes, (ii) melanin transfer from melanocytes to keratinocytes, and (iii) melanin internalization by keratinocytes [26]. Melanocytes produce two different types of melanin: the brown-black eumelanin and the yellow-red pheomelanin [27]. Generating an epidermal melanin unit, one melanocyte supplies approximately 36-40 associated keratinocytes with pigment-containing melanosomes by transport through its dendrites [28, 29]. After internalizing, the melanosomes locate above the nuclei within the keratinocytes to protect the genome from UV irradiation-induced DNA damage [27].

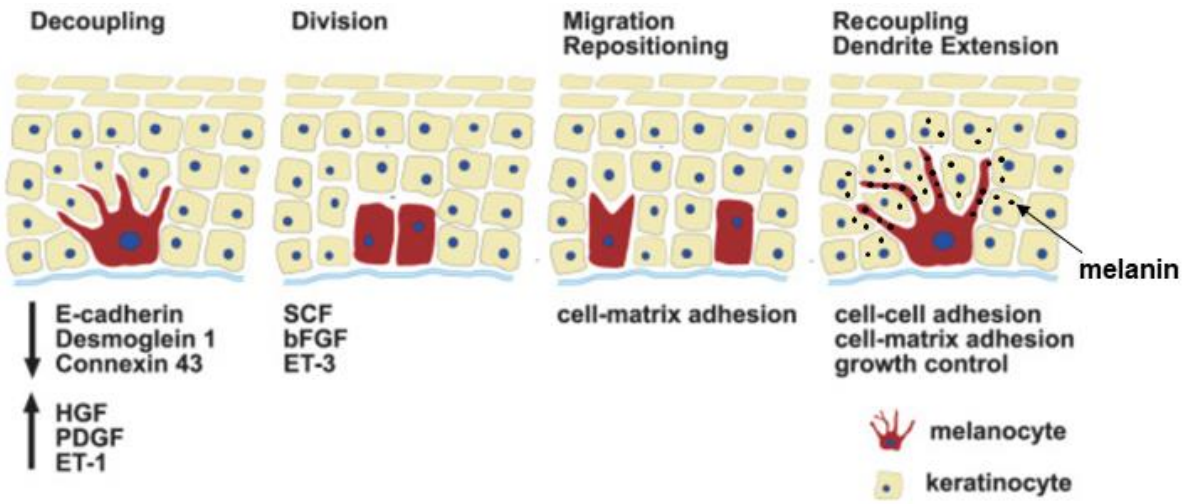

Figure 1. Crosstalk of melanocytes and keratinocytes in the basal membrane.
Cell division requires decoupling from the BM by downregulation of adhesion proteins and upregulation of growth factors. Cell-matrix adhesion allows migration to reposition. Recoupling to the BM, cell-cell adhesion and dendrite extension to provide keratinocytes with melanin. Modified from [6].

Once the balance of the melanin unit is deregulated, enhanced proliferation of melanocytes and extensive production of melanin can occur resulting in transformation into nevus or melanoma [6, 30]. Depending on skin area where the melanocytes are proliferating, nevi can be distinguished as junctional (epidermis), dermal (dermis) or compound (overlapping in the epidermis and dermis) [31]. Benign nevi can transform into melanoma by transition into the radial growth phase (RGP) (Figure 2). In this phase, which is considered the first malignant state, melanoma cells still express E-cadherin and spread along the basal membrane still holding contact to keratinocytes [6, 31]. However, since E-cadherin is considered the major adhesion molecule of epidermal melanocytes and keratinocytes, its expression is lost in most melanoma releasing them from keratinocyte control [6]. This downregulation leading to complete loss of E-cadherin takes place during the vertical growth phase (VGP) (Figure 2). This phase is a more dangerous stage of melanoma progression in which the tumor invades the underlying dermal tissue and can gain metastatic potential [31]. Attenuation of E-cadherin expression can be accomplished by HGF (Hepatocyte Growth Factor), PDGF (Platelet-Derived Growth Factor), ET-1 (Endothelin-1) and the snail family of transcription factors, which are expressed in melanoma but not melanocytes [6, 32-34]. Upon E-cadherin and P-cadherin downregulation N-cadherin expression is upregulated, referred to as “cadherin switch”, which leads to a change of melanoma binding partners from keratinocytes to fibroblasts and endothelial cells [35]. Moreover, enhanced expression of proteases, especially matrix-metalloproteinases (MMPs),

increases aggressiveness and invasiveness facilitating melanoma cells to cross the basement membrane and invade the dermis by proteolysis of the extracellular matrix (ECM) [36]. Degradation of the ECM by increased MMP activity and gained migratory properties due to loss of adhesion proteins favors melanoma metastasis [37].

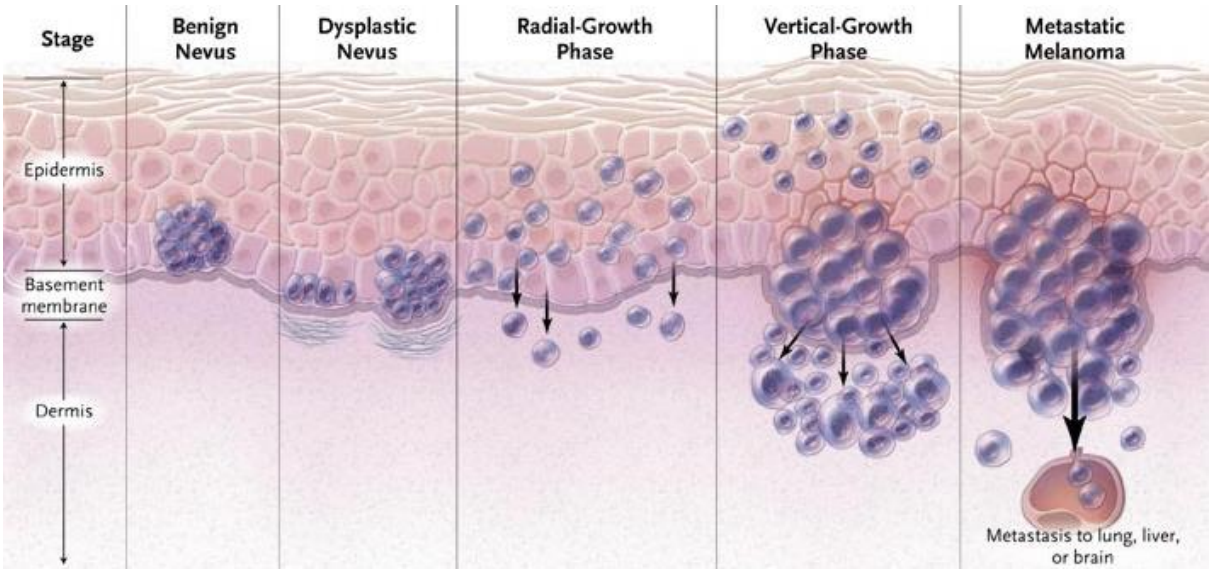

Figure 2. Stages of melanoma development.
Benign nevi can start to grow abnormally and transform into dysplastic nevi. The malignant state is achieved by accelerated growth in the radial-growth phase (RGP). In the following vertical-growth phase (VGP) melanocytes are released from keratinocyte control, pass the basement membrane (BM) and metastases leave the primary tumor. Modified from [38].

After leaving the primary tumor, melanoma cells' dissemination to distant tissues and organs occurs in different ways. Melanoma cells that have undergone epithelial-to-mesenchymal transition (EMT), acquire more mesenchymal-type characteristics [39] and become more migratory and metastatic. Those cells can actively move into the surrounding tissue and intravasate into blood- or lymphatic vessels allowing them to circulate [37, 40]. On the contrary, non-EMT tumor cells, may be shed from the primary tumor into blood- or lymphatic vessels [40], or attach to motile EMT tumor cells, thus passively invading [41]. However, regardless of how melanoma cells dissociated from the primary tumor, they have to overcome several obstacles when circulating. They have to overcome anoikis, described as cells' death when detached from ECM, shear stress of blood stream or lymphatic fluid, and the immune system within and outside the vessels [42]. When arrived at distant sites by extravasating through the endothelium, melanoma cells can undergo mesenchymal-epithelial transition (MET), the reversible process of EMT, and proliferate to grow into a metastasis [42, 43]. Otherwise, if adapting to the new microenvironment is not possible or if the current

circumstances are not suitable, the tumor cell can change into a dormant state in which it can persist until environmental conditions are proper to start proliferating again [42].

1.1.3 Tumor microenvironment

The tumor microenvironment (TME) describes the entity of cellular and non-cellular components of the tumor-encompassing niche [44]. The ECM accounts for the non-cellular part of the TME and I will introduce this subject in separate paragraph. The cellular component of the TME, besides the proliferating tumor cells, comprises infiltrating immune cells and numerous stromal cell types, including fibroblasts that are activated into a cancer-associated fibroblasts type of cell (CAFs), vascular cells, and adipose cells (Figure 3) [44]. The malignant tumor cells and the dynamic TME closely cross-communicate [44, 45]. They influence each other either by direct contact or by autocrine and paracrine signal transduction, and autophagy, which in turn regulates tumor growth, survival, metastasis and therapeutic resistance [46].

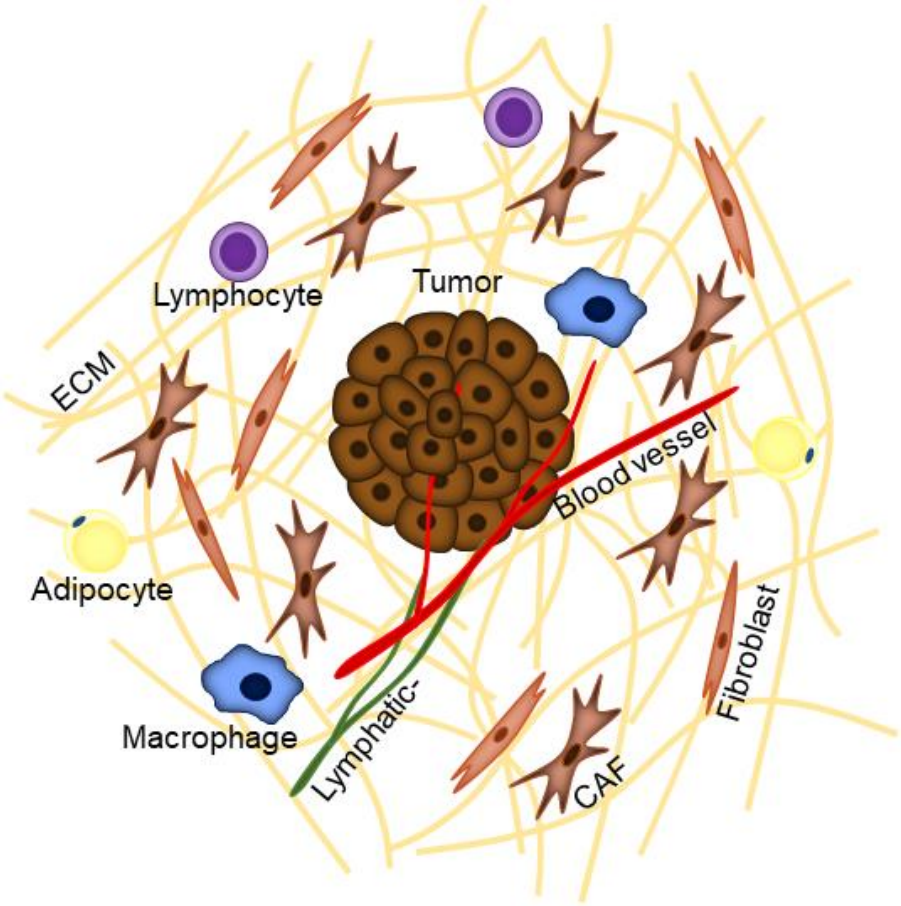

Figure 3. The tumor microenvironment consisting of numerous different cell types and the non-cellular structural extracellular matrix.

Tumor infiltration by immune cells is described as universally accepted for many types of cancers [47, 48]. It indicates that tumor cells are recognized by the host's innate and adaptive immune response to eliminate tumor cells and counteract tumor progression, an event referred to as immunosurveillance [49]. Accompanying with this, several studies demonstrate a correlation of inflammatory tumor infiltrates and positive patient's prognosis [50-53]. However, tumor cells have developed several strategies to overcome immunosurveillance. In contrary to this, a number of studies have considered tumor infiltration by immune cells to have a tumor promoting effect [54-56]. Among them, macrophages are considered to have an important role in tumor growth. In mammary tumors it has been described that macrophages are recruited to the invasive front of cancer cells to promote migration and invasion through secretion of soluble factors, as for instance EGF (epidermal growth factor) [57, 58]. In addition, they support angiogenesis by secretion of VEGF (vascular endothelial growth factor) and may regulate collagen fibrillogenesis [57, 58]. This, leading to movement of the invasive tumor cells along collagen fibers, which are attached to blood vessels, facilitates penetration of the tumor cells into those vessels [59]. Further, regulatory T-cells are recruited to the tumor to down-regulate the host's anti-tumor response and conduct pro-angiogenic reprogramming of the TME to support the tumor [56, 60, 61]. However, besides the mentioned, plenty of other immune cells, like neutrophils, dendritic cells, lymphoid cells, myeloid-derived suppressor cells, and NK (natural killer) cells hold a significant role in influencing and contributing to tumor growth [56, 62]. Cancer infiltrating immune cells are able to communicate with cancer-associated adipocytes (CAA) protecting the tumor from the host's anti-tumor immune response [63]. Cancer associated adipocytes (CAA) mainly have metabolic functions but promote tumor growth and metastasis through enhanced secretion of inflammatory factors, like IL-1β, Il-6, and IL-10, and matrix metalloproteinases [64]. Lymph vessels ensure drainage of fluids and cells from the tumor to lymph nodes and lymphoid secondary organs [65]. Further, blood vessels promote tumor growth by providing nutrients and oxygen [66]. During tumorigenesis EC morphology and functionality, on both cellular and molecular level, often are unbalanced [67]. Continuous overexpression of pro-angiogenic factors, including VEGF, fibroblast growth factor 2, platelet derived growth factor, angiopoietins, ephrins, apelin and chemokines, promote steadly angiogenesis of tumor vessels [68, 69]. However, maturation of these newly formed blood vessels is disturbed and they exhibit irregular vessel diameters [69].

Moreover, defective formation of the vessels' EC monolayer and cell junctions leads to large intercellular openings increasing vessel leakiness. This causes increased interstitial fluid pressure, reduced blood flow and enhanced intratumoral hypoxia [70, 71]. Altered cancer cell heterogeneity, resistance and disturbed drug supply to the tumor are further consequences of these features [66]. Increased hypoxia, which is observed in the majority of cancer types, induces the stabilization of the heterodimeric transcriptional factor complex, hypoxia-induced factor (HIF). When under hypoxic conditions the HIF α-subunit is stabilized, transcription of several earlier mentioned pro-angiogenic genes is upregulated to promote angiogenesis [69, 72]. Another targed that is regulated by HIF is a member of the glycolytic pathway, namely carbonic anhydrase IX (CAIX) [73]. CAIX regulates the pH level within hypoxia-induced acidosis by hydroxylating carbon dioxides, making it an important marker for tumor hypoxia [74]. The major component of many cancers' TME are cancer-associated fibroblasts (CAFs) [75]. CAF lack epithelial and endothelial cell markers but express mesenchymal ones, such as vimentin (VIM), alpha-smooth muscle actin (α-SMA), fibroblast activation protein (FAP), platelet-derived growth factor alpha (PDGF-α) [46]. However, these markers are not specific to CAFs as on the one hand, they can be expressed also by other mesenchymal cell types and on the other hand, as a result of their great heterogeneity, different CAF subpopulations can express different combinations of these markers [46]. Fibroblasts can be activated into CAFs by a number of different stimuli, including growth factors (transforming growth factor beta (TGFβ), hepatocyte growth factor (HGF), fibroblast growth factor (FGF), PDGF), transcription factors (nuclear factor-kappaB (NF-κB), heat shock factor-1 (HSF-1)), metalloproteinases (MMPs), cytokines (interleukin-1 (IL-1), interleukin-6 (IL-6)), reactive oxygen species (ROS), but also by various cancer therapy approaches [46]. Likewise, changes in physical and mechanical properties of the surrounding microenvironment, such as increased tissue stiffness can activate CAFs [76, 77]. CAFs are crucial regulators within the TME. They secrete soluble factors, such as growth factors, cytokines, chemokines, and other effector molecules to communicate with the malignant cancer cells as well as with the other cells of the TME to promote the tumor and the immune response [46, 78]. Consequently, it has been shown that CAF-mediated secretion if IL-6 has a beneficial effect on proliferation, migration and drug resistance of bladder and ovarian cancer cells [79, 80]. Further, paracrine secretion of CAF-TGFβ can activate HOX transcription in breast cancer cells, which induces EMT and promotes breast

cancer metastasis [81]. A further crucial feature of CAFs during tumor growth is the remodeling of the ECM. CAFs reshape the ECM by increased production, modification and degradation of matrix molecules creating an altered microenvironment that favors the tumor [82]. Enhanced expression and activation of MMPs allows CAFs to specifically degrade parts of the ECM to clear paths that facilitate tumor cell migration and invasion into the surrounding tissue [83, 84]. However, while CAFs have been predominantly considered to have a tumor-supportive role in the past, some recent studies have also shown a tumor-suppressive effect of specific CAF subpopulations demonstrating their heterogeneity [46, 85].

1.2 Extracellular matrix

The ECM represents the non-cellular compartment of the microenvironment in all tissues and organs that serves as a scaffold rendering structure and stability [86]. It consists of a variety of extracellular molecules, like collagen, glycoproteins (such as fibronectin and tenascins), proteoglycans (such as heparan sulphate proteoglycans, versican and hyaluronan) and glycosaminoglycans that are secreted by resident cells and, whose composition and organization differs dependently from tissue and condition [87]. As a highly dynamic network, the ECM molecules undergo permanent enzymatic and non-enzymatic remodeling as well as posttranslational modification [88]. Besides its supportive role, the ECM also has mechanical properties, like elasticity, tensile strength and tissue stiffness. This in turn can regulate cellular functions, such as proliferation, apoptosis, migration and differentiation in normal skin homeostasis and under pathological conditions [87, 88].

Collagen type I, not only accounting for the major part of the ECM, is also one of the best documented components of the peritumoral matrix of many cancers being involved in regulation of tumor growth [86, 89, 90]. Therefore, the following subparagraph will concentrate on the description of collagens.

1.2.1 Collagens

Collagens are a large superfamily of extracellular proteins comprising 29 different types that can be divided into different classes dependent on their structure [91]. Namely the fibrillar (types I, II, III, V, XI, XXIV, XXVII), the fibril-associated collagens with interrupted triple helices (FACITs) (types IX, XII, XIV, XVI, XIX, XX, XXI, XXII, XXVI), the network forming (types IV, VIII, X), the anchoring fibrils (type VII) and the

transmembrane (types XVII, XXV) collagens [92]. Collagens have been shown to have a regulatory impact on several cellular processes including proliferation, apoptosis, differentiation, adhesion, migration and invasion [90, 93-97].

They are the most abundant proteins comprising up to 30% of the ECM in vertebrates and have a contributing role in a number of functions like in maintaining tissue structure, stability and mechanical properties [92, 98]. Collagens have a long half-life with 117 years in cartilage (type II collagen) and 15 years in skin (type I collagen) [99], and 74 days in mice skin (type I collagen) [100].

The molecular structure of all members of the collagen family unifies one triple helical collagenous and two non-helical regions at both ends of the collagen molecule [91]. In fibril-forming collagens, three α polypeptide chains are arranged in a uniformly shaped coiled-coil structure to generate the collagen triple helix. This structure can be formed by either three identical or different left-handed α-chains generating right-handed homotrimers, such as e.g. collagen type II and III, or heterotrimers, like collagen type I, V and IX, respectively [101]. The triple helix sequence contains Gly-X-Y repeats, with potential interruptions, in which each X and Y can stand for a proline or hydroxyproline [91, 101]. Interchain hydrogen bonds between two glycines, prolines or hydroxyprolines, respectively, of adjacent α-chains stabilize the triple helix [101].

Synthesis of collagen starts with the transcription of genes encoding the different α-chains, for instance COL1A1 and COL1A2 for collagen type I. The collagen mRNA translocates to the rough endoplasmatic reticulum (rER) where it is translated and the generated pre-pro-collagen molecule is elongated into the rER lumen with the N-terminus first (Figure 4) [91, 102]. Simultaneously, the signal peptide is removed and the nascent, unfolded polypeptide α-chain is posttranslationally modified. These modifications include proline and lysine hydroxylation by prolyl 3-hydroxylase (3-PH), prolyl 4-hydroxylase (4-PH), and lysyl hydroxylase (LH), respectively [103]. While prolyl 3-hydroxylation is less prevalent, prolyl 4-hydroxylation occurs more commonly (99% of proline hydroxylations) and has an important role in hydrogen bond formation and triple helix stability [103]. Hydroxyproline comprises about 10% of the amino acids in collagen and is commonly present at the Y position of Gly-X-Y repeats, which makes it a marker for collagen [91]. Specific hydroxylysines can be a target for additional modification via O-linked glycosylation. In this process, which is catalyzed by hydroxylyl galactosyltransferases (GT) and galactosylhydroxylysyl glucosyltransferases (GGT), galactose and glucose are added to the 5-hydroxyl group

generating galactosylhydroxylysine (G-Hyl) and glucosylgalactosylhydroxylysine (GG-Hyl) [102, 104]. Following this, three α-chains align at the C-terminal pro-peptide of each polypeptide chain and form a triple helix from the C-terminus to the N-terminus through a zipper-like folding mechanism that requires approximately 14 minutes of time to fold the whole procollagen molecule [91, 105]. In the case of collagen type I, during translation the pre-pro-collagen polypeptide chains arrange in so-called collagenosomes, which are distinct disk-shaped structures, sized 0.5-1 μM in diameter and 200-400 nm in thickness, at the ER membrane [106]. As procollagen folding takes place in the collagenosome center, proper formation and organization of this structure is essential [106]. Since unlike collagen biosynthesis, which starts at the N-terminus, triple helix formation is initiated at the C-terminus, several chaperone proteins, such as prolyl 4-hydroxylase (P4-H), peptidyl prolyl cis-trans isomerases (PPIases), protein disulfide isomerase (PDI) and heat shock protein 47 (hsp47), among others, prevent the α-chains from associating with each other before completion of the translation process [107, 108]. The procollagen molecule generated this way, translocates from the ER to the Golgi apparatus and is then secreted into the extracellular space. Afterwards, the procollagen C- and N-terminal pro-peptides are shed by a disintegrin and metalloproteinase with thrombospondin motifs (ADAMTS), bone morphogenic protein 1 (BMP1)/Tolloid-like proteinases and Meprins, generating a mature collagen molecule that spontaneously arrange in parallel and longitudinal structures building collagen fibrils [104, 109].

Specific proline and lysine residues of the C- and N-terminal telopeptides, which are disclosed upon removal of the pro-peptides at both termini, undergo oxidative deamination by lysyl oxidase (LOX). This results in generation of Lys^{ald} (α-aminoadipic acid-δ-semialdehyde) and Hyl^{ald} (δ-hydroxy, α-aminoadipic acid-δ-semialdehyde), the respective aldehyde form, that is necessary for the formation of covalent inter- and intramolecular cross-links during collagen fibril synthesis [104]. Depending on their composition and formation, different types of crosslinks can be distinguished that specifically occur in certain tissues. They are generated in the telopeptides of collagen molecules in pathways originating either from Hyl^{ald}, being predominant for stiff tissues, such as bone, cartilage and fibrotic tissue, or Lys^{ald}, found in soft tissues like skin (Figure 5) [110].

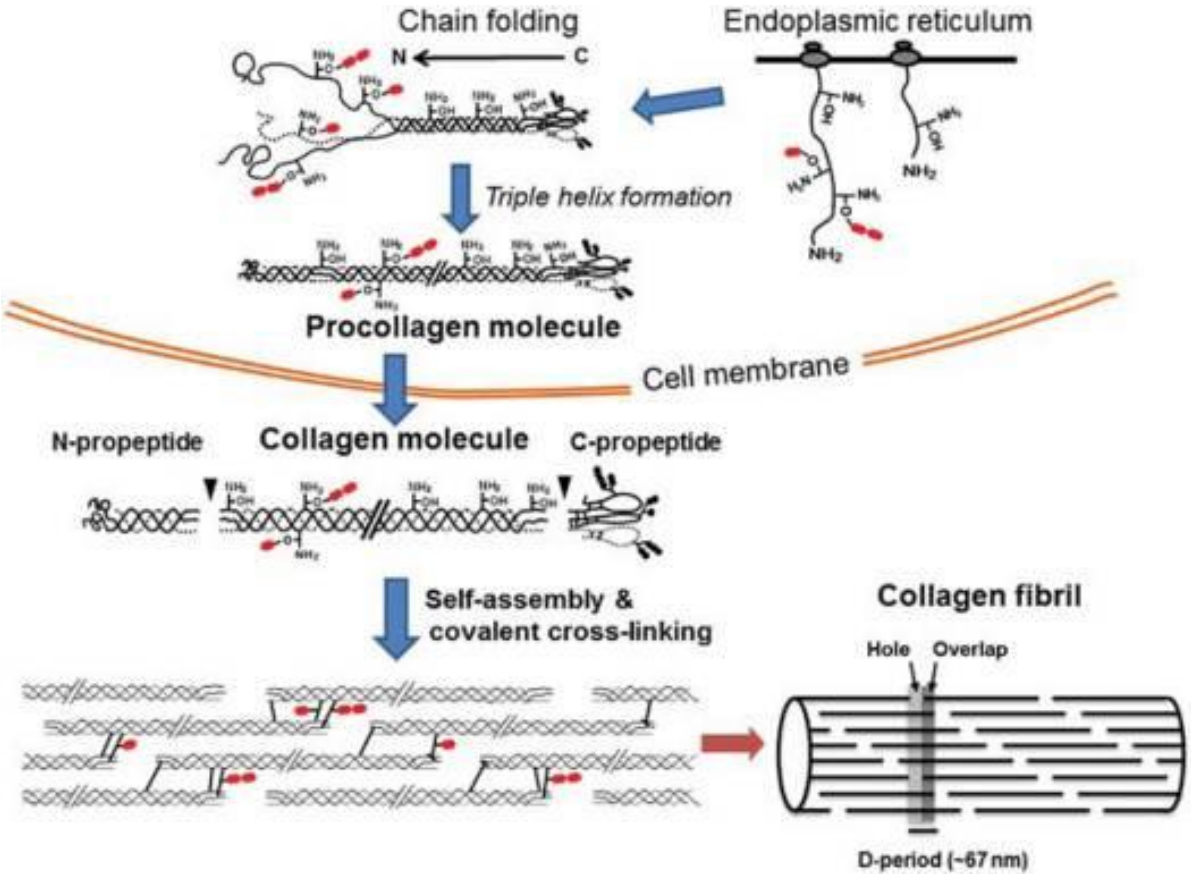

Figure 4. Collagen biosynthesis.
Collagen mRNA is translated at the endoplasmatic reticulum (ER) with simultaneously removing the signal peptide and hydroxylation of lysine- and proline residues. Afterwards chain folding occurs by three α-chains fold in a zipper-like manner from the C- to the N-terminus and following triple helix formation. The generated procollagen molecule is released into the extracellular space where both propeptides are removed and the mature collagen molecule assembles into a collagen fibril and cross linking takes place [104].

One Hyl^{ald} can react with the ε-amino group of an hydroxylysine residue that is located within the helical part of an adjacent collagen molecule generating an intermolecular deH-DHLNL (dehydro-dihydroxylysinonorleucine) crosslink, referred to as almidine crosslink [104]. This crosslink is a divalent and immature type that can be reduced again by reducing agents and can act as a marker for newly synthesized collagen [104, 111]. Condensation of two deH-DHLNL crosslinks with each other, releases one helical hydroxylysine residue and results in the formation of a stable, trivalent Pyr (pyridinoline) crosslink, which can link two or three collagen molecules [112, 113]. Further trivalent end products being formed in this pathway, but less commonly are d-Pyr (deoxypyridinoline) crosslinks (two telopeptidyl Hyl^{ald} and one helical lysine) , Prl (pyrrole) crosslinks (one telopeptidyl Hyl^{ald} and Lys^{ald} each, and one helical hydroxylysine) and d-Prl (deoxypyrrole) crosslinks (one telopeptidyl Hyl^{ald} and Lys^{ald} each, and one helical lysine) [114-116].

In soft tissues, such as the skin, the telopeptidyl Lys^{ald} reacts with a helical hydroxylysine residue from a juxtaposed collagen molecule, generating the divalent deH-HLNL (dehydro-hydroxylysinonorleucine) crosslink. By reacting with a helical histidine residue, the divalent deH-HLNL crosslink can mature into the trivalent HHL (histidinohydroxylysinonorleucine) crosslink, which resistant against UV light and therefore the prevalent collagen crosslink type in skin and cornea [117, 118]. Another predominant crosslink in soft tissues, which is present especially in the skin [119, 120], is the deH-HHMD (dehydro-histidinohydroxymerodesmosine) crosslink, formed by two telopeptidyl Lys^{ald}, one helical histidine and a helical hydroxylysine residue, making it the only tetravalent crosslink having the most complex structure [104, 121].

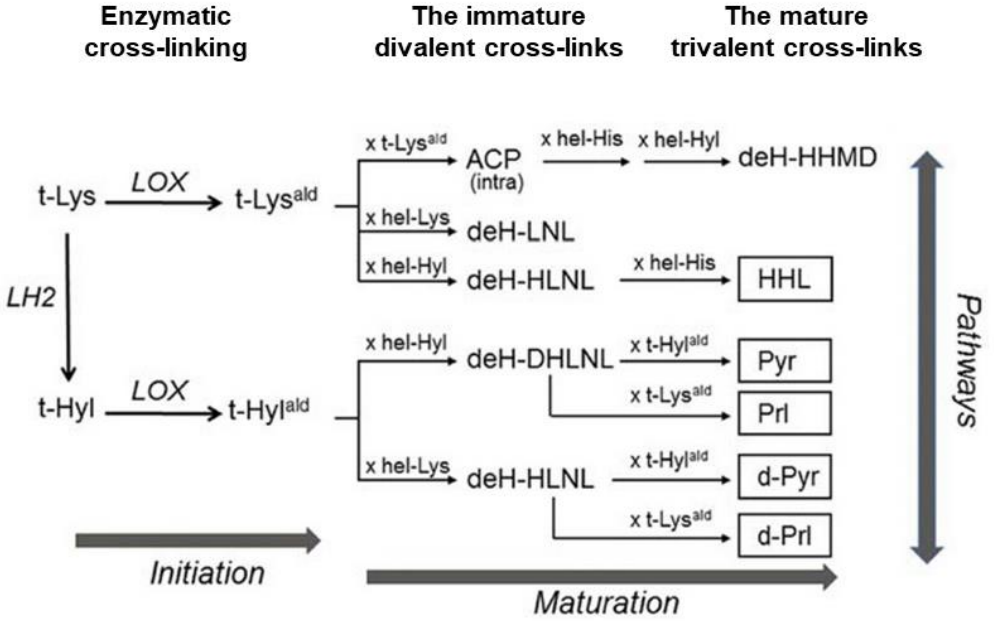

Figure 5. Pathways of LOX-mediated collagen cross-linking.
The scheme displays initiation and maturation of immature divalent cross-links into mature trivalent (or tetravalent) cross-links. t, telopeptidyl; hel, helical; ald, aldehyde; d-, deoxyde-; H, dehydro. Modified from [104].

1.2.2 ECM in cancer

The ECM is a major component of the TME and a critical regulator of tumor growth. In cancer ECM synthesis, modification and degradation dynamics are deregulated leading to different composition, density and mechanical properties compared to physiological ECM [122]. As tumors often are desmoplastic, their fibrotic microenvironment is designated by increased deposition, altered organization, reduced turnover, altered force-mediated remodeling, and enhanced post-translational

modifications of matrix molecules [88, 122]. Many cells of the TME may contribute to production and deposition of matrix proteins, however the main producer of the ECM are fibroblasts that produce massive amounts of the ECM [123]. Tumor cells also exhibit altered expression of matrix proteins, such as collagen types I and III, and matrix modifying enzymes like lysyl oxidases (LOX) and LOX-like proteins (LOXL) [86, 124, 125]. Although, several studies described the tumor promoting role of fibroplasia and stiffening of tumor matrix [126-129], ECM proteins can have either tumor-suppressing or tumor-promoting properties. The best-known alteration in tumor ECM is the abnormal accumulation of fibrillar collagen accompanied by increased numbers of crosslinks and stiffness [89]. Increased remodeling of matrix molecules leads to reorganized collagen arrangement being characterized by packed and linearized interstitial collagen fibers at the tumor invasive front [130]. This cancer-specific pattern, referred to as tumor-associated collagen signature (TACS) [131], has tumor-supportive effects, especially concerning cell proliferation, migration, metastasis, and responses to treatments [130, 132]. Indeed, increased fibrillar collagens orientation accompanied by increased stiffness has been detected at the invasive front of human breast cancer [133]. In addition, extensive deposition of fibronectin, hyaluronic acid (HA) and tenascin C resembles a desmoplastic fibrotic phenotype attributed to many cancers with poor prognosis [134, 135].

ECM proteins' posttranslational modifications (PTMs) control their arrangement and localization and regulate processes, such as interactions with other molecules and cellular receptors, trafficking and degradation [136]. Deregulation of these PTMs during tumor growth can result in morphological and functional changes of the ECM. Under physiological conditions enzymes like PLOD and LOX are involved in the proper folding and crosslinking of collagen fibers. Tissue transglutaminase 2 (TG2) catalyzes crosslinks in fibronectin, heparan sulfate proteoglycan (HSPG), fibrinogen and collagen type IV. These enzymes are often upregulated in cancer, leading to increased crosslinking and linearization of ECM molecules [137]. Further, HSPG is modified by endosulphatases that are upregulated in many cancers. Altering of the sulfation pattern of HSPG can lead to differential regulation of various receptor tyrosine kinase signaling pathways resulting in impaired or extensive growth factor release [138].

A different way to modify the tumor ECM is proteolytic processing by several enzymes, including MMPs, ADAMs, ADAMTS and specific serine- and cysteine proteases [139]. Processing of the ECM can have tumor-promoting or tumor-antagonizing effects [140,

141]. Matrix degradation by MMP8 for instance has been shown to be tumor supportive in ovarian cancer and hepatocellular carcinoma [142, 143]. In contrast, low MMP8 expression correlated with worse prognosis in tongue squamous cell carcinoma patients, and *in vitro,* MMP8 acted anti-invasive by impairing VEGF-C expression [144]. However, most matrix-degrading events support tumor progression by leaving space for the deposition of the new tumor-derived matrix and facilitating tumor cell migration and invasion [145]. Further, the processing of matrix proteins can generate bioactive fragments, called matrikines, such as endostatin, the NC1 piece of type XIX collagen, or those derived from elastin act in a tumor-promoting or suppressing way [146-148].

1.3. MMPs

1.3.1 Structure

The matrix metalloproteinases (MMPs), also called matrixins, are a family of calcium (Ca^{2+})-dependent zinc (Zn^{2+})-containing endopeptidases. They belong to the superfamily of metzincins, including astacins, serralysins, pappalysins, adamalysins (ADAMs and ADAMTS having, in addition, thrombospondin-like motifs) [149, 150]. Based on their structure and substrate specificity, the MMPs can be classified into six major subgroups: collagenases (MMP1, MMP8, MMP13); gelatinases (MMP2, MMP9); stromelysins (MMP3, MMP10, MMP11); matrilysins (MMP7, MMP26); membrane-type MMPs (MMP14, MMP15, MMP16, MMP24) and other unspecified MMPs (Figure 6) [151]. These proteases are composed of multiple domains, including a signal peptide, the pro-peptide domain, the catalytic domain, the hinge region, and the hemopexin domain (PEX). The signal peptide, comprising 17-19 amino acids, is located at the N-terminus of the MMPs and is responsible for the translocation up to the cell membrane or secretion into the extracellular space. The pro-peptide domain (consisting of 77-87 amino acids) contains a consensus cysteine-switch sequence PRCGXPD, which binds the Zn^{2+} of the catalytic domain keeping the protease inactive [152]. The highest homology among all MMPs shows the 170 amino acid sized catalytic domain, containing the conserved Zn^{2+} binding motif HEXXHXXGXXH and methionine, which forms a ‘Met-turn’ [151]. The proline-rich hinge region is a highly motile element responsible for protein flexibility, and the hemopexin domain regulates protein binding [153, 154]. Collagenases share this general domain structure. They degrade fibrillar collagen types I, II, and III by binding them with the hemopexin domain and cleaving

with the catalytic domain. This cleavage event occurs in the triple-helical part of the collagen molecule three-fourth from the N-terminus, generating the typical N-terminal three quarter and C-terminal one quarter fragments [151]. In contrast, both gelatinases (MMP2 and MMP9) contain three unique fibronectin type II modules in their catalytic domain that allows them to degrade denaturated collagens [149]. MMP7 and MMP26 representing the matrilysins, lack the hemopexin domain but nevertheless degrade collagens and other ECM proteins [155].

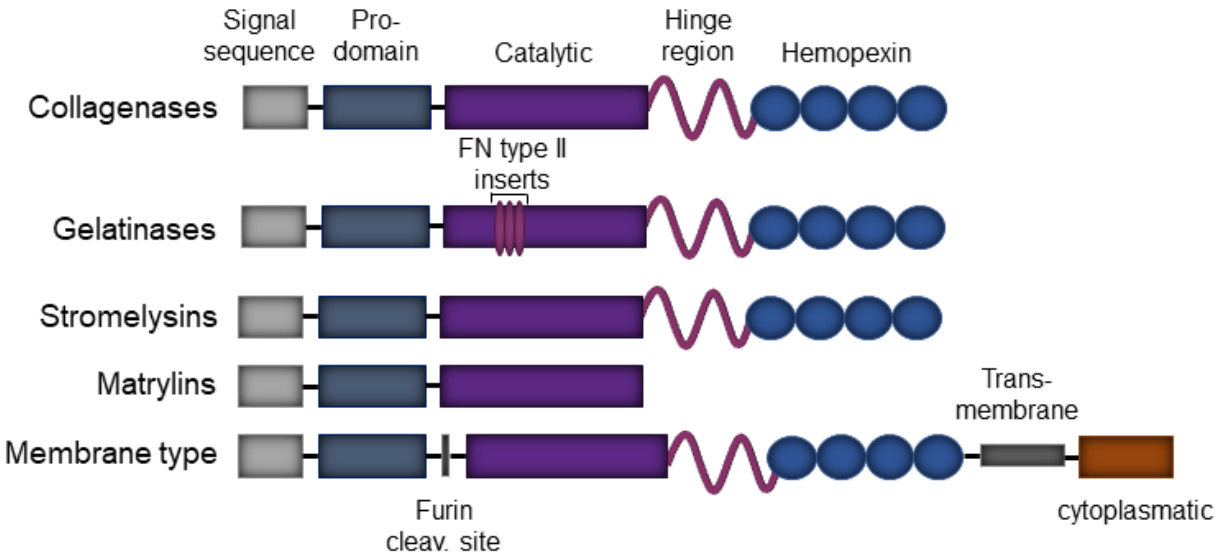

Figure 6. The family of matrix metalloproteinases.
These proteases are grouped into collagenases, gelatinases, stromelysins, matrilysins, membrane-type MMPs and others, unspecified (not included in this figure).

1.3.2 Regulation and activity

MMPs are expressed in several different tissues and cell types time and context-dependent. MMP synthesis, secretion, and activation are tightly regulated [155-157]. MMPs, are synthesized as pre-proenzyme and are transformed to proMMPs during the translational process at the ER by removing the signal peptide [158]. ProMMP latency is maintained by binding the thiol group from the free cysteine in the pro-domain to the zinc ion (Zn^{2+}) of the catalytic domain, thereby preventing substrate binding [149, 152]. To activate the proenzyme, this interaction needs to be interrupted, a process referred to as the “cysteine switch”. The switch can be induced by reducing the thiol group with reactive oxygen species (ROS) or non-physiological agents like alkylating agents such as heavy metal ions and disulfides. These result in autoproteolysis of the pro-domain [159, 160]. Further, the pro-domain can be directly shed by another

protease. Allosteric disruption of the pro-domain conformation can impede thiol-Zn2+ interaction and allow a water molecule to bind the zinc ion of active MMPs [152, 160]. Approximately one-third of all MMPs, including MT-MMPs, are activated through cleavage by the type I membrane subtilisin-like serine protease furin [161]. Furin recognizes an RXKR or RRKR sequence located between the pro- and the catalytic domain of the MMPs, whose cleavage leads to the removal of the pro-domain [160]. Being active in the Golgi apparatus, the activation of MMPs mediated by furin occurs intracellularly and before secretion or assembly into the cell membrane [161, 162]. The remaining proMMPs are secreted as inactive proenzymes and are activated extracellularly. Further activation may occur by “mutual MMPs-activation” of MMPs. For example, MMP3 can activate proMMP1 and proMMP7 [163, 164]. Another best described proMMP-activation process by another MMP is the MMP14-mediated proMMP2 activation [165-167]. Thereby, MMP14 activates proMMP2 in a cooperative action with the tissue inhibitor of metalloproteinase 2 (TIMP2) at the cell surface. To initiate this activation mechanism, C-terminal TIMP2 tightly interacts with MMP2 by binding to its C-terminal hemopexin domain. This leaves the inhibitory N-terminal part of TIMP2 free to bind the catalytic domain of MMP14 rendering it inactive [158, 168]. Afterwards, this generated ternary complex formed in a stoichiometric ratio of 1:1:1, directs the pro-domain of proMMP2 to another active MMP14 that clusters in this complex, and activates the proenzyme [158]. This activation mechanism occurs in the presence of low concentrations of TIMP2, but high TIMP2 concentrations impede the second MMP14 to activate MMP2 [169, 170].

1.3.3 MMPs role in physiology and pathology

MMPs' primary function was limited to the degradation of ECM proteins. However, studies with mice harboring full-body deletions of distinct MMPs show that these proteases are involved in processing a variety of additional proteins. For example, cell surface receptor and growth factors proteolytic activation lead to the modulation of various developmental processes, including angiogenesis, wound healing, and immune response [171-178]. Despite their multiple roles, knock-out mice exhibit only mild phenotypes and are viable with few exceptions.

In bone development, MMPs are involved in matrix turnover during the two main bone ossification processes, the endochondral and intramembranous. Deletion of MMP2, MMP9, MMP13, and MMP14, led to impaired bone growth because of irregularities in

development and vascularization of growth plates, which resulted in diminished bone growth and body size [172, 179-181]. MMP14 deficient mice, in contrast to the other MMP knock-out models, show a very severe phenotype resulting in the early death of mice [172].

Deregulation of these proteases in various organs implicated them across multiple disease processes. In cardiovascular diseases, MMP1 MMP2, MMP9, and MMP12 contribute to myocardial fibrosis, atherosclerotic vascular wall thickening, and plaque fracture [182-186]. MMPs are essential contributors in degrading the atherosclerotic plaque, mainly consisting of collagen types I and III. The resulting plaque rupture can lead to coronary artery diseases, venous thromboembolism, and stroke [187, 188]. In contrast, another study showed that MMP3 and MMP9 inhibit atherosclerotic plaque growth, counteracting the pathological state [184].

In addition, MMP2, MMP3, MMP9, among others, are upregulated in arthritis, where they impair standard joint functionality by cleaving the non-collagenous ECM of the joints [189]. In addition to this, uncontrolled MMP expression and activity have been associated with various cancer types [190, 191]. For instance, metastasis to distant organs in breast cancer patients has been correlated to upregulated MMP1, MMP2, MMP7, MMP9, MMP11, and MMP13 [192, 193]. Further, MMP12 and MMP13 are increased in mouse lung tumors [194]. Moreover, increased MMP9 levels have been linked to poor patients' outcomes in breast, lung, colon, gastric, pancreas, and prostate cancers [195-199]. By degrading the ECM, generating bioactive fragments, and releasing growth factors, MMPs play an essential role in tumor growth, metastasis, and invasion [200]. The tumor surrounding ECM represents a physical barrier that must be overcome by the tumor cells during expansion, invasion, and metastasis. To promote the tumor cells' invasion to adjacent tissues, MT-MMPs, such as MMP14, localize at the cells' invading front in structures named invadopodia, where focalized proteolysis takes place [201]. Apart from that, activated secreted MMPs, including MMP2 and MMP9, degrade matrix proteins and facilitate invasion [201, 202]. On the contrary, some MMPs can have a tumor counteracting effect. Mice deficient for MMP8 are more susceptible to the development of papilloma tumors [203], but in breast cancer, its overexpression decreases the metastatic potential [204]. Moreover, in the absence of MMP9 in bone-marrow cells, mice develop epithelial tumors in which keratinocyte differentiation is greatly diminished by the lack of keratin 10 (K10) suppressing keratin

intermediate filaments and increasing vimentin to a more aggressive and higher-grade tumor [205].

1.4 MMP14

1.4.1 Structure and functions

MMP14 is the first described MT-MMP and was identified as a cellular receptor and activator for pro-MMP2 [206]. MMP14 consists of multiple domains, highly conserved within this proteinase family, and contains a transmembrane domain and a cytoplasmatic tail (Figure 6). Activation of MMP14 is a two-step process. Besides the furin recognition site, RRKR, a further cleavage event within the pro-domain of MMP14 is necessary to generate an active enzyme [207, 208]. The MMP14 pro-domain consists of three-helix bundled structures and a “bait” loop region that links the first two helices [207]. Furin cleavage alone is not sufficient to activate MMP14 since the intact pro-domain still is an efficient inhibitor of MMP14 [207]. Intradomain cleavage of either the PGDL or PQSL sequence, or both, within the pro-domain “bait” loop region starts the MMP14 activation process [207]. This cleavage event can be performed by various MMPs, including MMP2, MMP9, MMP14 (autoproteolysis), MMP15, MMP16, MMP24, and MMP25 generates the activation intermediate [208]. Moreover, also trypsin can activate MMP14 *in vitro* [209].

The transmembrane domain anchors the enzyme to the cell membrane, and together with the hemopexin, allows protein homodimerization [210]. MMP14 homodimer formation is important for MMP2 activation [158, 211] and cleavage pericellular collagen types I, II, and III at the cell surface [212]. Besides collagen, several other proteins are among MMP14 substrates, although mostly demonstrated *in vitro* and only partly *in vivo*. These include other ECM proteins (fibronectin, vitronectin, laminins 1, -2/4, -5, perlecan, fibrinogen), enzymes and proenzymes (proMMP2, proMMP13 and ADAM9), receptors (CD44, ICAM-I, EphA2, LRP1), cytokines (IL-8, SDF-1, MCP-3) and growth factors (CTGF, HB-EGF) [210, 213-215]. MMP14 controls many cellular processes, including proliferation, migration, invasion, and differentiation in physiological and pathological conditions [213-216]. However, apart from its proteolytic properties, MMP14 is capable of acting in a proteolysis-independent manner. For example, forming a complex with TIMP-1, MMP14, through its cytoplasmatic tail can activate ERK1/2, leading to upregulation of cell proliferation and migration in breast cancer cells independently of proteolysis [217]. Moreover, through either activity of the

cytoplasmic domain or trafficking to the nuclear compartment, MMP14 initiates the activation of a phosphoinositide 3-kinase δ (PI3Kδ)/Akt/GSK3β signaling cascade [218, 219] and controls motility and inflammatory response of macrophages independently of protease-activity. In addition, MMP14 has been shown to control transcription of target genes, including vascular endothelial growth factor A (VEGF-A) by forming a complex with VEGFR-2 and Src to phosphorylate Akt and mTOR [225]. It is also implicated in the transcription of several cytokines, such as interleukin-6 (IL-6), -12 (IL-12), and -33 (IL-33) [220, 221].

1.4.2 MMP14 knock-out models

1.4.2.1 Complete knock-out models

Mice carrying a full-body deletion of this protease suffer from severe defects in connective tissues, organs, and bone development that lead to early death [172, 222, 223]. In the first available MMP14 knockout mouse model, gene deletion was achieved by replacing the first half of 3' exon 1 to the 3' end of exon 5 with a PGK controlled HPRT minigene [172]. The resulting protein lacked the amino acid residues 6-274, including five pro-domain residues and eight catalytic domain residues, generating an inactive polypeptide [172]. Almost simultaneously, another MMP14 knockout mouse model was described. In this case, MMP14 deletion was performed by partly removing exon four and replacing it with a neomycin cassette with the pgk1 promoter [222]. Because both generated MMP14 deletion mice developed similar severe skeletal and vascular phenotypes, they will be described together [172, 222]. Mice with MMP14 deletion exhibited no obvious phenotype directly after birth, but body weight and size were reduced five days after delivery, and one-third died before weaning [172]. They develop severe skeletal dysplasia with impaired long bone formation. They have delayed growth and vascularization of the unmineralized epiphyseal cartilage resulting from disturbed ossification and replenishment of progenitor cells, critical for bone growth [172, 222].

Further, loss of MMP14 dependent remodeling leads to progressive osteopenia and arthritis due to extensive overgrowth in the whole skeleton. It is most severe in joints, ligaments, tendons, synovial capsules, and articular cartilage, where bones are associated with soft tissues [172, 222]. Another characteristic of the MMP14 deletion is cranial dysmorphism that develops early after birth. Because of the lack of MMP14 collagenolytic activity, the embryonic cranial cartilage, which usually is removed shortly

after delivery, stays in place. Moreover, ligaments and sutures are not correctly remodeled, leading to disturbed cartilage dissolution, increased bone degradation, and reduced bone formation affecting cranial morphogenesis [172, 222]. In mice that lived longer than three months, loss of collagenolytic activity of fibroblasts led to fibrosis of soft tissues [172, 222].

In a third, more recent, MMP14 knockout model, exons 4 and 5, which code for the catalytic domain, were removed [223]. Apart from the earlier mentioned abnormalities, these mice exhibit cardiac defects, including a thickened muscular wall of the right ventricle, ventricular septum hypertrophy, and extensive collagen type I accumulation in heart tissue. However, these mice also newly show upregulation of the senescence markers p16 and p21 leading to enhanced senescence in the heart, kidney, and adipose tissue [223]. On a cellular level, loss of MMP14 altered nuclear and cytoskeletal morphology, resulting in impaired organization and connectivity between nuclear envelope and cytoskeleton that was further dependent on the surrounding ECM [223]. These characteristics have also been found in aging diseases, rendering a link to the found senescence phenotype [223-225]. Moreover, metabolic changes were detected as a result of the deletion of MMP14 [223, 226]. In the absence of MMP14 tissue glygogen and lipid levels [226], and systemic blood sugar levels were markedly lower, accompanied by reduced levels of insulin-like growth factor 1 (IGF-1), increased circulating growth hormone (GH) [223] and decreased triglyceride levels in blood plasma [226].

1.4.2.2 Tissue-specific knock-out models

Because of the early death of mice with constitutive and complete deletion of MMP14, its functional role could be analyzed predominantly during embryonic or early postnatal development. Generation of tissue-specific deletion of MMP14 allowed to circumvent premature death and investigate the distinct functions of this protease also in adulthood.

The contribution of MMP14 to skin repair during wound healing was investigated by a specific deletion in the epidermis [227]. In these mice, floxed exons 2-4 of the MMP14 gene were removed by the Cre-recombinase controlled by the keratin 14 promotor. These mice did not display any overt phenotype, and when challenged by skin excisional wounding, they could restore tissue integrity completely [233]. However, they showed a transitory phenotype with reduced vascular regression due to impaired

keratinocytes-mediated proteolytic release of endostatin from collagen type XVIII [227]. These data highlighted the critical role of MMP14 expression in keratinocytes for epidermal-dermal crosstalk in the regulation of vascular homeostasis [227]. MMP14 deficiency in macrophages (using the LysM-Cre driven deletion) results in increased corneal vascularization by lymphatic vessels [228], but this deletion did not affect either skin development or repair [229]. However, when exposed to skin irritants, the influx of monocytes, macrophages, and T-cells in treated skin was reduced without macrophage-MMP14. This process was accompanied by reduced levels of several proinflammatory cytokines, such as IL-1β, IL-2, IL-6, IL-9, IFN-γ, MIG, and MIP-2. *In vitro*, MMP14-deficient macrophage migration on fibronectin was significantly decreased [229]. In hearts after myocardial infarction (MI), macrophage-specific MMP14 (LysM-Cre driven) deletion results in attenuated post-MI cardiac dysfunction, accompanied by reduced fibrosis and preserved cardiac capillary network [230]. *In vitro*, the ability of MMP14-deficient macrophages to induce endothelial to mesenchymal transition (EndMT) in co-cultured endothelial cells (EC) was diminished, which correlates with reduced numbers of cells undergoing EndMT in heart post-MI [230].

Specific deletion of MMP14 in endothelial cells (EC) using the Tie2-Cre driven deletion, results in a mild cranial dysmorphia with slightly delayed suture closure. Still, long bone development, ossification, and skin development were not altered [231]. Tendon-specific deletion of MMP14 (Scx-Cre driven) leads to a limb phenotype with dorsiflexion of the paws, a dome-shaped skull and, impairment of skeletal and cranial growth [232]. Moreover, these mice exhibited smaller tail and Achilles tendon size with accumulated fibronectin but not collagen type I, pointing to altered tendon development. This was due to impaired collagen fibril release from the plasma membrane fibripositors where fibrils are anchored by fibronectin to a cell-surface receptor whose identity is unclear [232].

Further, mice lacking MMP14 in the dermal fibroblasts display a fibrosis-like skin phenotype and formation of fibrotic tendons as a result of impaired collagenolysis [233]. Induction of fibrosis by bleomycin injections in the skin was not altered, but the resolution of fibrotic lesions was reduced by the absence of fibroblast-MMP14. This, together with the lack of fibrillar collagen type I degradation by MMP14-deleted fibroblasts *in vitro*, shows the importance of MMP14 as a collagenolytic enzyme in skin homeostatic remodeling [233]. Another model emphasizing the essential role of the

collagenolytic function of MMP14 in tissue remodeling was produced by Sftpc-Cre driven alveolar epithelial cell-specific deletion of MMP14 to investigate idiopathic pulmonary fibrosis (IPF) [234]. In this study, MMP14-alveolar epithelial deletion led to more severe bleomycin-induced lung fibrosis and delayed resolution, corroborating the findings in mice harboring the fibroblast-specific deletion of MMP14 [233, 234].

1.4.3 MMP14 in cancer

MMP14, is often upregulated in many different cancer types [235]. In patients who have lung cancer, breast cancer, gastric cancer, esophageal cancer, colorectal cancer, ovarian cancer, Merkel cell carcinoma, pleural mesotheliomas, and glioma, high MMP14 expression has been correlated with poor prognosis [236]. The activity of this protease in breast and gastric cancer cells and stroma promotes its progression by regulating cellular processes like proliferation, migration, metastasis, and invasion [237-239]. During tumor growth, MMP14 can act in different ways to support the tumor: (I) cleavage of the ECM to either release bioactive fragments for activation of signaling pathways or for cell migration, (II) binding of signaling molecules on the cell surface leading to interaction with other cell-surface proteins or initiation of intracellular signaling via the cytoplasmatic domain, (III) intracellular proteolysis and (IV) by regulating transcription of other genes [240].

MMP14 is critical for proteolytic cleavage of interstitial ECM during cellular migration of tumor cells, endothelial cells and fibroblasts [241-243]. The mesenchymal migration mode is the most common way for movement used by cells. It is mediated by β1 integrin-dependent substrate binding, ECM degradation, and the formation of actin-rich protrusions called invadopodia [244, 245]. Invadopodia are formed in a Rac1-dependent manner and represent the leading edge of the moving cell [246]. MMP14 forms a complex with β1-integrins enabling directional cell traction and ECM degradation to drive cell motility [245]. In this way, through degradation and reorganization of the collagen fibers within the pericellular ECM, the cell builds paths, which can be used and expanded by other cells [247]. Focal adhesions connecting cytoskeleton and ECM also contain active MMP14 [248]. α2β1 integrins bind intact collagen fibers, but collagen processing into gelatin exposes cryptic RGD sites that are recognized and bound by αvβ3 integrins [249, 250]. This shift in the integrin-based binding of collagen from α2β1- to αvβ3 results in FAK phosphorylation at Tyr576 and Tyr577, followed by ERK activation through c-Src, and promotes tumor cell migration

and proliferation [248, 249]. Further, MMP14 processes the laminin 332 (laminin 5) γ2 chain in tumors but not quiescent tissues [251]. The released cleavage fragments, detected in malignant melanoma and gastric cancer cells, bind to the epidermal growth factor (EGF) receptor to enhance cell adhesion, migration, and vascular tube formation *in vivo* and *in vitro* [252-254]. Independently of expression in tumor cells, stromal cells expressing MMP14 can induce tumor cell invasion and metastasis through paracrine signal transduction. MMP14 activates transforming growth factor-β (TGF-β) and releases it by proteolytically processing the latent TGF-β binding protein (LTBP-1) [255, 256]. In turn, activation of TGF- β signaling induces CULT1 and subsequently Wnt5, which leads to EMT, causing prostate cancer cells to adopt a metastatic phenotype [255].

MMP14 is expressed in melanoma already in the early transformation from nevi to malignant cells and continuously increases during melanoma development [257]. In highly invasive melanoma, MMP14 expression is required for tumor cell invasion [257, 258]. Accordingly, MMP14 activity has been linked to a cooperative invasion process that allows poorly invasive melanoma cells to co-invade with highly invasive melanoma cells [259]. Thereby, the invasive cells degrade and remodel the ECM, and deposit collagen and fibronectin to build supportive tracks that facilitate the poorly invasive melanoma cells to move [257]. Another signaling molecule that is described to be strongly reactivated in melanoma and controlling tumor growth is Notch1 [260], and MMP14 has been shown to process and activate Notch1 leading to sustained melanoma growth [261].

1.5 Aim of the project

The ECM is a significant component of the TME that plays an essential role in regulating tumor growth. In cancer, deposition, remodeling, and degradation of matrix proteins are highly deregulated due to altered expression or to proteolytic activities, well know from MMPs. MMP14 is considered a major modifier of the ECM during cancer growth and progression for many types of tumors. In melanoma, MMP14 is highly expressed and active at the tumor-stroma border, in both tumor and stromal cells, with supporting functions for growth and invasion [241, 267-269]. Indeed, the expression of MMP14 in tumors is often associated with poor patients' survival.

We could previously show that the expression of MMP14 in fibroblasts has a crucial role in collagen homeostasis in the skin *in vivo* [233]. In particular, lack of collagen processing by MMP14 in fibroblasts led to collagen accumulation and tissue stiffness, which are two tissue features frequently observed in tumors. In breast, lung, and colorectal cancer, desmoplasia is strongly linked to the tumor's aggressiveness [262]. In contrast, in melanoma, a desmoplastic response around tumors is not prominent (apart from a specific subtype with better prognosis [263]) and a clear link to progression was not established.

Using the mouse model with deletion of MMP14 in fibroblasts, the overall aim of this work was to investigate the cell-specific role for MMP14, collagen accumulation, and tissue tension in melanoma growth.

For this, we used murine melanoma cells and monitored, as a function of time, the growth of grafted tumor cells *in vivo* in mice lacking MMP14 in dermal fibroblasts ($MMP14^{Sf-/-}$). Tumor specimens were analyzed for processes and features essential in tumorigenesis and possibly altered upon MMP14 deletion. These included fibroblast activation, tumor cell proliferation, apoptosis, vascularization, and inflammatory response. These were investigated by immunofluorescence staining and relative quantification.

To identify alterations in collagens in the peritumoral tissues, hydroxyproline (content), cross-linkage (content and pattern), and fibrils structures (picrosirius red staining) were investigated. Collagen fiber structure and organization were analyzed by second harmonic generation (SHG) microscopy, and mechanical properties were studied by atomic force microscopy (AFM). Furthermore, the peritumoral matrix composition was investigated using proteome analysis as an unbiased approach.

The distinct effect of MMP14-modified ECM structure and composition on melanoma invasion was investigated using *ex vivo* invasion assays with decellularized and devitalized skin composites. In addition, by proteome-, western blot- and protein array analysis the MMP14-dependent fibroblast matrix and media composition alterations were investigated. Last, using primary fibroblasts from control and MMP14$^{Sf-/-}$ mice skin and murine melanoma cell lines, *in vitro* culture systems were used to investigate whether and how fibroblast matrix and conditioned medium, or identified altered matrices, affect on a cellular level melanoma cells proliferation, apoptosis, cell adhesion, and migration.

2 Material and Methods

2.1 Materials

2.1.1 Chemicals

All chemicals, unless otherwise indicated, were purchased in analytical grade from Merck (Darmstadt, Germany), Carl Roth (Karlsruhe, Germany), Merck (Darmstadt, Germany), Gibco (Karlsruhe, Germany), Serva (Heidelberg, Germany), TH Geyer GmbH (Lohmar, Germany), Biochrom (Berlin, Germany), and Riedel-de Haën (Seelze, Germany).

2.1.2 Cell culture material

Plastic equipment for cell culture was purchased from Greiner AG (Kremsmünster, Austria) and BD Biosciences (Heidelberg, Germany). Tissue culture plates with defined stiffness grade were from Ibidi (Gräfelfing, Germany). DMEM (Dulbecco's Modified Eagle Medium) cell culture medium was purchased from Gibco (Karlsruhe, Germany), antibiotics (penicillin/streptomycin), L-glutamine and EDTA (ethylenediaminetetraacetic acid) were from Biochrom Merck (Berlin, Germany). Trypsin was from Thermo Fisher (Darmstadt, Germany). FCS (fetal calf serum) was from PAA (Cölbe, Germany) and ascorbate from Sigma (Taufkirchen, Germany). Human recombinant fibronectin was from Roche GmbH (Mannheim, Germany), Matrigel (Growth Factor reduced MatrigelTM Matrix) was purchased from BD Bioscience (Heidelberg, Germany), acid extracted bovine collagen type I was from Curacyte Discovery GmbH (Leipzig, Germany). Collagen type XIV was provided by Prof. Manuel Koch (Institute for Dental Research and Oral Musculoskeletal Biology and Center for Biochemistry, University of Cologne, Germany). Dispase II and DNase I were purchased from Roche GmbH (Mannheim, Germany), collagenase type I from Worthington Biochemical Corporation (Lakewood, NJ, USA), mitomycin-c was from Sigma-Aldrich (Schnelldorf, Germany).

2.1.3 Consumable materials

1.5% agar Noble: BD Biosciences (Heidelberg, Germany)
10xPCR Buffer +Mg: Applied Biosystems (California, US)
Agarose: Bio-Budget (Krefeld, Germany)
Betaisodona: Mundipharma GmbH (Limburg, Germany)
Bleomycin: Medac GmbH (Wedel, Germany)

CAA (chloroacetamide): Merck (Darmstadt, Germany)
Chemiluminescence Reagent ECL: Thermo Scientific (Asbach, Germany)
cisplatin (cis-Diammineplatinum (II) dichloride): Merck (Darmstadt, Germany)
CL-XPosureTM Film: Thermo Fisher (Karlsruhe, Germany)
Cover glasses: TH-Geyer GmbH (Lohmar, Germany)
Cryomolds (standard, intermediate): Sakura (Zoeterwoude, Netherlands)
CXR Reference Dye (30µm): Promega GmbH (Mannheim, Germany)
dNTP Mix (10mM): Fermentas (Sankt Leon-Roth, Germany)
DTT (dithiothreitol): Thermo Scientific (Asbach, Germany)
Embedding cassettes: VWR (Pennsylvania, US)
Endopeptidase Lys-C: Thermo Fisher (Karlsruhe, Germany)
Eppendorf tubes (1.5 ml, 2 ml): Eppendorf (Hamburg, Germany)
Falcon tubes 15ml, 50ml: BD Bioscience (Heidelberg, Germany)
Filter 0,2µm: Pall Corporation (Dreieich, Germany)
GeneRulerTM 1kb DNA Ladder: Thermo Fisher (Karlsruhe, Germany)
Glas pipettes: TH Geyer GmbH (Lohmar, Germany)
GLC^{TM} Mounting Medium: Sakura (Zoeterwoude, Netherlands)
GoTaq® qPCR Master Mix (2X): Promega (Walldorf, Germany)
Immu-mount: Thermo Scientific (Asbach, Germany)
Microscope Polysine slides: Thermo Scientific (Asbach, Germany)
Nitrocellulose western blotting Membrane AmershamTM Protran® (Ø 0.45 µm; Ø 0.2 µm): Merck (Darmstadt, Germany)
Normal goat serum: Dako Agilent (Waldbronn, Germany)
NuPAGE® Antioxidant: Thermo Fisher (Karlsruhe, Germany)
NuPAGE® Bis-Tris Mini Gels (4-12%): Thermo Fisher (Karlsruhe, Germany)
NuPAGE® MES running buffer: Thermo Fisher (Karlsruhe, Germany)
Oligo d(T)16 50µm: Thermo Fisher (Karlsruhe, Germany)
PageRulerTM Plus Prestained Proteinladder: Thermo Fisher (Karlsruhe, Germany)
PageRulerTM Unstained: Thermo Fisher (Karlsruhe, Germany)
Paraffin (Paraplast Tissue Embedding Medium): McCormick Scientific (Maarn, Netherlands)
PBS Dulbecco w/o Ca^{2+} w/o Mg^{2+}: Biochrom GmbH (Berlin, Germany)
PCR tubes (0.5 ml): Peqlab Biotechnologie GmbH (Erlangen, Germany)
Pipette tips: Sarstaedt (Nümbrecht, Germany)

Ponceau Red Solution: Merck (Darmstadt, Germany)
Protein G SepharoseTM 4 Fast Flow: GE Healthcare Bio-Sciences AB (Uppsala, Sweden)
Proteinase K: Thermo Fisher (Karlsruhe, Germany)
Proteinladder: Thermo Fisher (Karlsruhe, Germany)
RedSafeTM: iNtRON Biotechnology (South Korea)
REDTaq® ReadyMix™: Merck (Darmstadt, Germany)
Reverse Transcriptase MuL V (50U/µl): Applied Biosystems (California, US)
RNase Inhibitor (20U/µl): Thermo Fisher (Karlsruhe, Germany)
RNAzol™ B: Wak-Chemie Medical GmbH (Steinbach, Germany)
Sirius Red F3B: Merck (Darmstadt, Germany)
Syringes and needls: BD Biosciences (Heidelberg, Germany)
Tamoxifen pellets: Harlan laboratories (Venray, Netherlands)
TEAB (Triethylammonium bicarbonate): Thermo Fisher (Karlsruhe, Germany)
Tween ®: Merck (Darmstadt, Germany)
Weigert's iron hematoxylin: Waldeck GmbH (Münster, Germany)
Whatman paper: VWR (Bruchsal, Germany)

2.1.4 Buffers and reagents

Running buffer (10X) pH 8.3: SDS (35mM), Trizma® base (250nM), Glycine (1.92M) (PAGE)
Anode buffer I pH 10.2: Trizma® base (300mM), 20% methanol
Anode buffer II pH 10.4: Trizma® base (25mM), 20% methanol
Cathode buffer pH 7.6: Amoinocaproic acid (40mM), 20% methanol
Coomassie Destain solution: 10% methanol, 10% acetic acid
Coomassie Stain 2.5%: Coomassie® briliant blue G250, 45% methanol, 10% acetic acid
crystal violet stain: 0.5% crystal violet, 20% methanol
DNA loading buffer (6X): 30% glycerol, 0.25% bromophenol blue, 0.25% Xylol Cyanole
DNA lysis buffer: 0.1 M Tris/HCl pH 8.5, 5mM EDTA, 0.2% SDS, 0.2M NaCl
Cell removal Buffer: 20mM NH_4OH, 0.5% TritonX-100 in PBS
Formaldehyde fixation solution: 4% Paraformaldehyde, PBS, HCl/NaOH pH 7.4
Laemmli buffer (5X): Trizma® HCl (60mM) pH 6.8, 25% glycerol, 2% SDS, 2-Mercaptothanol (14.4M), 0.1% Bromophenol blue

Extraction buffer: 8M Urea, 0.2% SDS, 0.5M TEAB, 5mM TCEP

RIPA buffer pH 7.4: Trizma® base (50mM), NaCl (150nM), 1% NP-40, 2% Deoxycholic Acid, 1%SDS

TBE buffer pH 8: Trizma® base (90mM), boric acid (90mM), EDTA (20mM)

TBS (10X) pH 7.6: Trizma® HCl (50mM), Trizma® base (20mM), NaCl (150mM)

TBST: TBS (1x), 0.5% Tween®20

TE-Buffer: Trizma® base (10mM) pH 7.2, 1mM EDTA

PBST: PBS + Tween® 20 0.5 % (v/v)

PBS: 136 mM NaCl; 2.6 mM KCl; 10nM Na_2HPO_4; 1.5 mM KH_2PO_4; pH 7.4

2.1.5 Kits

Table 1. Kits for cell- and protein analysis.

Kit	Cat No/Company
Cell Proliferation ELISA, BrdU (colorimetric) kit	11 647 229 001, Roche (Mannheim, Germany)
Cell Death Detection ELISA Plus Kit	11 774 425 001, Roche (Mannheim, Germany)
Proteome Profiler – Mouse XL Cytokine Array Kit	ARY028, R&D Systems (Wiesbaden, Germany)
PierceTM BCA Protein Assay Kit	23227, Thermo Fisher Scientific (Schwerte, Germany)

2.1.6 Antibodies

Table 2. Mouse antibodies used for immunofluorescence stainings.

Antigen	Antibody Cat. No	Source	Dilution
CD16/32	553141	BD Biosciences (Heidelberg, Germany)	1:200
CD31	557355	BD Biosciences (Heidelberg, Germany)	1:1000
CD45	MCA1388	Bio-Rad AbD Serotec GmbH (Puchheim, Germany)	1:250
CD68	MCA1957GA	Bio-Rad AbD Serotec GmbH (Puchheim, Germany)	1:60
cleaved caspase 3	9661-S	Cell Signaling (Frankfurt, Germany)	1:200
Collagen type XIV	clone KR47	Manuel Koch, Biochemie	1:5000
Keratin 6	PRB-169P	Covance (Münster, Germany)	1:1000
Ki67	M7249	Dako Agilent (Waldbronn, Germany)	1:100

Ly6G	127625	Biolegend (Amsterdam, Netherlands)	1:200
LYVE-1	ab14917	Abcam (Berlin, Germany)	1:1000
PDGFRα	AF1062	R&D Systems (Wiesbaden, Germany)	1:100
TRP-2	sc-10451	Santa Cruz Biotechnology (Heidelberg, Germany)	1:100
αSMA Cy3	C6198	Merck (Darmstadt, Germany)	1:200
goat 488nm	A11055	Thermo Fisher Scientific (Schwerte, Germany)	1:1000
rabbit 488	A11034	Thermo Fisher Scientific (Schwerte, Germany)	1:1000
rabbit 594nm	A11037	Thermo Fisher Scientific (Schwerte, Germany)	1:1000
rat 488	A11006	Thermo Fisher Scientific (Schwerte, Germany)	1:1000
rat 594	A11007	Thermo Fisher Scientific (Schwerte, Germany)	1:1000

Table 3. Mouse antibodies used for immunoblot analysis.

Antigen	**Antibody Cat. No**	**Source**	**Dilution**
Actin	#2928H	MPBiomedicals (Eschwege, Germany)	1:2000
Collagen type I	2031503505	Quartett (Berlin, Germany)	1:500
Collagen type VI	-	Raimund Wagener, Biochemie	1:500
Collagen type XII	clone KR33 (KV137)	Manuel Koch, Biochemie	1:2000
Collagen type XIV	clone KR47	Manuel Koch, Biochemie	1:2000
PCNA	#133900	Thermo Fisher Scientific (Schwerte, Germany)	1:1000
mouse HRP	P0260	Dako Agilent (Waldbronn, Germany)	1:2000
rabbit HRP	P0217	Dako Agilent (Waldbronn, Germany)	1:2000

2.1.7 Laboratory equipment

Bio Photometer: Eppendorf (Hamburg, Germany)

Cell culture incubator HERA cell 150i CO2: Thermo Fisher Scientific (Karlsruhe, Germany)

Cryostat Microm HM 560: Thermo Scientific (Asbach, Germany)

Eppendorf Centrifuge 5415 R or C: Eppendorf (Hamburg, Germany)

Fluorescence Microscope Keyence BZ-9000: Keyence (Osaka, Japan)

GelDoc power supply Easy-Cast Electrophoresis System Model 2B, Owl Scientific Model 40-0911: Thermo Scientific (Asbach, Germany)

Heraeus® Megafuge® 1.0 R: Heraeus GmbH (Hanau, Germany)

JPK NanoWizard4 atomic force microscope: Bruker Nano GmbH (Karlsruhe, Germany)

KY-F75U camera: JVC (Wayne, USA)

Megafuge ST Plus Series Centrifuge: Thermo Scientific (Asbach, Germany)

Microscope Leica DM 4000 B: Leica (Wetzlar, Germany)

Microtome Epredia™ Shandon™ Finesse™ 325: Thermo Scientific (Asbach, Germany)

Migration microscope Olympus XM10 camera: Olympus (Tokyo, Japan)

Mixer Mill MM3000: Retsch (Haan, Germany)

Nanodrop 2000 Spectrometer: Thermo Scientific (Asbach, Germany)

Neubauer-counting chamber: BRAND GmbH (Wertheim, Germany)

Nikon Eclipse TS100: Nikon (Tokyo, Japan)

Nikon Eclipse TS2: Nikon (Tokyo, Japan)

PCR Thermocycler T3000: Biometra (Göttingen, Germany)

pH-meter InoCG710: Schott (Mainz, Germany)

Photometer Eppendorf Bio: Eppendorf (Hamburg, Germany)

Pipette boy accu-jet® pro: BRAND GmbH (Wertheim, Germany)

Pipettes 10µl: Eppendorf (Hamburg, Germany)

Pipettes, 20, 200, 1000µl: GILSON (Hessen, Germany)

Precision caliper: Mitutoyo (Neuss, Germany)

Real-time PCR Step One Plus Real-time PCR System, with the StepOneTM Software v2.1: Thermo Fisher (Karlsruhe, Germany)

Rotator Stuart SB2: VWR (Bruchsal, Germany)

Semi-dry transfer system: Merck (Darmstadt, Germany)

Shaker IKA HS250 basic: IKA Werke GmbH (Breisgau, Germany)

upright multiphoton microscope (TCS SP8 MP-OPO): Leica (Wetzlar, Germany)

Victor3TM Multilabel plate reader: Perkin Elmer (Wellesley, MA, USA)

Vortex-Genie 2^{TM}: Bender & Hobein GmbH (Hanfröste, Germany)

Waterbath Julabo-SW20: Julabo (Seelbach, Germany)

Western blot Curix 60 developing machine: AGFA (Mortsel, Belgium)

Western blot Dual Gel Caster Chamber SE245: Hoefer Inc. (Massachusetts, USA)

Western blot vertical electrophorese system mighty small SE250/SE260: Hoefer Inc. (Massachusetts, USA)

X-ray detection cassettes (Cronex Quanta III): Heinrich Faust GmbH (Cologne, Germany)

2.2 Methods

2.2.1 Cell Culture

B16F0 [264], B16F1 (CRL-6323, ATCC®, Wesel, Germany), HCmel12 [265] and BDVII [266] cells and primary isolated fibroblasts were grown DMEM medium (+4.5 g/l D-Glucose, L-Glutamine) supplemented with 10% FCS, 2 mM L-glutamine, 100 U/ml penicillin and 100 µg/ml streptomycin, and 0.05 g/l L-ascorbic acid was added to the fibroblast's media. Cells were grown at 37°C, 5% CO_2 and passaged every 2-3 days after washing with Dulbecco´s PBS (1x) and treated with 0.02% Trypsin/ 0.1% EDTA. Cells were counted using a Neubauer chamber. For coating tissue culture plates, recombinant collagen type I or collagen type XIV were diluted in PBS, and fibronectin in PBS containing 0.1 M $CaCl_2$, and incubated o/n at 4°C. Afterwards, plates were rinsed with PBS and free uncoated surfaces blocked with 1% heat-inactivated BSA for 1h at RT. For analysis of melanoma apoptosis in fibroblast c.m. 100ng/ml recombinant GROα (ab202817, Abcam) was added to $MMP14^{Sf+/+}$ c.m., and either 13µM MMP3 inhibitor (MMP3i) (444225, Merck) or 1µg/ml of a neutralizing antibody against GROα (α-GROα) (MAB453-100, R&D Systems) was added to $MMP14^{Sf-/-}$ c.m.

2.2.1.1 Isolation of primary fibroblasts

After adult mice were sacrificed, their back skin shaved and dissected with a scalpel. Following washes in PBS and disinfection in betaisodona for 2 min, in 70% EtOH for 1 min and twice in PBS for 1 min, the skin was placed (dermis downside) in a P5 petri dish on top of 5 ml dispase II (5 mg/ml in serum free DMEM) and incubated overnight (o/n) at 4°C. Afterwards, the skin was washed with serum-free DMEM and the epidermis was removed from the dermis. After shredding the dermis into small pieces, it was transferred into a falcon containing sterile 400 U/ml collagenase type I in serum-free DMEM and stirred for 90 min at 37°C. The solution was centrifuged at 315 x g for 5 min at RT and supernatant was removed. The pellet was resuspended in 10 ml complete DMEM containing 20% FCS and AA (antibiotic and antifungal), and seeded into a P10 petri dish.

2.2.1.2 Preparation of fibroblast deposited matrix and conditioned medium

Primary fibroblasts were cultured in complete DMEM with ascorbate for 14 days, the medium was changed every 2-3 days. Fibroblasts were removed from matrix by adding 20mM NH4OH and 0.5% TritonX-100 for 1 min at RT and washed gently with PBS. The matrix was visualized by staining with 0.25 % Coomassie Brilliant blue for 10 min at RT, washed with PBS and photos recorded using a light microscope equipped with DISKUS 4.50.1638 software.

To prepare fibroblasts supernatants, cells were washed twice with PBS and incubated with serum-free DMEM for 24 h. The medium was collected and spun down for 5 min at 315 x g to remove cellular debris. Supernatants (= conditioned medium; c.m.) were used immediately for B16F1 treatment experiments or stored at -20°C for further use.

2.2.1.3 Melanoma spheroids

Spheroids were produced using the liquid overlay method as previously described [267]. Shortly, 5000 B16F1 cells were seeded in a 96-well plate coated with 1.5% agar Noble and incubated for 72h at 37°C and 5% CO_2, in which cells organized into a three-dimensional structure. Spheroids were harvested using a pipette and placed into an Eppendorf tube. The medium was removed, and spheroids were transferred into a solution of bovine collagen type I containing 1M NaOH, 175mM $NaHCO_3$, 3% FCS, 2mM L-glutamine, 100U/ml penicillin, and 100µg/ml streptomycin. After incubation at 37°C for 1h, polymerized collagen gels were covered with complete DMEM.

2.2.1.4 Colony outgrowth assay

B16F1 cells were washed twice with PBS and treated with 0.1% FCS DMEM with 1.6 µg/ml mitomycin-C in 0.1% FCS DMEM for 2 h at 37°C to inhibit cell growth. A metal ring (diameter: 0.5 cm^2) was placed on the fibroblast matrix or recombinant protein coating. B16F1 cells were washed with PBS, trypsinized and counted. 200.000 cells were seeded in the metal rings and let adhere for 3 h. After removal of the ring, suspended cells were removed by washing with PBS and serum-free DMEM was added. Two positions per well were chosen to monitor cell migration and pictures were taken every 30 min. Pictures were analysed using ImageJ software (http://rsb.info.nih.gov/ij; version ImageJ 1.53a), by measuring the surface covered by cells at selected time points. Migrated surface was calculated by subtracting the cell-

covered surface at the beginning (time point 0) from cell-covered surface at selected time points (covered surface at x h – covered surface at 0 h = migrated surface).

2.2.1.5 Proliferation assay

B16F1 cells were starved in serum-free DMEM for 24 h before treating them with fibroblast conditioned medium (2.2.1.3) or seeding them in tissue culture plates coated with recombinant collagen type I, type XIV, or fibroblast-deposited matrix. B16F1 cells were seeded in a density of 40.000 cells/cm^2 into the wells of a 96-well plate and let adhere o/n at 37 °C and 5 % CO_2. Cell proliferation was analysed using the Cell Proliferation ELISA ® Kit according to the manufacturer's instructions. Briefly, B16F1 cells were labelled with BrdU labelling reagent (10µM final concentration per well) for 4 h at 37 °C and then lysed with 200 µl "FixDenat" for 30 min at RT. After removing the solution thoroughly, 100 µl of the anti-BrdU-peroxidase conjugated antibody was added for 1.5 h at RT. After washing, 100 µl substrate solution was added and incubated for approximately 25 min at RT until color development was sufficient for photometric detection. The color development was blocked by addition of 25 µl 1 M H_2SO_4 and measured at 450 nm using Victor^{3TM} 1420 Multilabel Counter.

2.2.1.6 Cell death assay

B16F1 cells were seeded in a density of 40.000 cells/cm^2 into the wells of a 96-well plate and incubated O/N at 37 °C and 5 % CO_2. Cells were either seeded directly on coated wells or treated with fibroblast c.m. after adhesion. B16F1 cells irradiated with 0.1 J/cm^2 UV-B were used as positive control. Cell death was analysed with Cell Death Detection ELISA Plus Kit according to the manufacturer's instructions. Briefly, B16F1 cells were lysed with 200 µl lysis buffer for 30 min at RT and then labelled with an immunoreagent containing an anti-histone-biotin and an anti-DNA-peroxidase conjugated antibody for 2 h at RT while shaking at 300 rpm. "ABTS substrate solution" was added to the wells and incubated for approximately 20 min at RT until color development was sufficient for photometric detection. The process was stopped by addition of "ABTS stop solution" and color development was measured at 405 nm (reference wavelength 490 nm) using Victor^{3TM} 1420 Multilabel Counter.

2.2.1.7 Adhesion assay

B16F1 adhesion assays were performed as previously described [268]. Briefly, cells were seeded (60.000 cells/ cm^2) in protein coated 96-well plates and incubated 2 h at 37°C, 5% CO_2. Afterwards, wells were rinsed with PBS to removed not adhered cells and remaining cells were fixed with 4% paraformaldehyde (PFA) for 10 min at RT. After washing, the fixed cells were stained with crystal violet (0.5% Crystal Violet in 20% MetOH) for 15 min at RT. Crystal violet stain was removed and after washing with PBS the retained stain was eluted from the cells by addition of 0.1M sodium citrate and measured at 595nm using Victor^{3TM} 1420 Multilabel Counter.

2.2.1.8 *Ex vivo* invasion assays

Mouse back skin punch biopsies (8 mm) were incubated in 5mg/ml dispase II in serum-free DMEM o/n at 4 °C to remove the epidermis and basement membrane. Afterwards, skins were washed in PBS and epidermis was removed. To devitalize deepidermized skin biopsies, they were frozen at -80 °C for 30 min and thawed in the water bath at 37 °C in three cycles. For decellularization of skin biopsies we used a published procedure [269]. Skin biopsies were incubated in 0.1 % Triton X-100 for 1 h for cell lysis, then they were incubated in 2 % sodium deoxycholate for 24 h, to solubilize cellular and membrane components. Afterwards biopsies were washed in 1M NaCl for 1h and incubated in 1.3 mM $MgSO_4$, 2 mM $CaCl_2$, 30 µg/ml DNase I for 1 h to remove nuclear parts of the dermal cells. All incubation steps of the decellularization process were performed at 4°C, with stirring and with addition of 100 U/ml penicillin and 100 µg/ml streptomycin. The devitalized and decellularized skin biopsies were placed on a metal net in a 6-well plate, and 1 x 10^5 B16F1 cells were seeded on the dermis (Figure 7). The specimens were incubated at the air-liquid surface for 3 weeks at 37 °C and 5 % CO_2 and medium was renewed every 2-3 days. For further analysis, one half on each skin biopsy was embedded in Tissue-Tek ® and frozen on dry ice, and the other half was fixed in 4 % PFA for 1h at 4 °C and embedded in paraffin. Sections were stained with hematoxylin and eosin (H&E) and distance invaded or tumor load of B16F1 cells into the skin composites were quantified.

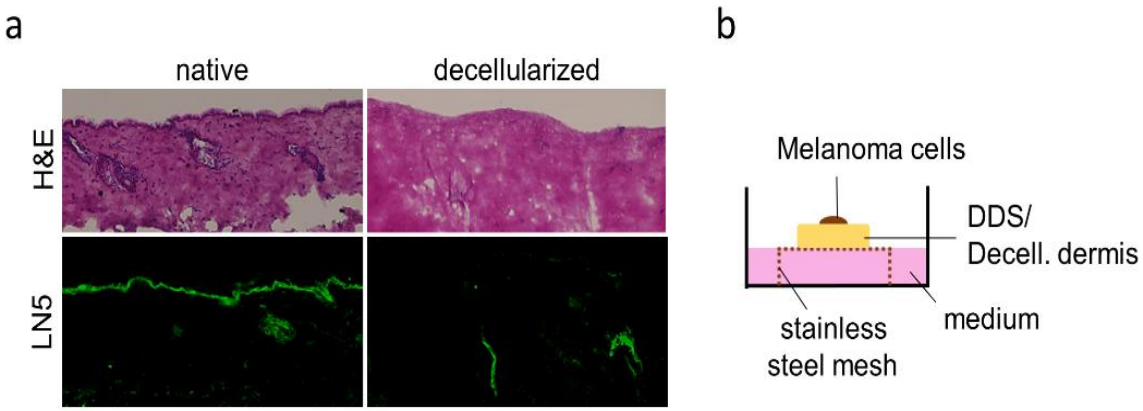

Figure 7. Skin biopsies and *ex vivo* invasion assay.
(a) H&E staining of native and decellularized skin sections. Immunofluoresence staining for laminin 332 (LN5). (b) Assembly of a skin composite on the metal net within a tissue culture well filled with medium. Melanoma cells were seeded on top of the skin composite. H&E, hematoxylin & eosin; LN5, laminin 332; DDS, de-epidermized devitalized skin; Decell. dermis, decellularized dermis.

2.2.2 Protein Analysis

2.2.2.1 SDS PAGE and Western Blot

Cell lysates were prepared using the RIPA extraction buffer supplemented with protease inhibitor. Fibroblast matrix was solubilized in 8 M Urea supplemented with protease inhibitor after cells were removed using 20 mM NH_4OH and 0.5 % TritonX-100 for 1 min at RT followed by washes in PBS. All collected lysates were homogenized using Mixer Mill at 30 Hz for 2 min. Protein concentration was determined by Pierce® BCA protein assay, according to the manufacturer's instructions, or, for matrix lysates, by measuring the optical density using the Nanodrop 2000 Spectrometer. Equal amounts of protein (10-20 µg) were separated under reducing conditions by SDS-PAGE using an 8 % (for matrix lysates and supernatants) or 10 % (for cell lysates) polyacrylamide gel. Separated proteins were transferred to a nitrocellulose membrane by semi-dry blotting system. Transfer efficiency was confirmed by Ponceau S staining. The membrane was blocked in PBST containing 5 % milk powder for 1 h at RT and incubated with the primary antibody O/N at 4°C. After washing three times for 5 min at RT in PBST, the membrane was incubated for 1 h at RT with the HRP-conjugated secondary antibody. After extensive washing with PBST, membrane was incubated in Chemiluminescence Reagent ECL for 1 min at RT and bound antibodies were visualized in a x-ray detection cassette. Detected protein were normalized to the corresponding Ponceau S staining.

2.2.2.2 Proteome analysis

Peritumoral tissue was macrodissected from cryosections (400 µm), lysed in a tube containing 0.1% Triton X-100 with protease inhibitors and homogenized using Mixer Mill MM3000 at 30 Hz for 2 min. Further decellularization of the tissue was performed as for skin biopsies (2.2.1.9) [269]. After a final centrifugation step, ECM proteins were extracted from the pellet with 8M Urea, 0.2% SDS, 0.5M TEAB, 5mM TCEP, or from fibroblast matrix after removal of fibroblasts (2.2.1.2.). Afterward, samples were precipitated with acetone and resuspended in 8M urea. Samples were reduced with 5 mM DTT (dithiothreitol) for 1 h at 37 °C and alkylated with 40 mM CAA (chloroacetamide) at RT in the dark for 30 min. 1 µg endopeptidase Lys-C was added and incubated at 37 °C for 4 h. Samples were diluted with 50 mM TEAB until the urea concentration reached 2 M. Trypsin was added in an enzyme-protein ratio of 1:75 (w/w) and incubated o/n at 37 °C. Salts and impurities were removed by stage tip purification and samples were analyzed by HPLC mass spectrometry. This analysis was performed with the support of the Proteomics Facility of the CECAD at the University of Cologne.

2.2.2.3 Mouse XL Cytokine Array Kit

Fibroblast conditioned medium was prepared and collected as previously described (2.2.1.3). For analysis of a number of 111 secreted soluble factors the Proteome Profiler™ - Mouse XL Cytokine Array Kit was used according to the manufacturer's instructions. Shortly, the nitrocellulose membrane with bound antibodies against selected cytokines was blocked in "Array Buffer 6" for 1 h at RT while shaking. Fibroblast conditioned media were mixed to half volume of "Array Buffer 4" and incubated with the nitrocellulose membrane o/n at 4 °C on a shaker. Afterwards, the nitrocellulose membrane was washed 3 x 10 min in 1 x wash buffer to remove unbound soluble factors and incubated with a cocktail of biotinylated detection antibodies for 1 h at RT while shaking. After removing unbound antibodies by washing 3 x 10 min in 1 x wash buffer, the membrane was incubated in 1 x Streptavidin - HRP on a shaker for 30 min at RT and washed again. Membrane was placed in an x-ray detection cassette and incubated with the chemiluminescent detection reagent for 1 min. The signal corresponding to protein amount bound to each capture spot on the membrane was visualized in an x-ray detection cassette using enhanced chemiluminescence and quantified by densitometric measurement using ImageJ software

(http://rsb.info.nih.gov/ij; version ImageJ 1.53a). Reference dots for positive and negative (background) controls are on the membrane.

2.2.3 Analysis of nucleid acids

2.2.3.1 DNA isolation and genotyping

Mouse tail tips were lysed in 300 µl DNA lysis buffer + 1 µl Proteinase K at 56 °C while shaking on 300 rpm o/n. Lysates were centrifuged at 16.000 x g for 10 min at RT to remove hairs and undigested tissue. The supernatant was transferred into a new tube, DNA was precipitated by addition of 300 µl 100 % EtOH and centrifuged at 16.000 x g for 10 min at RT. DNA pellet was washed with 70 % EtOH twice, let dry with open lid for 10 min at RT and solved in TE-buffer. Genotyping of mice was perfomed in a total volume of 25 µl including 1 µl genomic DNA, 12.5 µl RedTaq, 0.5 µl forward primer, 0.5 µl reverse primer and 10.5 µl H_20. Primers used for genotyping are listed in table 4.

Table 4. Primers used for mouse genotyping.

Primer	**Sequence (5' - 3'; f, forward; r, reverse)**	**Tm (°C)**	**No. of cycles**	**Product size (bp)**
1314_30	f GAG GCA GAG GCA GAA CAA GC	60	35	MMP14fl/wt: 165 MMP14fl/fl: 285,
1314_31	r GAG CAT CAG AAA GTT GAG AGG			
SC 1(+)	f GTC CAA TTT ACT GAC CGT ACA C	50	35	cre-recombinase: 350
SC 3(-)	r CTG TCA CTT GGT CGT GGC AGC			
1314_30	f GAG GCA GAG GCA GAA CAA GC	60	35	deletion: 400
rev1	r CCA CCA AGA AGA TGT CAT TCC			

2.2.3.2 RNA isolation

Sub confluent (70-80 %) primary fibroblasts were washed with PBS and lysed with RNAzol^{TM} B for 5 min on ice. Afterwards, lysates were collected by scraping and transferred into a tube. RNA was extracted by addition of 1/5 volume of chloroform, inverting for 15 sec and incubation on ice for 3 min. Samples were centrifuged at 16.000 x g for 15 min at 4°C. The upper, colorless phase was transferred into a new tube and RNA was precipitated by addition of 1 volume isopropanol o/n at -80 °C. After centrifugation at 16.000 x g for 10 min at 4°C, the RNA pellet was washed twice with 70 % EtOH, dried on ice and solved in 30µl RNase-free H_2O. The quality of RNA was analysed by electrophoresis on a 1% agarose-TBE gel and concentration was determined by optical density measurement at 260 nm and 280 nm via NanoDrop 2000 Spectrometer.

2.2.3.3 Reverse transcription - polymerase chain reaction (RT-PCR)

1 µg RNA was reverse transcribed into cDNA using dNTPs (10 mM), oligo dT 16 primers (50 µM), RNase inhibitor 20 U/µl, reverse transcriptase 50 U/µl and 10 X PCR buffer I containing 15 mM $MgCl_2$. Reverse transcription was performed using the following conditions: 21 °C 10 min; 42 °C 30 min; 99 °C 5 min. The house keeping gene, S26, used as control, was amplified using 1 µl cDNA, 12.5 µl REDTaq® ReadyMix™ with $MgCl_2$, and 10 mM forward (5' – 3': AATGTGCAGCCCATTCGCTG) and reverse (5' – 3': CTTCCGTCCTTACAAAACGG) primers. PCR reaction was performed using the following conditions: 94 °C 1 min (denaturation), 56 °C 1 min (annealing), 72 °C 1 min (elongation), 72 °C 10 min (final extension) for 30 cycles of amplification. The PCR product was mixed with DNA loading buffer and separated on 1.8 % TBE agarose gel via electrophoresis.

2.2.3.4 Quantitative real-time PCR

For quantitative real-time PCR 1 µl cDNA was amplified with GoTaq® qPCR Master Mix (2 X), forward and reverse primers (10 mM) and CxR Reference Dye in triplicates and 20 µl total volume each. The amplification reaction and quantitative measurement was performed using the StepOnePlus Real-Time PCR system with the StepOne™ Software v2.1 from Applied Biosystems. The specificity of the PCR products was confirmed with melting curve analysis. The expression levels were normalized to the house keeping gene, S26, and quantified by calculating the fold induction by the comparative ΔΔCt method [270]. Primers used for analysis are listed in table 5.

Table 5. Primers used for quantitative real-time PCR.

Gene	**Sequence (5' - 3'; f, forward; r, reverse)**	**Tm (°C)**	**No. of cycles**
COL6A1	f GATGAGGGTGAAGTGGGAGA r CAGCACGAAGAGGATGTAGTCAA	60	40
COL12A1	f AGACATTGTGTTGCTGGTGGA r GAGAAATGAAGCTTCGCACAGT	60	40
COL14A1	f TGGTGGAGAGCCTGACCCGG r GCATCCCACCTGACGCGCAT	60	40

2.2.4 *In vivo* experiments

2.2.4.1 Animal housing

Mice were kept in the animal facility of the Institute for Pharmacology of the University of Cologne in cages covered with air filters and continuous ventilation system under pathogen-free conditions with 12 h light-dark cycle and access to food and water ad libitum. All animal experiments were performed in compliance with German Regulations for Welfare of Laboratory Animals and were approved by the Regierungspräsidium Köln, Germany (NRW authorization 50.203.2-K 37a; 84-02.04.2016.A012; 84-02.04.2016.A013; 84-02.05.40.17.073).

2.2.4.2 Tumor grafting and skin treatment

Mice with the inducible fibroblast-specific deletion of MMP14 were generated by crossing mice with the floxed MMP14 gene (exons 2 - 4) to mice expressing a fusion protein with the catalytic subunit of the cre recombinase fused to the estrogen receptor domain under control of a fibroblast-specific regulatory fragment of the pro - α2 (I) collagen gene [227, 271]. To induce the fibroblast-specific deletion of MMP14, the offspring of these mice, at 4 weeks of age, was fed with tamoxifen (400 mg/ml pellets) for five weeks and the phenotype was allowed to develop for further five weeks. To induce skin fibrosis control mice were treated with intradermal injections of 100µg bleomycin, or NaCl for control mice, five days a week over a period of four weeks. Afterwards, 0.5 x 10^6 B16F1 cells were injected intradermally into the flank of mice and tumor growth was followed and documented over time.

For chemotherapeutic treatment, mice received a single intraperitoneal injection with cisplatin (10 mg/kg), or NaCl as control, at day 5 after B16F1 cell injection. Tumor sizes (height, width and length) were measured using a precision caliper. When tumors reached a maximal allowed size, mice were sacrificed by cervical dislocation, and tumors and selected organs were collected and stored appropriately for further analysis.

2.2.5 Tissue Analysis

2.2.5.1 Hematoxylin and Eosin (H&E) staining

Paraffin sections of B16F1 tumors (2.2.4.2) and *ex vivo* invasion assays (2.2.1.9) were deparaffinized in xylol for 20 min, followed by a graded alcohol series for 1 min each, isopropanol, 96 % EtOH, 75 % EtOH, aqua bidest. Afterwards, deparaffinized sections

were stained for 5 min in hematoxylin solution and rinsed three times with lukewarm H_2O. After staining for 5 sec in eosin sections were rinsed with H_2O. Sections were dehydrated by ascending alcohol series and mounted in GLC™ Mounting Medium.

2.2.5.2 Immunofluorescence staining

Cryosections were fixed with 1 % PFA for 8 min at RT and washed with PBS. Then permeabilized with ice-cold acetone (-20 °C) for 5min, dried, and blocked with 10 % NGS in PBS at RT for 30min. Primary antibody diluted in 1% BSA in PBS was added to the sections and incubated in a humidified chamber o/n at 4°C. After washing three times with PBS, sections were incubated in secondary antibody in 1% BSA in PBS in a humidified chamber for 1h at RT. After washing three times with PBS, sections were mounted with Immumount and stored at 4°C. For quantifications of fluorescence intensities and number of positive cells, we used ImageJ software. The numbers of Ki67 and cleaved (cl.) caspase 3 positive cells were quantified in the central section of different tumor specimens or within invaded tumor nests (invasion assays) as percentage of the total numbers of nuclei stained by DAPI. For quantification of the intensity of expression of CD31, LYVE-1, CD45, Collagen type XIV, αSMA, PDGFRα the percentage of signal area within the peritumoral tissue (100 µm radius from tumor) relative to tissue area was determined.

2.2.5.3 Picrosirius red staining

Sections were deparaffinized, stained in Weigert's iron hematoxylin for 5min, and rinsed several times with fresh and lukewarm water. Sections were differentiated in 1 % HCl in 70% ethanol until the cytoplasm was destained and rinsed several times in warm water. Sections were stained in 0.5% PicroSirius red staining solution (Sirius Red F3B in saturated picric acid) for 1h and rinsed twice with 0.5 % acetic acid. Then sections were dehydrated three times with isopropanol, dipped twice in xylol, and embedded in a xylol- based GLC mounting medium.

2.2.5.4 Atomic Force Microscopy (AFM)

For this analysis freshly cut 20µm cryosections using a JPK NanoWizard4 atomic force microscope mounted on a Zeiss Axio observer Z1 widefield fluorescence microscope and operated via JPK SPMControl Software v.6. Cryosections were equilibrated in PBS supplemented with protease inhibitors, and measurements were performed within

20 min after sectioning the samples. For micromechanical measurements, spherical silicon dioxide beads with a diameter of 3.5 µm glued onto tip-less silicon nitride cantilevers (CP-PNPLSiO-B-5, NanoAndMore GmbH, Wetzlar, Germany) with a nominal spring constant of 0.08 Nm−1 were used. Measurements were performed using the Quantitative Imaging (QI) Mode with a pixel time of 500 ms (approach and retraction), ensuring detection of elastic properties only. Forces of up to 2 nN were applied. The AFM measurements and following quantification were performed by Matthias Rübsam (CECAD) at the University of Cologne. For each biological replicate, we analyzed 50-200 force curves of various dermal and peritumoral locations. All analyses were performed with JPK Data Processing Software (Bruker Nano GmbH, Herzogenrath, Germany). Prior to fitting the Hertz model corrected by the tip geometry to obtain Young's Modulus (Poisson's ratio of 0.5), the offset was removed from the baseline, contact point was identified, and cantilever bending was subtracted from all force curves.

2.2.5.5 Second Harmonic Generation (SHG)

Deparaffinized tissue sections of 6 µm thickness were analysed using an upright multiphoton microscope (TCS SP8 MP-OPO, Leica), equipped with a Ti:Sa laser (Chame-leon Vision II; Coherent) tuned to 1050 nm. For acquisition of the pictures LAS X software (Leica Microsystems) was used. Collagen fiber alignment and waviness were quantified using ImageJ software as previously described [272, 273]. SHG analysis was performed in the Imaging facility of the CECAD at the University of Cologne.

2.2.6 Statistics

Statistical analysis was performed using GraphPad Prism version 7.05 for Windows (GraphPad Software, La Jolla, CA, USA, www.praphpad.com). Student's t-test was used for data analysis, with $p<0.05$ considered to be statistically significant. Kolmogorov-Smirnov test was used for AFM analysis.

3 Results

3.1 Role of stromal MMP14 in melanoma growth

3.1.1 B16F1 tumor growth is reduced in MMP14$^{Sf-/-}$ skin

Altered expression of MMPs, including that of MMP14, was demonstrated in several types of cancer, including melanoma [235, 240, 274, 275]. Besides in cancer cells, MMP14 is expressed by stromal cells, mainly by fibroblasts that are considered the most effective regulators of dermal matrix remodeling [276]. Mice lacking MMP14 specifically in fibroblast display thickened skin, enhanced collagen accumulation, and increased tissue stiffness, all ascribed to impaired collagen degradation [233]. A comparable altered environment is found around tumors, contributing to tumor progression [126, 129]. However, the role of these alterations during melanoma development and progression has been controversial [277-279]. Using the MMP14-fibroblast deficiency model, we aimed to address the role of collagen and stiffness increase in melanoma growth.

To this end, B16F1 melanoma cells were injected intradermally into the flank of MMP14$^{Sf-/-}$ and control mice, and tumor growth was followed over time. Melanoma growth was reduced in MMP14$^{Sf-/-}$ compared to control mice as detected by measuring tumor size and analyzing tumor cross-sections until the last experimental day (at this time, tumor size in control reached the maximal ethical accepted size for these experiments). Tumor sections showed a more prominent matrix accumulation around the melanomas developed in MMP14$^{Sf-/-}$ compared to control mice as detected by H&E and by Sirius red staining observed with polarized light (Figure 8a). The latter showed increased accumulation of fibrillar collagen in MMP14$^{Sf-/-}$ compared to control mice, as shown earlier in the skin (Figure 8a) [280]. Six days after cell injection, tumor size displayed measurable differences with an average tumor size of 29.83 mm^3 in MMP14$^{Sf-/-}$ mice and 63.95 mm^3 in controls (Figure 8b). With exception of the final day, at each documented time-point throughout the experiment, tumor growth in MMP14$^{Sf-/-}$ mice was reduced, although not significantly, compared to control. On day 13, the difference in tumor size was significant, with an average number of 362.60 mm^3 in MMP14$^{Sf-/-}$ and 925.10 mm^3 in control littermates (Figure 8b). Despite the different tumor sizes, the number of metastasis in lung, liver, and lymph nodes of MMP14$^{Sf-/-}$ versus controls were not altered (Figure 8c). Moreover, the ratio of proliferating cells within the tumor, counted after immunofluorescence staining with the proliferation marker Ki67, was decreased in MMP14$^{Sf-/-}$ compared to control littermates (Figure 8d).

This indicates that the reduced melanoma growth might result from diminished cellular proliferation.

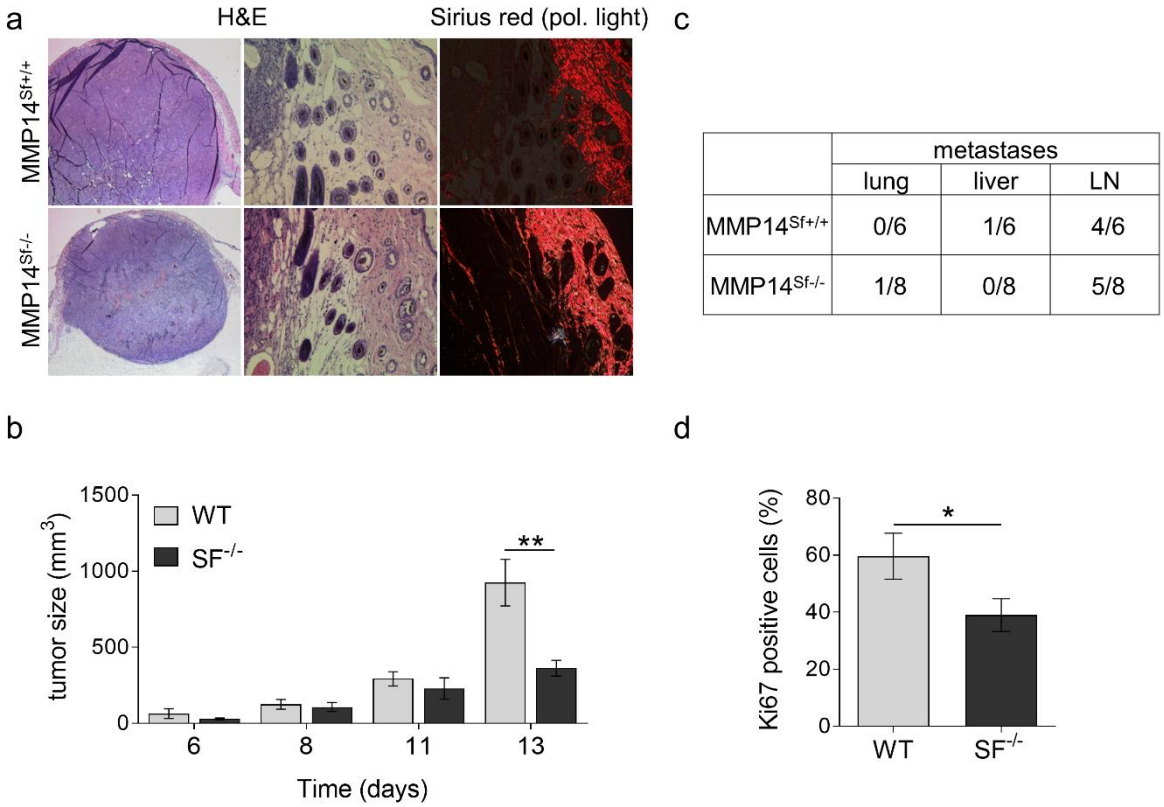

	metastases		
	lung	liver	LN
MMP14$^{Sf+/+}$	0/6	1/6	4/6
MMP14$^{Sf-/-}$	1/8	0/8	5/8

Figure 8. B16F1 melanoma growth in MMP14$^{Sf-/-}$ and control mice.
(a) H&E and Picrosirius red staining of sections from B16F1 tumors. (b) Time-course of B16F1 growth. (c) The ratio of organs with metastasis was determined by PCR amplification of GFP expressed by melanoma cells (lower). (d) Percentage of Ki67 positive melanoma cells within the tumor. Mean +/- SEM; MMP14$^{Sf+/+}$ (WT; control) n=6; MMP14$^{Sf-/-}$ (SF$^{-/-}$) n=8; *p<0.05; **p<0.01.

3.1.1.1 Reduced vascularization in MMP14$^{Sf-/-}$ peritumoral tissue

During tumor growth, angiogenesis and lymph angiogenesis are critical processes that supply nutrients, oxygen, and inflammatory cells to the growing tumor [281]. To investigate if in the absence of stromal MMP14 vascularization is altered, thus leading to reduced melanoma growth in MMP14$^{Sf-/-}$ mice, we performed immunofluorescence staining and quantification of blood and lymphatic vessels in B16F1 tumors of control and MMP14$^{Sf-/-}$ mice. Analysis of the endothelial cell marker, PECAM/CD31, showed a significant reduction in the percentage of blood vessels in the tumor of MMP14$^{Sf-/-}$ mice compared to controls (Figure 9a). In addition, hypoxia, analyzed by carbonic anhydrase IX (CAIX) detection, was lower in tumors from MMP14$^{Sf-/-}$ mice compared to controls (Figure 9b). No differences in the amounts of alpha SMA-positive cells were detected around the vessels and the tumors (Figure 9a). On the contrary, lymph

vessels, analyzed using LYVE-1, were comparable in both mouse genotypes (Figure 9a). When analyzing tumors of a similar size, regardless of of the genotype and time-point, vascularization was not changed in both genotypes.

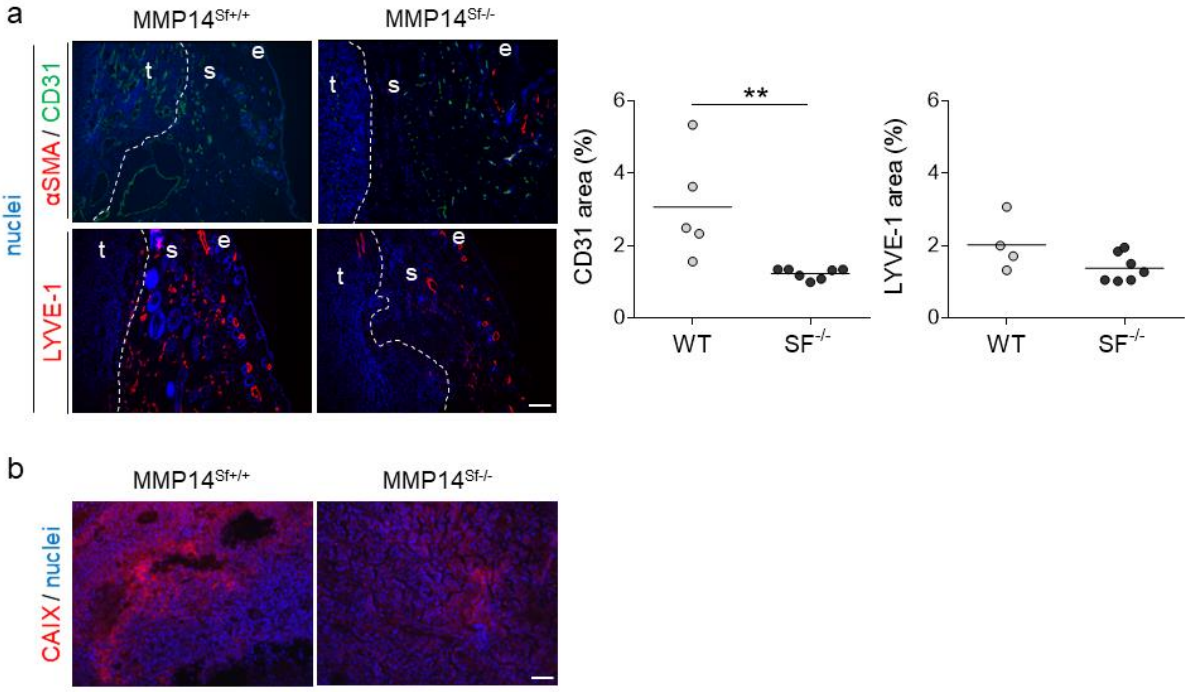

Figure 9. Analysis of vascularization and hypoxia in B16F1 melanoma of MMP14$^{Sf-/-}$ and control mice.
(a) Immunofluorescence staining for CD31 (green) and LYVE-1 (red), and (b) carbonic anhydrase 9 (CAIX) (red) in tumor-sections. The graphs are depicting the average positive cells as percentages. Mean +/- SEM; MMP14$^{Sf+/+}$ (WT; control) n= 4-5; MMP14$^{Sf-/-}$ (SF$^{-/-}$) n= 7; t= tumor; s= stroma; e= epidermis; **p<0.01; scale: 100µm.

3.1.1.2 Decreased amounts of inflammatory cells in MMP14$^{Sf-/-}$ peritumoral tissue

Tumor-infiltrating immune cells are a crucial part of the tumor microenvironment. During early tumorigenesis, tumor-antagonizing immune cells being part of the innate and adaptive immune system, detect and kill tumor cells. As tumor growth progresses, the tumor can escape immune surveillance by mutations in gene expression and infiltration of tumor-promoting immune cells [282, 283]. Of importance, changes in the ECM during aging, including decreased collagen density and increased collagen fiber alignment leading to altered tissue mechanics, promote tumor cell growth and metastasis but impaired T-cell motility [284]. The immune cells of the tumor microenvironment include T cells (CD8$^+$ cytotoxic, CD4$^+$ effector T cells, regulatory T cells), natural killer (NK) cells, macrophages (M1/M2), neutrophils (N1/N2), dendritic cells (DCs) and myeloid-derived suppressor cells (MDSCs). These cells can act in a

tumor-suppressing or -promoting way dependent on immune cell polarization, activation state, and stage of tumor growth [283, 285].

To analyze if fibroblast-MMP14 has a role in the immune cell response during melanoma growth, we analyzed the leukocyte marker CD45 (hematopoietic cells, e.g. T-cells, B-cells, neutrophils). In tumor sections of MMP14$^{Sf-/-}$ mice, CD45 levels were significantly reduced compared to tumor tissue of control mice (Figure 10a). In addition, we investigated CD16/32 expression as a marker for NK cells that are cytotoxic lymphocytes and have been shown to have an anti-tumor effect [286-288]. Further, we analyzed macrophages (CD68) and neutrophils (Ly6G) which can affect the tumor either positively or negatively depending on the polarization state [64, 285]. The expression of these immune cell markers was comparable in tumor sections of both genotypes. Together, these data indicate that fibroblast-MMP14, although it may affect recruitment of leukocytes, is not involved in the recruitment of macrophages, neutrophils, and NK cells to melanoma tumors (Figure 10b).

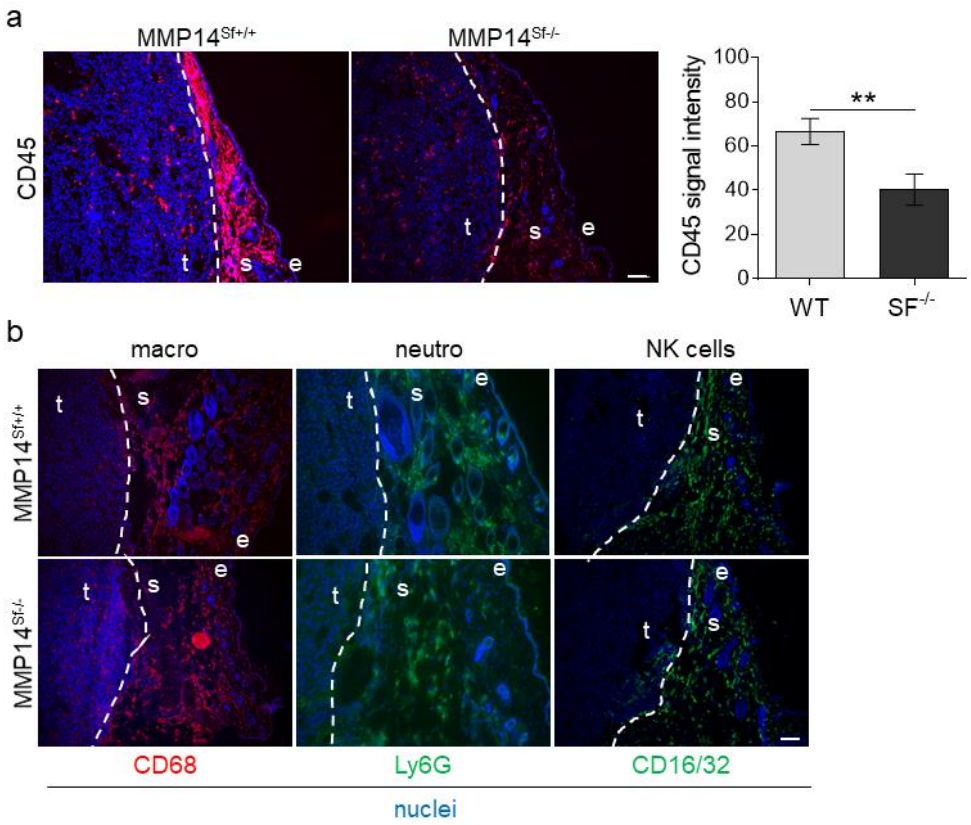

Figure 10. Analysis of immune cells in B16F1 tumors.
(a) Representative pictures of CD45 immunofluorescence staining (left) and quantification (right). The tumor-stroma border is visualized by the dashed line. (b) Immunofluorescence staining for macrophages (CD68, red), neutrophils (Ly6G, green) and NK cells (CD16/32, green) of tumor-stromal tissue. Mean +/- SEM; MMP14$^{Sf+/+}$ (WT; control) n= 4-6; MMP14$^{Sf-/-}$ (SF$^{-/-}$) n= 5-7; t= tumor; s= stroma; e= epidermis; **p<0.01; scale: 100µm.

3.1.2 B16F1 invasion in *ex vivo* skin composites

To investigate if the altered composition and modification of the extracellular environment in the skin of MMP14$^{Sf-/-}$ mice is sufficient to affect melanoma growth independently of active cellular crosstalk between melanoma and stromal cells, we used two *ex vivo* invasion systems. In these approaches, skin biopsies of MMP14$^{Sf-/-}$ and control mice were, after removal of the epidermis by dispase II treatment, either devitalized or chemically decellularized to inactivate or altogether remove resident cells from the tissue. In the devitalization process by freeze-thaw cycles, cells are destroyed by filling with frozen water crystals, which cause them to burst [289]. With this method, the skin composite retains the fibrillar microstructure of the ECM and the mechanical properties of the tissue [289, 290]. However, cellular content, including the cell membrane, cellular proteins, and a significant part of DNA, remain in the tissue [289]. This approach allowed us to analyze melanoma-ECM crosstalk within an almost intact tissue structure without active cellular crosstalk; remaining cellular content can potentially still influence melanoma cells. Thus, tissues were decellularized with Triton-X 100 and sodium deoxycholate to remove cellular components from the tissue [291]. However, the skin ultrastructure is disrupted using this method, including partly damaged collagen, and mechanical properties are altered [291-293].

Once both skin biopsies were either devitalized by three repeating freeze-thaw cycles or chemically decellularized, melanoma cells were seeded on top of the epidermis-free side. After three weeks of incubation, melanoma cells grew on the surface and invaded into the devitalized dermis of both mouse skin genotypes, as visible by H&E and TRP1 staining (Figure 11a). However, in MMP14$^{Sf-/-}$ composites, cells form smaller tumor nests (marked by dotted lines and indicated by white arrowheads) compared to controls (Figure 11a). Analysis of the proliferation marker Ki67 and the apoptosis marker cleaved (cl.) caspase 3, showed tendentially decreased cell proliferation, but not apoptosis in the tumor nests of MMP14$^{Sf-/-}$ skin composites when compared to control (Figure 11b).

To verify that this is an effect of the altered matrix and exclude the possibility of potential crosstalk of melanoma cells with remaining cellular components still present in this system, we decellularized the tissues. Afterwards, melanoma cells were seeded on control and MMP14$^{Sf-/-}$ decellularized biopsies and incubated for three weeks.

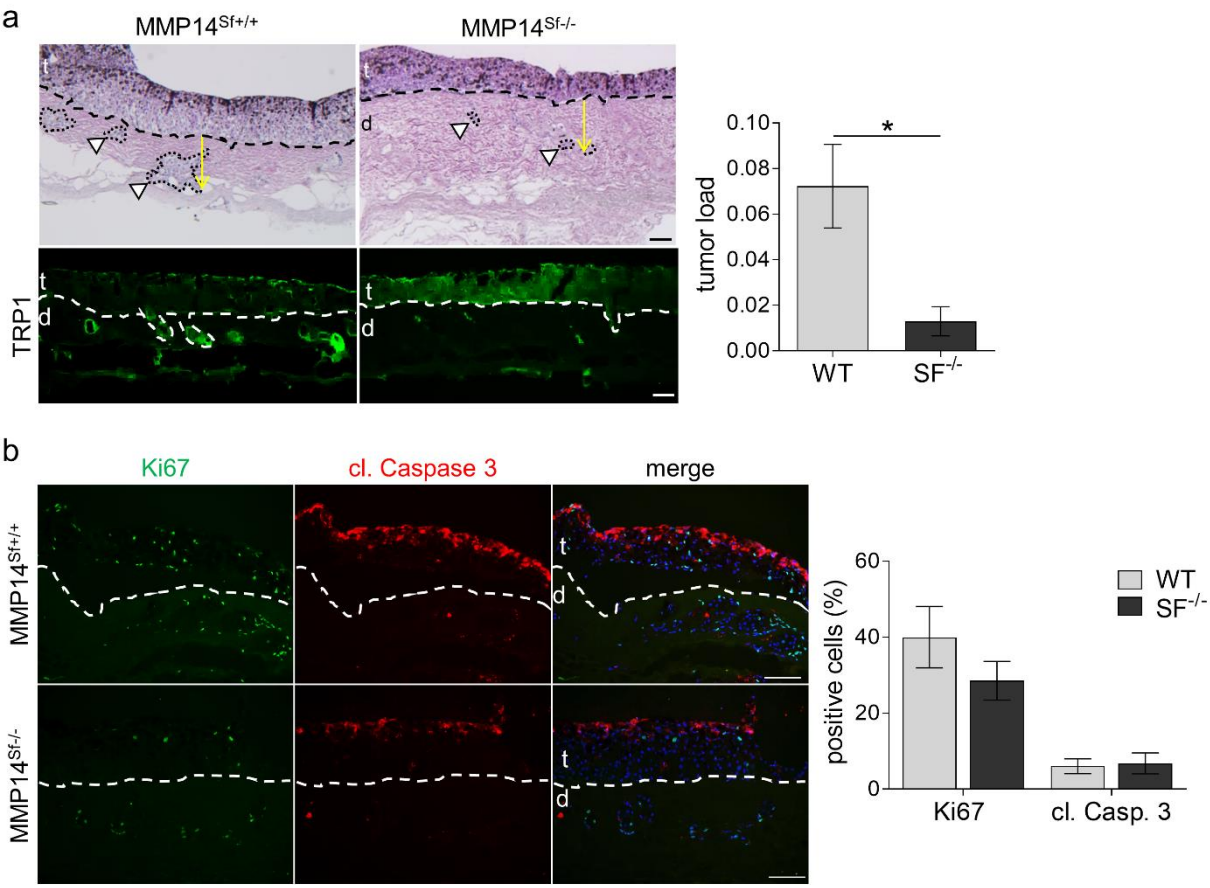

Figure 11. *Ex vivo* DDS assay with B16F1 cells.
(a) H&E and TRP1 (tyrosinase-related protein 1 used as marker for melanoma cells) staining of skin sections after three weeks of melanoma cell invasion (left), repeated four times in independent experiments. The dashed black line marks the border between melanoma cells and dermis, and invading tumor nests (white arrowhead) in the dermis are marked by a dotted line. The graph (right) depicts the size of tumor nests in μm^2 per μm^2 skin. (b) Ki67 and cleaved (cl.) caspase 3 immunofluorescence staining of DDS assay skin sections (left). Quantification of the average ratio of positive cells (right). Mean +/- SEM; $MMP14^{Sf+/+}$ (WT; control) n=4; $MMP14^{Sf-/-}$ ($SF^{-/-}$) n=4; DDS=de-epidermized devitalized skin; t=tumor; d=dermis; *p<0.05; scale: 100µm.

We detected growth of melanoma cells on the surface and invasion into the skin of both mouse genotypes (Figure 12a). As observed with the previous approach, tumor nests formed within the biopsies were smaller in $MMP14^{Sf-/-}$ skin than in control. Moreover, cellular proliferation was significantly decreased in tumor nests, and apoptosis was increased in $MMP14^{Sf-/-}$ skin composites compared to control skin (Figure 12b). This indicates that the matrix environment resulting from loss of fibroblast-MMP14 negatively affects melanoma growth independent of cellular crosstalk by regulating melanoma cell proliferation and apoptosis.

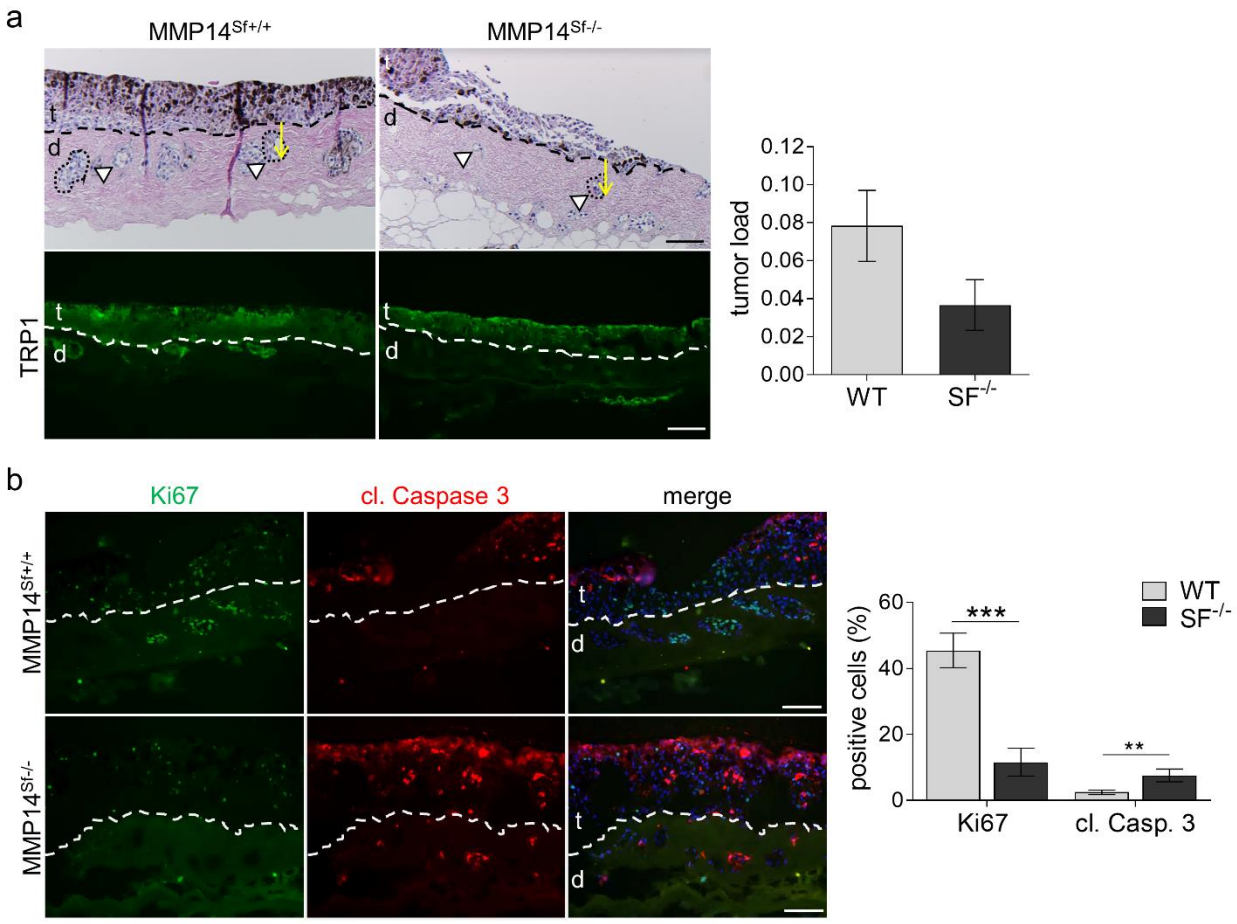

Figure 12. *Ex vivo* Decellularized skin assay with B16F1 cells.
(a) H&E and TRP1 (tyrosinase-related protein 1) staining of skin sections after three weeks of melanoma cell invasion (left), repeated four times in independent experiments. The border between melanoma cells and dermis is marked by the dashed black line and invading tumor nests (white arrowhead) in the dermis are marked by a dotted line. The graph (right) depicts the size of tumor nests in μm^2 per μm^2 skin. (b) Ki67 and cleaved (cl.) caspase 3 immunofluorescence staining of composites sections (left) and quantification of the average ratio of positive cells (right). Mean +/- SEM; MMP14$^{Sf+/+}$ (WT; control) n=6; MMP14$^{Sf-/-}$ (SF$^{-/-}$) n=4; t=tumor; d=dermis; **p<0.01; ***p<0.001; scale: 100µm.

3.2 Analysis of peritumoral tissue in MMP14$^{Sf-/-}$ mice

The ECM, particularly its most abundant component, collagen, represents a significant part, the structural one, of the tumor microenvironment (TME). Collagen fibers can affect tumor cells in a biochemical and biophysical way to promote tumor growth [138, 294-296]. Collagen remodeling, fiber structure and altered organization, provide a TME that influences cellular processes like proliferation, adhesion, and migration [296]. An important marker for tumor progression is the specific remodeling of collagen leading to a particular pattern of fiber alignment, referred to as tumor-associated collagen signatures [131, 297]. In agreement with these published data, besides altered

collagen type I content in the peritumoral tissue and skin of MMP14$^{Sf-/-}$ mice compared to control, we wanted to address possible changes in collagen fiber architecture.

We used Second Harmonic Generation (SHG) analysis to visualize collagen fibers in 3-dimensions and detected increased collagen fiber alignment, measured by a coherency parameter, in peritumoral tissue compared to normal skin independent of genotypes (Figure 13). Thereby, collagen fibers were mainly arranged parallel to the tumor. Moreover, fiber waviness was decreased in peritumoral tissue compared to the skin but comparable in MMP14$^{Sf-/-}$ and control (Figure 13). This indicates that although the absence of MMP14 in fibroblasts leads to collagen accumulation around the grown melanomas, these collagen fibrils' structure and arrangement are comparable to control mice tumors.

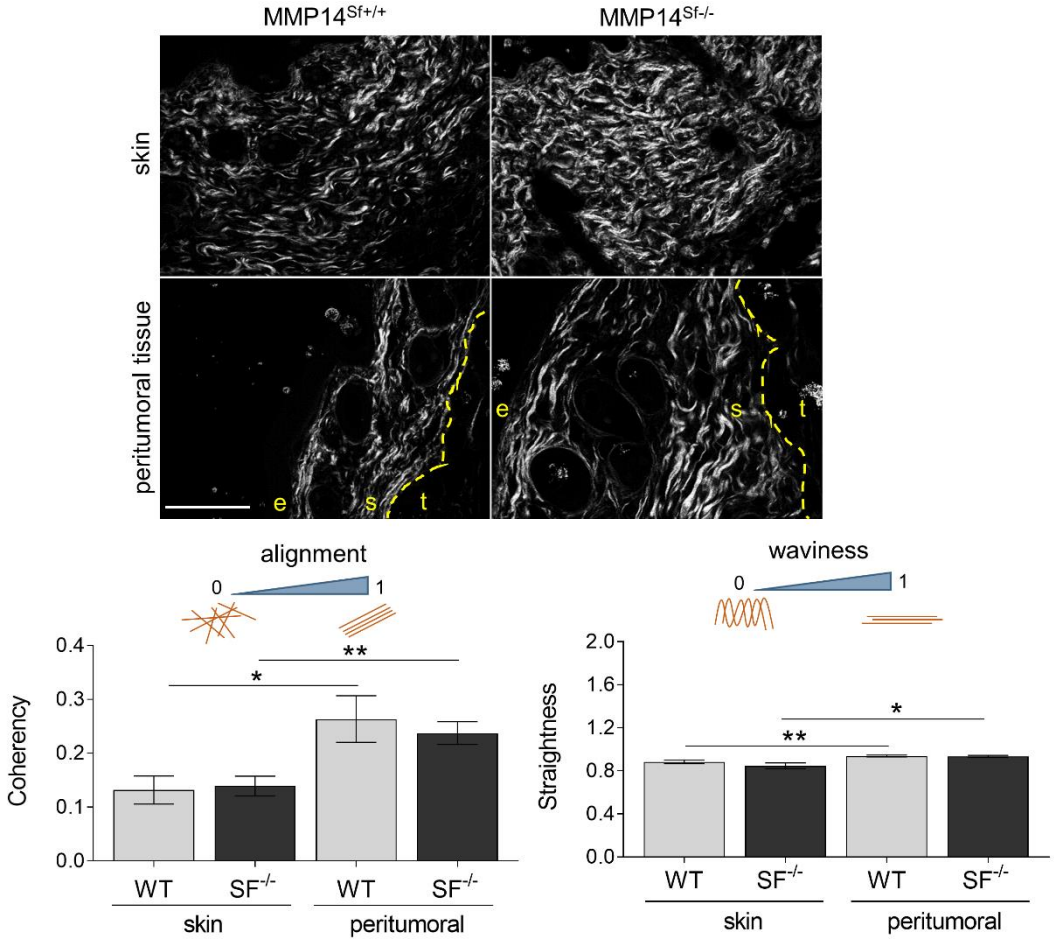

Figure 13. Second Harmonics Generation of skin and peritumoral tissue.
Second Harmonics Generation (SGH) analysis of skin and peritumoral tissue of grafted B16F1 melanoma in MMP14$^{Sf+/+}$ (WT; control) and MMP14$^{Sf-/-}$ (SF$^{-/-}$) mice (upper). Graphs depicting collagen fiber alignment and waviness determined by coherency (alignment) and a straightness parameter (waviness) (lower). The tumor-stroma border is visualized by the dashed line. Mean +/- SEM; peritumoral tissue (peritumoral); MMP14$^{Sf+/+}$ (WT; control) n=8; MMP14$^{Sf-/-}$ (SF$^{-/-}$) n=8; e= epidermis; s= stroma; t= tumor; *p<0.05; **p<0.01; scale: 100µm.

Apart from collagen fiber arrangements, similar to what was previously seen by Picrosirius red staining, also SHG displayed increased overall collagen in the skin of MMP14$^{Sf-/-}$ mice compared to control. Although to a reduced extent, this was also visible around melanomas. Consequently, we wanted to investigate if collagen accumulated in the peritumoral tissue of fibroblast-MMP14 deficient mice. For this, we removed the tumor and quantified the amount of hydroxyproline in the skin and peritumoral tissue. Both tissues exhibited increased collagen content in the absence of fibroblast-MMP14 compared to control (Figure 14a). On the contrary, non-collagenous proteins were not altered in both skin and peritumoral tissue of either genotype (Figure 14b).

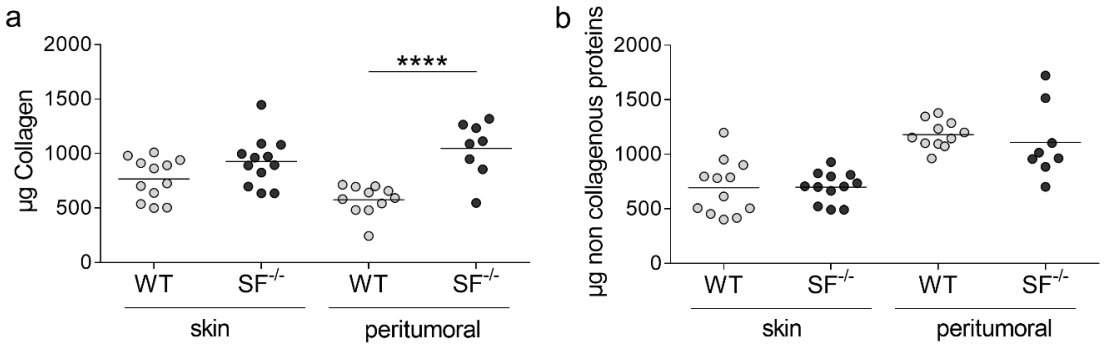

Figure 14. Analysis of protein content in skin and peritumoral tissue.
(a) Analysis of collagen amounts by hydroxyproline quantification, and (b) non-collagenous proteins via ELISA and photometric measurement. MMP14$^{Sf+/+}$ (WT; control); MMP14$^{Sf-/-}$ (SF$^{-/-}$); ****p<0.0001.

In further investigations, analysis of collagen cross-links was performed in cooperation with Prof. Jürgen Brinckmann from the University of Lübeck. These analyses showed no alteration in the amount of the divalent immature collagen cross-links DHLNL, which are predominant in stiff tissues, and HLNL, typical for soft tissues, in both genotypes when normalized to the number of collagen molecules (Figure 15a). Moreover, being a marker for newly synthesized collagen [111], these two types of collagen cross-links show that overall collagen synthesis is not altered due to the deletion of fibroblast-MMP14. Besides HLNL, HHMD cross-links, another collagen cross-link type that is lysine aldehyde-derived and occurs in soft tissues, was increased in peritumoral tissue of MMP14$^{Sf-/-}$ mice when compared to control and normalized to total collagen (Figure 15a). Moreover, hydroxylysine-derived collagen (hyl) cross-links, when normalized to the total amount of cross-links, were only slightly increased in the skin and peritumoral

tissue of MMP14$^{Sf-/-}$ mice to control (Figure 15b). The formation of collagen cross-links is regulated by two families of enzymes, namely the lysyl oxidases (LOXs), which oxidize the lysine residues of collagen fibrils, and the lysyl hydroxylases (LHs) that catalyze the hydroxylation of lysine residues of collagen fibrils [298]. In agreement with the cross-link analysis, transcript levels of LOX and LH2, which are responsible for the formation and composition of collagen cross-links, were also not significantly changed in the skin and peritumoral tissue of both genotypes (Figure 15c and d). An increase in LH2 was detected only in the skin from MMP14$^{Sf-/-}$ mice but not in peritumoral areas; this increase remains inexplicable since we did not see differences in cross-linkage.

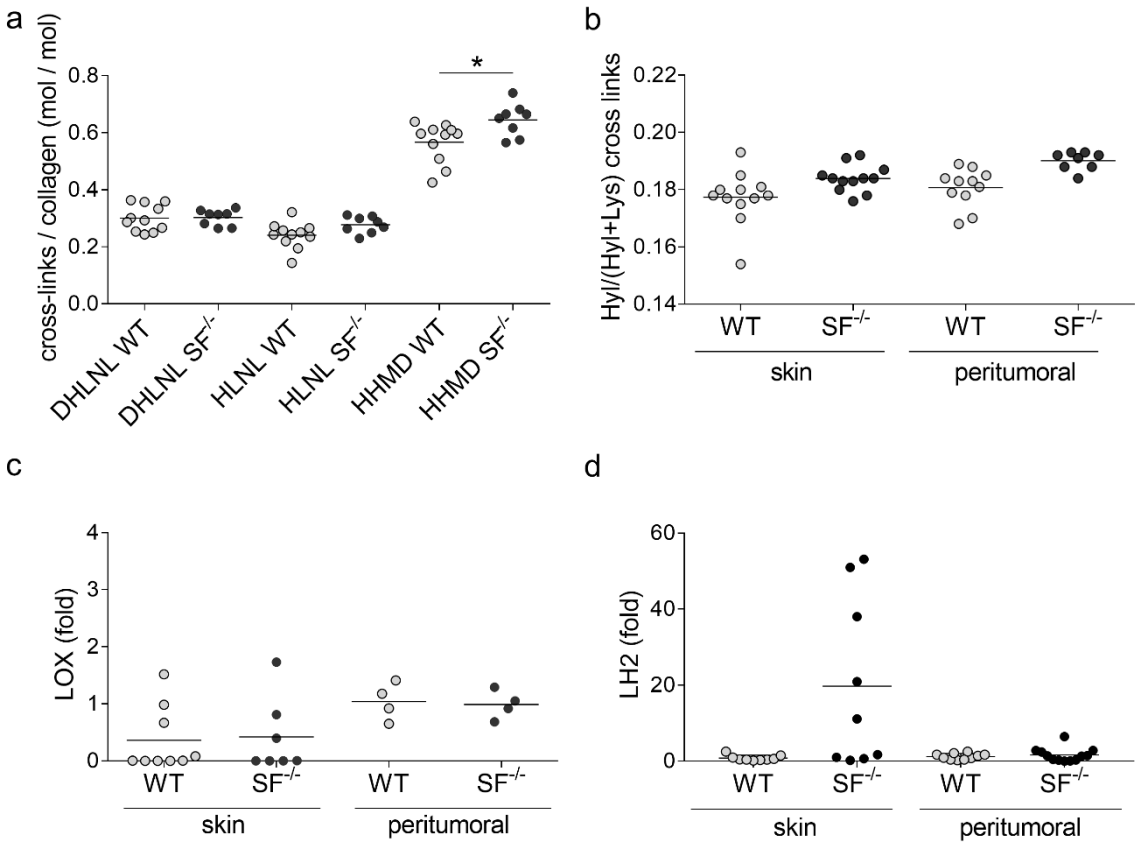

Figure 15. Analysis of collagen cross-link formation in the skin and peritumoral tissue.
(a) Analysis of collagen cross-links normalized to collagen content. (b) Hydroxylysine (hyl) – derived collagen cross-links normalized to total cross-links. (c) Transcript levels of LOX and (d) LH2 quantified by real-time PCR. Each dot represents one specimen per mouse. MMP14$^{Sf+/+}$ (WT; control); MMP14$^{Sf-/-}$ (SF$^{-/-}$; KO); DHLNL= dihydroxylysinonorleucine; HLNL= hydroxylysinonorleucine; HHMD= histidinohydroxymerodesmosine; *p<0.05.

3.2.1 Analysis of tissue stiffness in the skin and peritumoral tissue

Independently of alterations in collagen cross-linking, enhanced matrix abundance can cause altered tissue rigidity [299, 300]. Since in the peritumoral tissue of MMP14$^{Sf-/-}$ mice collagen content but not fibril architecture or cross-linkage was different, we

consequently wanted to address whether the increase in collagen amounts was sufficient to increase tissue stiffness. To investigate this, we used Atomic Force Microscopy (AFM), which allowed us to determine and localize the mechanical properties of healthy skin and peritumoral tissue without affecting the samples by prior treatment. This analysis showed that MMP14$^{Sf-/-}$ skin stiffness, as shown previously [233], is significantly increased compared to control (Figure 16). In early tumors, six days after cell injection, the rigidity of peritumoral tissue in MMP14$^{Sf-/-}$ mice was still increased compared to MMP14$^{Sf+/+}$ mice (Figure 16).

In contrast, on day 13 these alterations were not detected in peritumoral areas (Figure 16). At this time point, when stiffness dissipated, possible high amounts of collagens were sufficient to restrain the tumor growth.

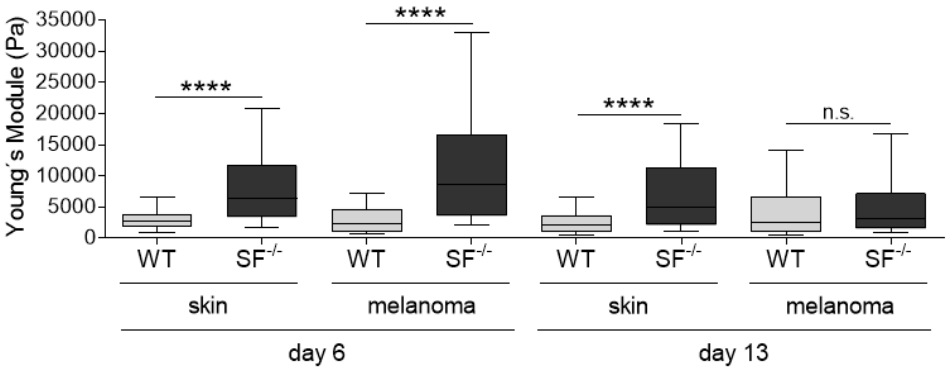

Figure 16. Atomic Force Microscopy of peritumoral tissue and skin.
Atomic Force Microscopy Analysis (AFM) of tissue stiffness, Young's Module, peritumoral tissue of melanomas and corresponding skin at 6 days (50-200 tissue measurements per mouse; WT n=2; SF$^{-/-}$ n=2) and at 13 days (200-500 tissue measurements per mouse; WT n=7; SF$^{-/-}$ n=7) after B16F1 intradermal cell injection. Mean +/- SEM; peritumoral tissue (melanoma); MMP14$^{Sf+/+}$ (WT; control), MMP14$^{Sf-/-}$ (SF$^{-/-}$); ****p<0.0001

3.3 Role for collagen type I on melanoma cell growth

3.3.1 Melanoma proliferation in 2D-culture on fibrillar and monomeric collagen type I

To further address the restraining role of collagens on melanoma growth, we used an *in vitro* approach using surfaces of defined stiffness and coatings of low and high collagen. We seeded B16F1 melanoma cells on plastic plates (1 GPa) with low (0.003 mg/ml) and high (0.3 mg/ml) concentrations of monomeric and fibrillar collagen type I, and FCS used as positive control. Cellular proliferation was analyzed by the BrdU incorporation method; this showed approximately 50 % fewer proliferating cells on all collagen type I coatings than FCS control (Figure 17). When plated on

monomeric type I collagen, melanoma cell proliferation was comparable on both concentrations. In contrast, the higher fibrillar collagen type I concentration significantly reduced melanoma cell proliferation, and lower concentrations led to levels of melanoma proliferation comparable to those detected on monomeric collagen (Figure 17). This indicates that, on high stiffness surfaces, only the native (fibrillar) state of type I collagen at higher concentrations negatively influences melanoma proliferation.

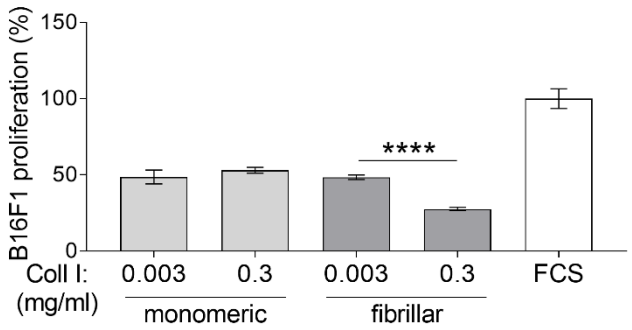

Figure 17. B16F1 cell proliferation on monomeric and fibrillar collagen type I coating.
BrdU incorporation analysis of B16F1 cells grown on tissue culture plates coated with monomeric and fibrillar collagen type I for 24 hours. Mean +/- SEM; collagen type I (Coll I); ****p<0.0001.

To investigate the role of increased fibrillar collagen type I combined with tissue rigidity on melanoma cells growth, we used an *in vitro* approach. We seeded melanoma cells on different stiff-coated surfaces (1.5 kPa, 15 kPa, 1 GPa) with low (0.03 mg/ml) and high (0.3 mg/ml) concentrations of fibrillar collagen type I, and fibronectin (0.01 mg/ml) as a positive control (Figure 18a). After 48 hours of culture on these surfaces, melanoma cells were lysed, proteins resolved, and the expression of the proliferation marker, PCNA, was analyzed by immunoblotting of cell lysates. On low amounts of type I collagen, we detected a gradual increase of proliferation from soft (1.5 kPa) to stiff (1 GPa) coated surfaces, showing a similar tendency also on fibronectin coating (Figure 18a). However, when cells were grown on high collagen concentrations, cellular proliferation was inversely correlated to tissue stiffness, showing the lowest proliferation on rigid surfaces (Figure 18a). Quantification of the average PCNA expression values of three independent experiments also confirmed these results (Figure 18a and b). We used another proliferation assay, BrdU incorporation, to corroborate this data and quantify active proliferation. To this end, we grew melanoma cells on high stiffness (1 GPa) surfaces coated with low (0.03 mg/ml) and high (0.3 mg/ml) amounts of collagen type I and FN, used as the positive control. Using this approach, we detected reduced melanoma cell proliferation on high collagen concentrations compared to lower collagen or positive control (Figure 18c). This

indicates that increased fibrillar collagen type I combined with high tissue stiffness, negatively influenced melanoma proliferation.

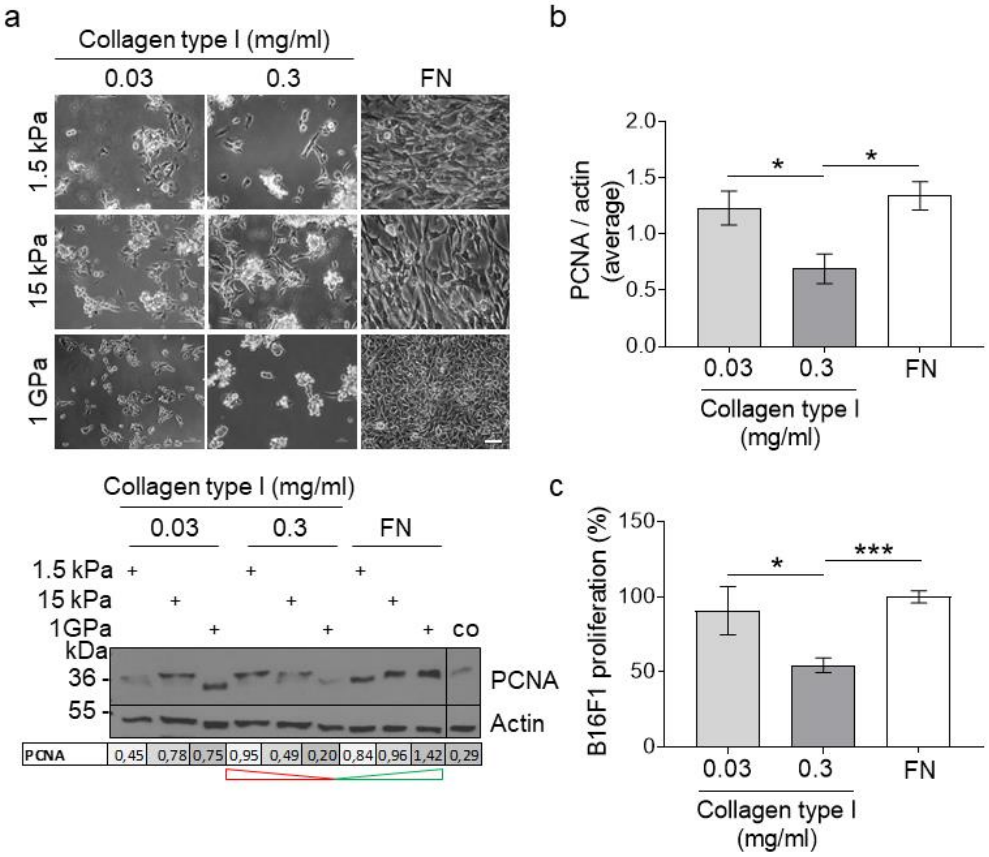

Figure 18. Analysis of B16F1 cell proliferation on stiffness plates coated with collagen type I. (a) B16F1 melanoma cells cultured on different stiff surfaces (1.5kPa, 15kPa and 1GPa) coated with low (0.03mg/ml) and high (0.3 mg/ml) concentrations of collagen type I and 0.01 mg/ml fibronectin (FN) for 48 hours (upper). Immunoblot analysis of PCNA levels of B16F1 lysates and density measurement of PCNA signal normalized to actin (lower), and (b) average PCNA values of three independent experiments. (c) BrdU incorporation analysis of B16F1 cells cultured on coated 1GPa tissue culture plates. Mean +/- SEM; *p<0.05; ***p<0.001; scale: 100µm.

3.3.2 Melanoma growth in 3D- spheroid culture within fibrillar collagen type I gels

Tumor progression is a complex multicellular process in a three-dimensional system, comprising cell-cell and cell-matrix interactions [301, 302]. Consequently, we analyzed how increased fibrillar collagen type I affects melanoma growth in a three-dimensional culture system. This may likely reflect the situation in the tumors at day 13 post-injection (Figure 8b and Figure 16). To address this, we generated melanoma cell spheroids using the liquid overlay method as described in the M&M section (section 2.2.1.4). Once formed, melanoma spheroids were embedded in increasing concentrations (0.3 mg/ml, 1 mg/ml, 2 mg/ml) of fibrillar collagen type I, with low stiffnesses of 0.8 Pa, 4 Pa, and 22 Pa [303]. Matrigel was used as the positive control, and spheroid growth was followed over time (Figure 19). Starting on day 3, the average

spheroid size in matrigel increased steadily, while spheroids in collagen gels did not grow noticeably during the first week of culture. After seven days, the average spheroid size in matrigel (0.21 mm^3) was more than three times larger than at the lowest collagen concentrations (0.06 mm^3). On day 9, while at the lowest concentration of collagen in gels, the average spheroid size was 0.09 mm^3, in 1 mg/ml and 2 mg/ml collagen gels, spheroids were about half of the size. On day 11, the average spheroid sizes grown in gels with the highest collagen concentrations (1 mg/ml; 2 mg/ml) increased modestly and remained significantly smaller than those grown in low concentrations (0.3 mg/ml) of collagen or matrigel until termination of the experiment at day 14. Interestingly, we observed single melanoma cells moving out the spheroid in matrigel and invading the surrounding tissue. On the contrary, no out-migrating cells were detected in spheroids growing in collagen type I gels where they were organized in a compact outer cell layer (Figure 19). Thus, increased fibrillar collagen type I inhibits melanoma growth in a three-dimensional system.

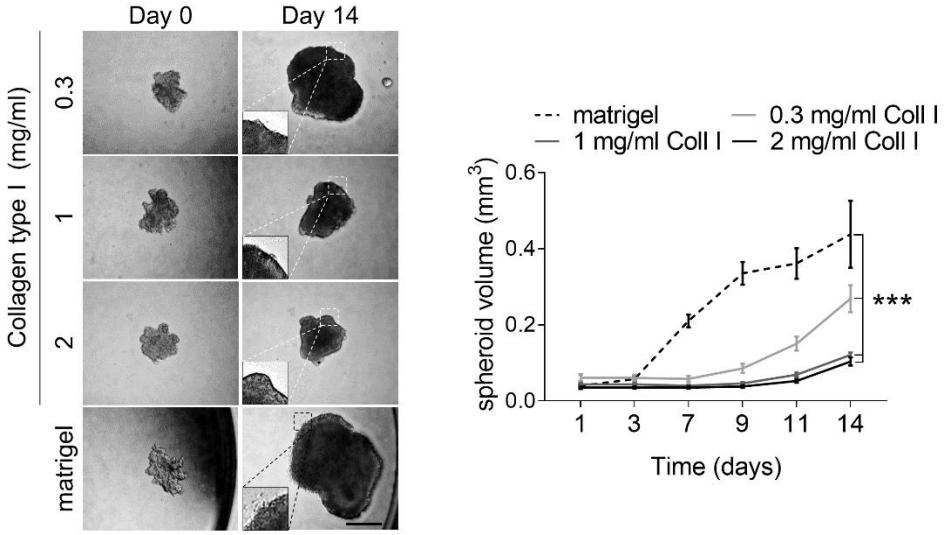

Figure 19. Melanoma spheroid growth in fibrillar collagen type I gels.
Mean +/- SEM. The average size of n=5-9 biological replicates of each condition is shown in the graph. Coll I=collagen type I; ***p<0.001; scale: 500µm.

3.4 Melanoma growth in a fibrotic microenvironment

The data above indicated enhanced collagen type I and increased stiffness negatively affect melanoma cell proliferation *in vitro*. To address *in vivo* whether these conditions inhibit melanoma growth, we undertook an approach where melanoma cells were grafted in fibrotic lesions rich in collagen and stiff [304-306]. Fibrotic lesions were generated in mice by daily intradermal bleomycin injections over four weeks, as

previously described [306, 307]. Bleomycin is a cytostatic drug used for chemotherapy. It interrupts the cell cycle by binding to the DNA of cancer cells, causing single- and double-strand breaks in a reactive oxygen species (ROS) dependent way [306, 308]. Overproduction of ROS results in an inflammatory response and subsequently activation of fibroblasts with an extensive production of collagen, other ECM proteins, and fibrogenic cytokines leading to fibrosis [304, 308]. The formation of skin fibrotic lesions was confirmed by microscopical analysis of H&E stained skin sections (Figure 20a). In these lesions and NaCl-treated control skin, melanoma cells were grafted intradermally, and tumor growth was followed over time. On day 4, after melanoma cell injection, tumors were visible and palpable only in NaCl-treated control skin. After eight days, when tumors were detected in both treated mice' skin, reduced tumor growth became visible in fibrotic areas compared to NaCl control and was most significant after day 11 post-injection (Figure 20b).

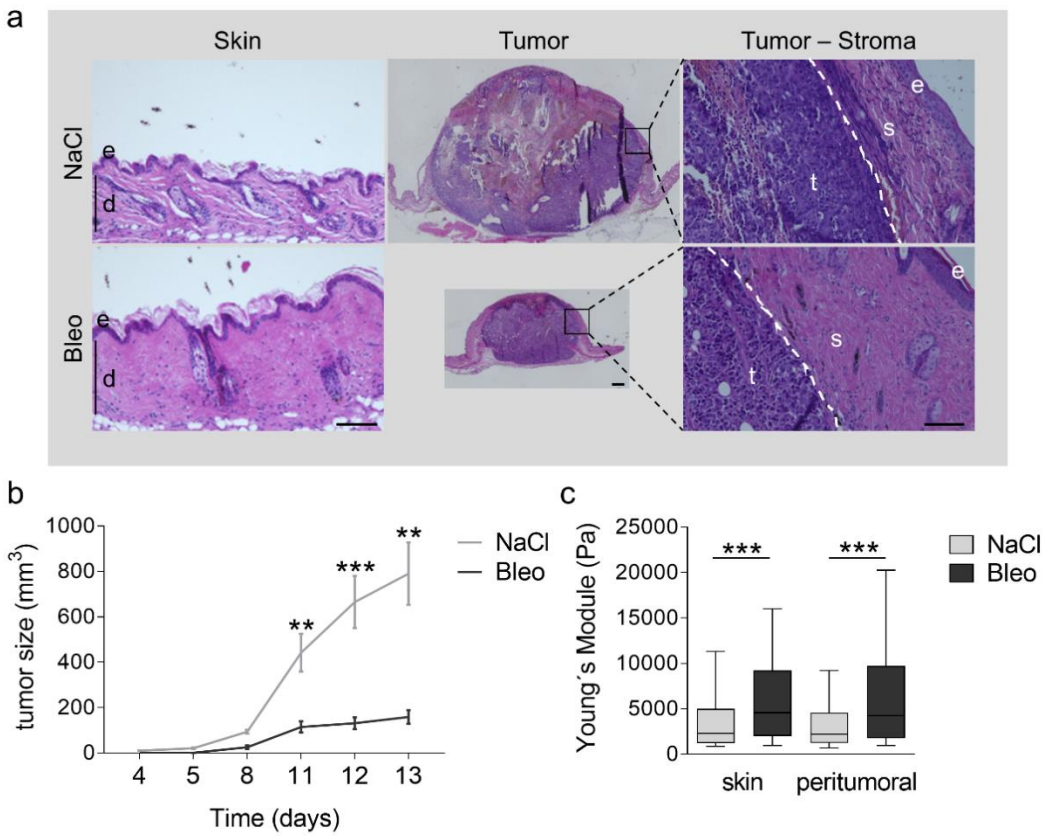

Figure 20. B16F1 melanoma growth in bleomycin-induced fibrotic skin.
(a) H&E stainings of representative sections of normal skin and melanoma. (b) Time course of melanoma growth in bleomycin-treated (Bleo) and control (NaCl) mice overtime. (c) Atomic Force Microscopy (AFM) to analyze tissue stiffness of skin (skin) and peritumoral tissue (peritumoral). The dashed line visualizes the tumor-stroma border. Mean +/- SEM; control (NaCl) n=8; bleomycin treated (Bleo) n=7; e= epidermis; d= dermis; s= stroma; t= tumor; **p<0.01; ***p<0.001, scale: 100µm.

The difference in tumor growth remained significant until the experiment was terminated. AFM analysis of peritumoral areas measured increased stiffness in the skin and the peritumoral regions of bleomycin-treated mice compared to NaCl control (Figure 20c). These data indicate that a collagen-rich stiff microenvironment inhibits *in vivo* melanoma growth. The data also suggest that the effect of MMP14 deletion in fibroblasts on melanoma growth is primarily mediated by the reduced collagen turn-over and accumulation in tissue rather than additional cellular alterations.

3.4.1 Melanoma cell proliferation in tumors developed in fibrotic skin

To investigate if reduced melanoma growth in fibrotic skin might result from altered cell proliferation or apoptosis, we performed immunofluorescence staining of tumor sections using Ki67, and cleaved caspase 3. This analysis showed minor changes in apoptosis but a significant reduction in melanoma cell proliferation in fibrotic skin compared to control tumors (Figure 21). These data, as also shown above with the fibroblast-MMP14 deleted mice (Figure 8d), indicated that a matrix-rich stiff environment inhibits melanoma growth *in vivo* by decreasing cellular proliferation.

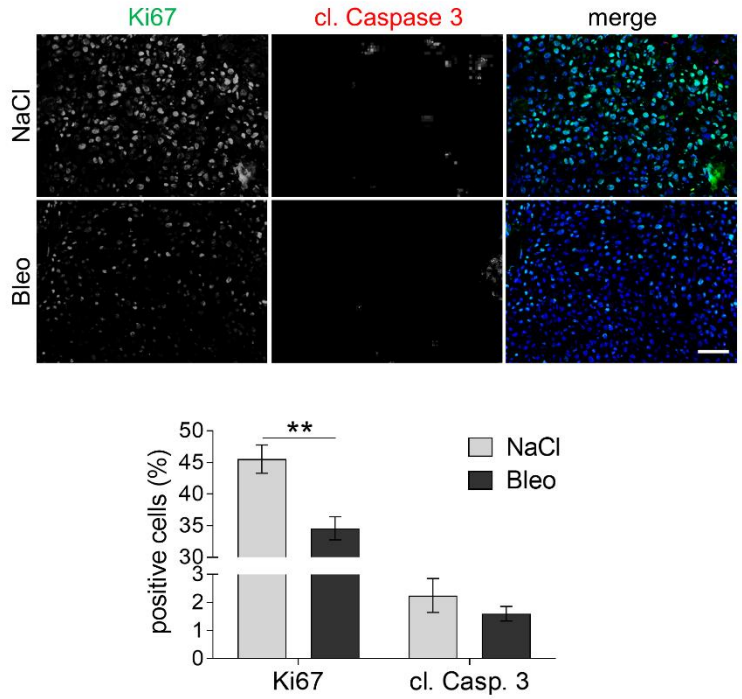

Figure 21. Ki67 and cleaved Caspase 3 staining in melanoma grown in fibrotic skin.
Immunofluorescence staining of Ki67 and cleaved (cl.) Caspase 3 in B16F1 tumors (upper) and the average ratio of positive cells (lower). Mean +/- SEM; control (NaCl) n=8; bleomycin treated (Bleo) n=7; **p<0.01; scale: 100µm.

3.4.2 Inflammatory cells and CAFs in fibrotic peritumoral tissue

Tissue fibrosis and tumor growth are accompanied by increased inflammatory response [282, 283, 308, 309]. To address if immune cell recruitment is altered during melanoma growth in fibrotic skin, we carried out an immunofluorescence staining for CD45. As observed in the MMP14$^{Sf-/-}$ mice tumors (Figure 10a), quantification of peritumoral tissue showed decreased CD45 signal intensity in tumors grown in fibrotic skin compared to control tumors (Figure 22).

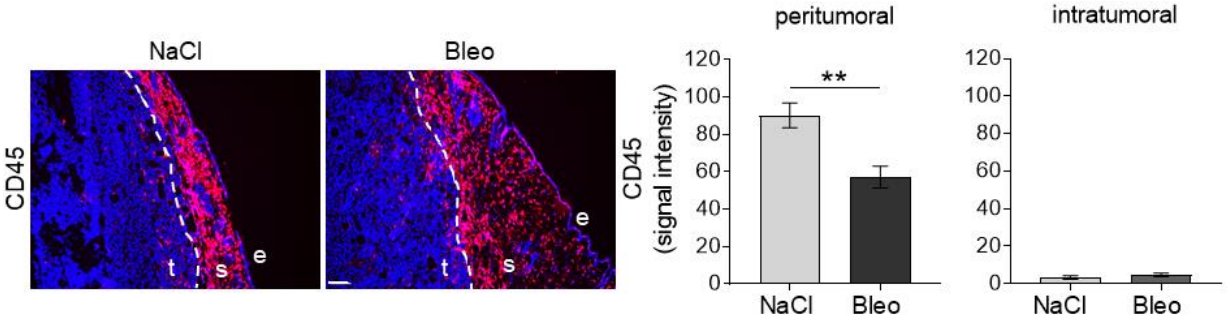

Figure 22. CD45 immunofluorescence staining of melanoma in fibrotic skin.
Representative pictures of immunofluorescence staining for CD45 in melanoma and peritumoral tissue (left). Quantification of average signal intensity per area is on the right. The dashed line visualizes the tumor-stroma border and analyzes peritumoral tissue (100µm radius from the tumor) (p) by the dotted line. Mean +/- SEM; control (NaCl) n=8; bleomycin treated (Bleo) n=7; t= tumor; p= peritumoral area; s= stroma, e= epidermis; **p<0.01; scale: 100µm.

Accumulation of collagen type I in the skin is also accompanied by activation of fibroblasts and their conversion into the so-called myofibroblasts [96, 310]. CAFs display markers and biological features of myofibroblasts [311-313].

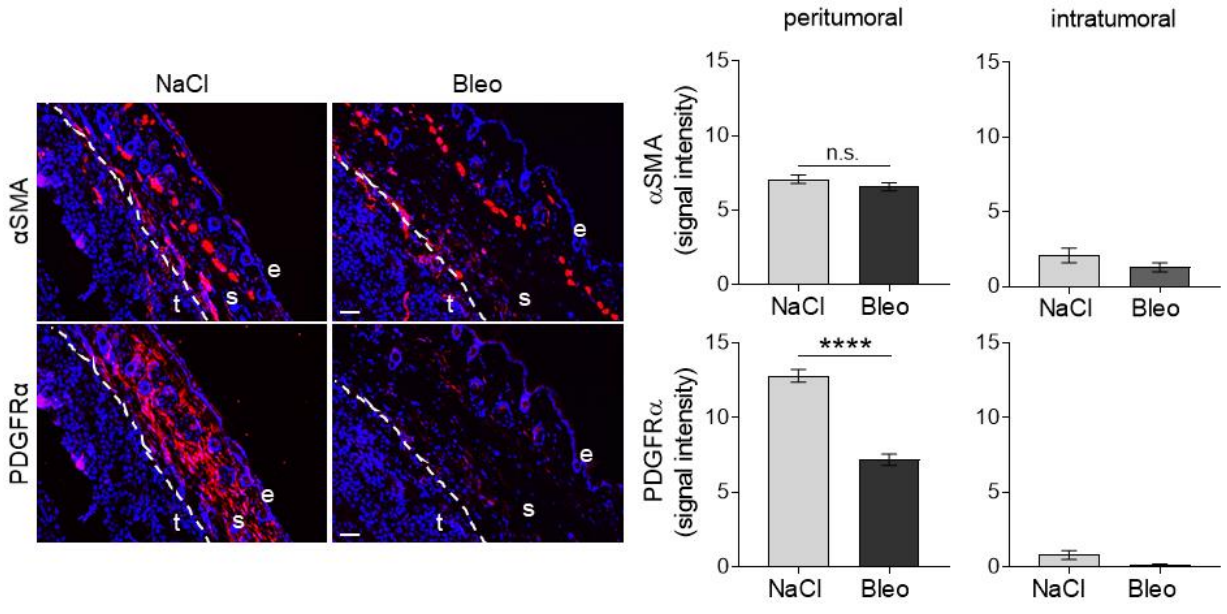

Figure 23. Immunofluorescence staining for PDGFRα and αSMA in peritumoral tissue of melanoma in fibrotic skin.

Representative pictures of PDGFRα and αSMA immunofluorescence staining of peritumoral tissue (left); right, quantification of average signal intensity per area. The dashed line marks the tumor-stroma border. Mean +/- SEM; control (NaCl) n=8; bleomycin treated (Bleo) n=7; t= tumor; p= peritumoral area; s= stroma, e= epidermis; ***p<0.001; scale: 100µm.

These cells occur around tumors and modulate growth [46, 313]. To analyze if numbers of fibroblasts (positive for PDGFRα [75] and CAFs (αSMA positive) [314] are altered in melanomas grown in control and fibrotic lesions, we used immunodetection on tissue sections. Although we did not detect differences in the amounts of CAFs located in peritumoral areas (Figure 23), the numbers of fibroblasts were decreased in the peritumoral regions of bleomycin-treated mice compared to controls (Figure 23). Moreover, intratumoral numbers of fibroblasts and CAFs were slightly reduced in melanoma of bleomycin-treated mice but not significantly.

3.5 Efficacy of chemotherapeutic treatment of melanoma in MMP14$^{Sf-/-}$ mice

We showed that collagen accumulation and increased tissue stiffness due to the deletion of fibroblast-MMP14 result in reduced melanoma growth (3.3). Enhanced collagen accumulation in peritumoral areas affected treatment by acting as a molecular sieve [90, 138]. The question raised on whether deletion of MMP14 in fibroblasts and restraining melanoma growth by structural microenvironmental alterations may synergize with chemotherapeutic treatment. Here we used a generally accepted anti-tumor drug, cisplatin, as an example. Cisplatin is an available cytostatic drug that interferes with DNA replication and increases cell death [315]. To address that, we injected B16F1 cells intradermally into the flank of MMP14$^{Sf-/-}$ and control mice. On day five after melanoma cell injection, when tumors were first detectable, mice were treated with a single intraperitoneal injection of cisplatin (10mg/kg) and we monitored tumor growth over time (Figure 24a). Already at day 8, three days after cisplatin treatment, the average tumor size in treated MMP14$^{Sf+/+}$ mice was significantly compared to untreated MMP14$^{Sf+/+}$ mice, but not in MMP14$^{Sf-/-}$ mice (Figure 24b). This delay of tumor growth in treated MMP14$^{Sf+/+}$ mice compared to untreated MMP14$^{Sf+/+}$ mice was detected until the termination of the experiment at day 13 (Figure 24b and c). However, in MMP14$^{Sf-/-}$ mice, cisplatin treatment did not further inhibit melanoma growth (Figure 24b and c). This indicates no improved chemotherapeutic effect of cisplatin using MMP14 as an additional target.

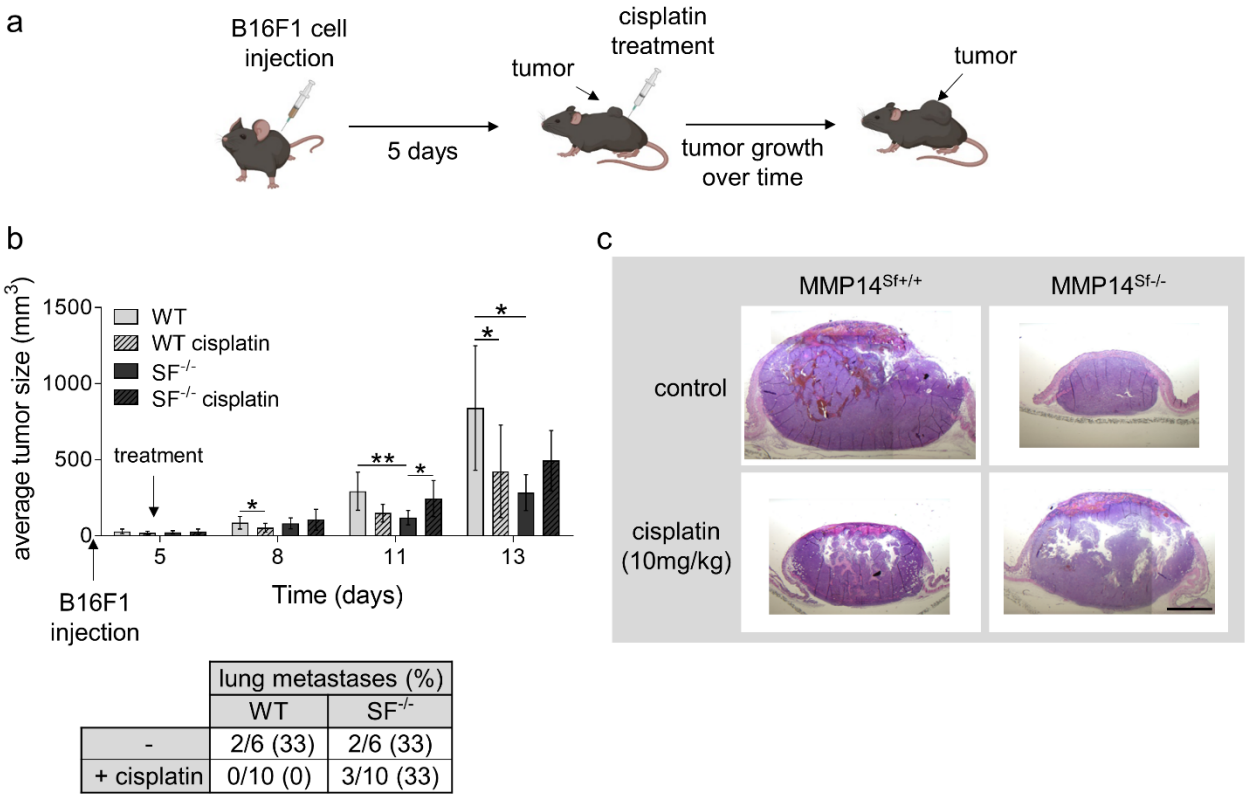

	lung metastases (%)	
	WT	$SF^{-/-}$
-	2/6 (33)	2/6 (33)
+ cisplatin	0/10 (0)	3/10 (33)

Figure 24. Chemotherapeutic treatment of B16F1 melanoma in $MMP14^{Sf-/-}$ mice.
(a) Schematic representation of experimental procedure. (b) Time course of melanoma growth after cisplatin treatment (10mg/kg, i.p.) (upper) and ratio of lungs with metastasis as determined by PCR amplification of GFP expressed in melanoma cells (lower). (c) H&E staining of representative tumors. Mean +/- SEM; $MMP14^{Sf+/+}$ (WT; control) n=6, with cisplatin n=10; $MMP14^{Sf-/-}$ ($SF^{-/-}$) n=6, with cisplatin n=10; *p<0.05; **p<0.01; scale: 500µm.

3.6 Analysis of peritumoral matrix in $MMP14^{Sf-/-}$ mice

3.6.1 Proteome analysis of peritumoral matrix proteins

We undertook a proteomic approach to investigate if apart of collagen type I, other collagens, or additional structural proteins of the peritumoral extracellular matrix are altered and contribute to the reduced tumor growth in $MMP14^{Sf-/-}$. The peritumoral tissue of grafted B16F1 melanoma tumors was macro-dissected (Figure 26a). Proteins were extracted with either SDS or SDS in urea to obtain proteins of different solubilities. Extracts were analyzed by mass spectrometry. In both approaches, several cellular proteins in the peritumoral tissue of $MMP14^{Sf-/-}$ were significantly altered compared to control mice, but only a few, and not changed considerably, were from the ECM (Figure 25). This was surprising since we previously detected (Figure 14) increased amounts of collagens in $MMP14^{Sf-/-}$ compared to control by hydroxyproline quantification. In contrast, non-collagenous proteins were not altered in both genotypes (Figure 14).

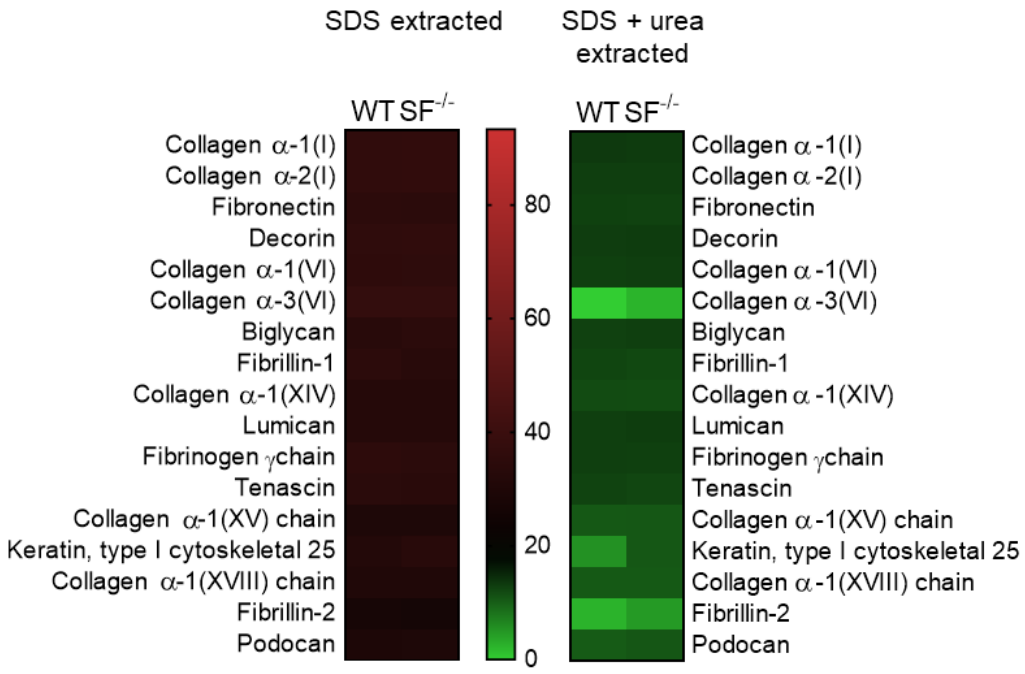

Figure 25. Proteome analysis of B16F1 melanoma peritumoral tissue.
Selected ECM proteins from extraction with SDS (left) and SDS in combination with urea (right). Mean +/- SD; MMP14$^{Sf+/+}$ (WT; control) n=4; MMP14$^{Sf-/-}$ (SF$^{-/-}$) n=4.

As large amounts of cellular proteins were extracted over ECM proteins, a possible reason for the reduced detection may be a solubility problem. To overcome this, we established a method to decellularize the tissue by extracting cellular proteins and enriching and concentrating the extracellular matrix proteins. We based the protocol on that previously published by Jiang et al. [269]. Efficacy of this method was confirmed by immunoblot analysis, where successful depletion of cell compartments was verified in lysates using actin immunodetection and enrichment of matrix proteins by detection of collagen type I (Figure 26a). Besides the α1 chain (138 kDa) and α2 chain (130 kDa) of collagen type I, an additional band with an approximate size of 120 kDa was detected (Figure 26a) that corresponds to isoforms of the α1 and α2 chains of collagen type I, which are generated by alternative splicing [316, 317]. Afterward, these samples underwent proteome analysis. This approach identified several differentially expressed extracellular matrix proteins significantly altered in peritumoral tissue of fibroblast lacking MMP14 compared to control (Figure 26b). Among these, collagen types I, VI, XIV, XV, and XVIII increased expression compared to control (Figure 26b). In addition, biglycan, lumican, podocan, decorin, fibrillin 1 and 2 were up-regulated in MMP14$^{Sf-/-}$ peritumoral tissue compared to control. In lysates from decellularized peritumoral tissue, we detected enhanced collagen type I expression in MMP14$^{Sf-/-}$ compared to control (Figure 27a), thus confirming the previous results (Figure 14a).

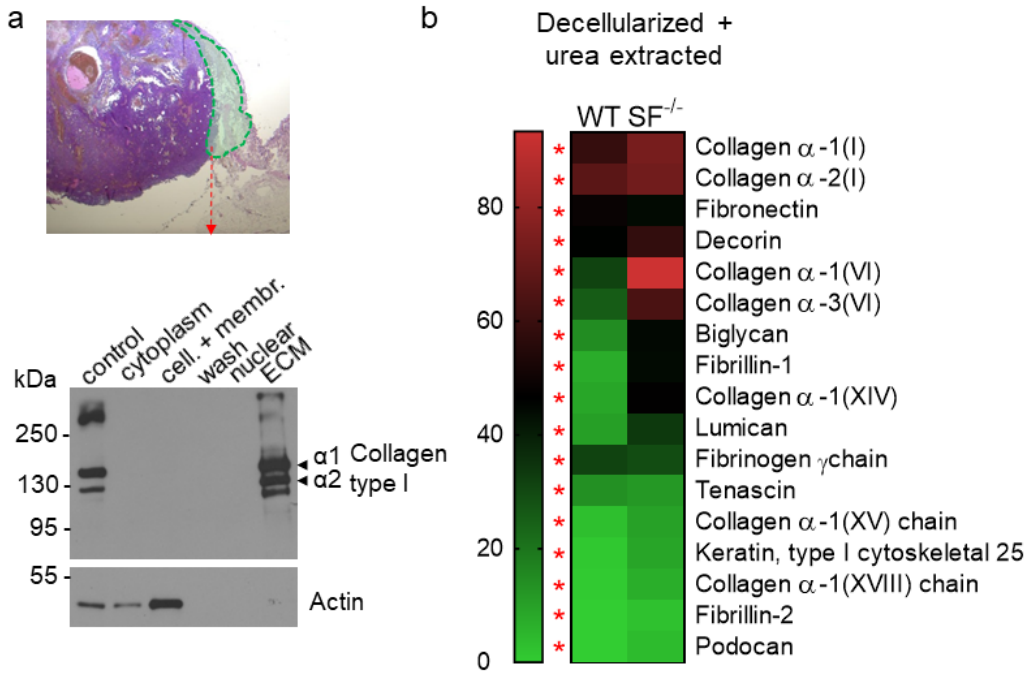

Figure 26. Analysis of decellularized B16F1 melanoma peritumoral tissue.
(a) Representative picture of B16F1 melanoma showing the dissected peritumoral tissue in green (upper). Immunoblot of the protein fractions extracted during decellularization of the tissue and enrichment of ECM proteins (lower panel). (b) Proteome analysis of B16F1 melanoma peritumoral tissue extracted with urea after decellularization. Significantly altered proteins are indicated (red star). Mean +/- SD; $MMP14^{Sf+/+}$ (WT; control) n=4; $MMP14^{Sf-/-}$ ($SF^{-/-}$) n=4.

Another collagen that was strongly up-regulated in those peritumoral tissues was type XIV collagen (Figure 26). Collagen type XIV is fibril-associated collagen (FACIT) that often occurs close to collagen type I fibrils in tissues of high mechanical stress [318]. Moreover, it is expressed in metastatic human melanoma cells, which also have high levels of collagen type I [319]. Collagen type XIV immunofluorescence staining on B16F1 tumor sections from control mice displayed strong immunostaining in areas adjacent to the tumor. At the same time, the remaining dermis was only modestly stained (Figure 27b). On the contrary, on tumor sections of $MMP14^{Sf-/-}$ mice, we detected enhanced collagen type XIV staining in the tumor at the periphery, in peritumoral areas, and beyond. Quantification of staining intensities showed a significant increase in collagen type XIV signal in peritumoral tissue of $MMP14^{Sf-/-}$ tumor sections compared to control (Figure 27b), confirming the result from the proteome analysis.

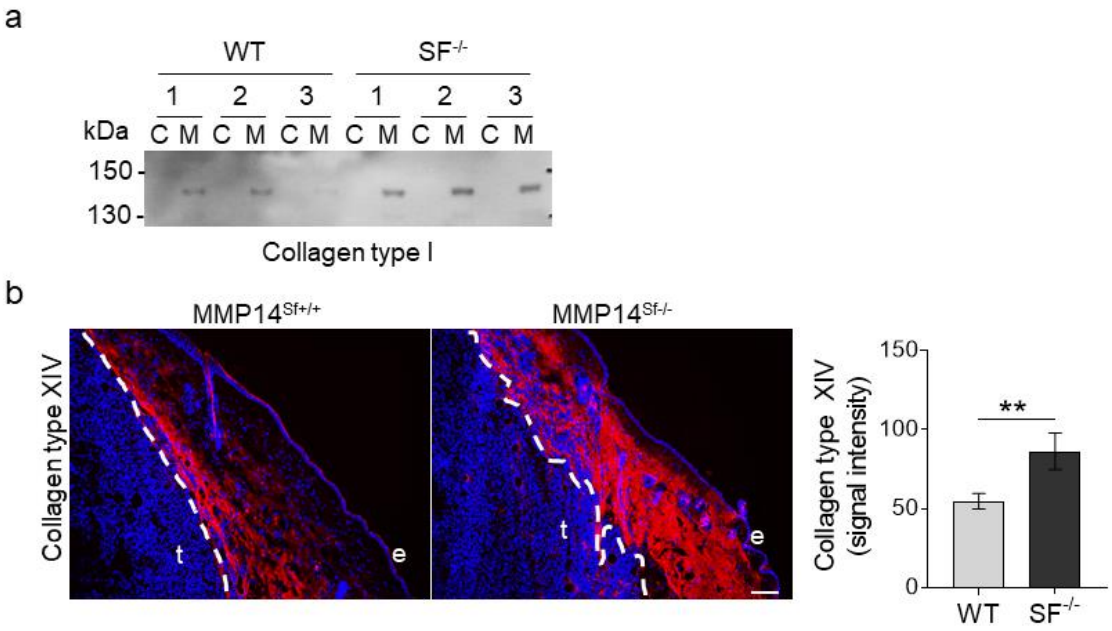

Figure 27. Collagen type I and XIV expression in B16F1 peritumoral tissue.
(a) Immunoblot analysis of three (1- 3) independent extracts from peritumoral MMP14$^{Sf+/+}$ (WT) and MMP14$^{Sf-/-}$ (SF$^{-/-}$) decellularized tissue (M) and control total lysates (C). (b) Representative pictures of collagen type XIV immunofluorescence staining and quantification of average signal intensity per peritumoral area (100µm radius from tumor) (right). The dashed line marks the tumor-stroma border. Mean +/- SEM; MMP14$^{Sf+/+}$ (WT; control) n=6; MMP14$^{Sf-/-}$ (SF$^{-/-}$) n=5; t= tumor; e= epidermis; **p<0.01; scale: 100µm.

3.7 Fibroblast proteome in the absence of MMP14

3.7.1 Fibroblast deposited matrix

3.7.1.1 Effect of fibroblast matrix on melanoma proliferation and apoptosis

To investigate the biological significance of matrix alterations induced by the deletion of MMP14 in fibroblasts on the growth of melanoma cells, we let primary fibroblasts secrete and deposit their matrix and used it as a growth substrate for B16F0, B16F1, and HCmel12 cells. For this, MMP14$^{Sf-/-}$ and primary control fibroblasts from 3 independent cell isolates per genotype were cultured for two weeks and allowed to deposit their matrix (Figure 28a). In the absence of MMP14 in fibroblasts, the produced fibroblasts matrix appears denser than wild-type cells, as visible by Coomassie blue staining (Figure 28a). After removing fibroblasts from their matrix, we seeded melanoma cells and analyzed cell proliferation and apoptosis. On the fibroblast matrix of both genotypes, cell proliferation of all three melanoma cell lines was significantly reduced compared to FCS coating used as a positive control, which contains multiple pro-proliferative growth factors and matrices [320] (Figure 28b). In addition, cell growth

of B16F0, B16F1, and HCmel12 cells on MMP14$^{Sf-/-}$ fibroblasts' matrix was significantly reduced compared to MMP14$^{Sf+/+}$ matrix (Figure 28b).

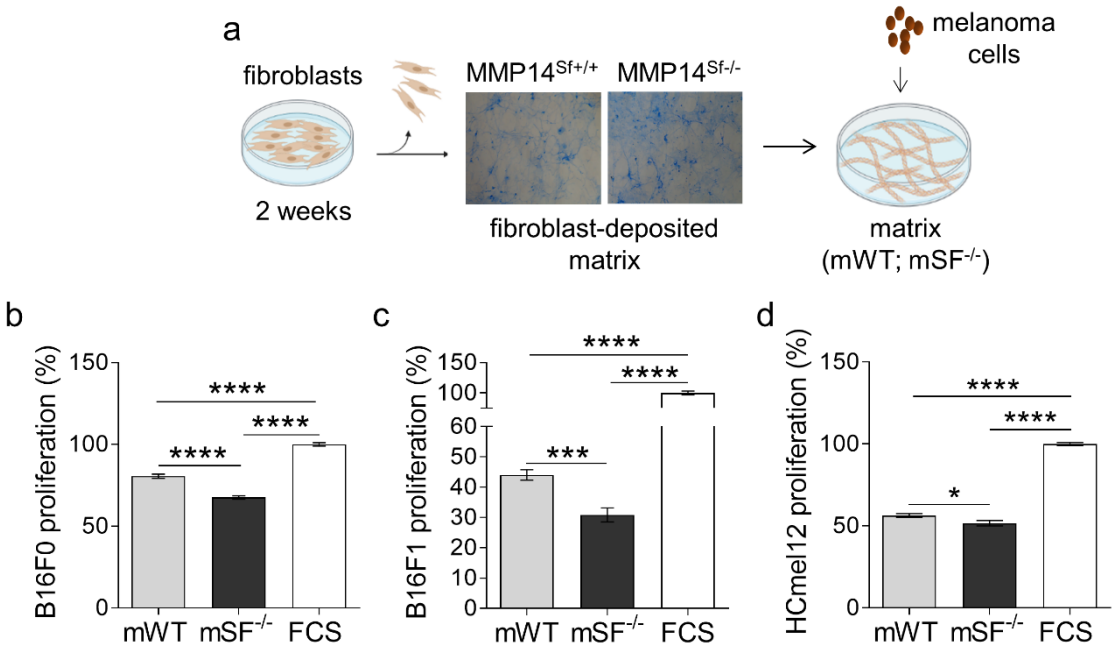

Figure 28. Analysis of melanoma cell proliferation on fibroblast matrix.
(a) Schematic representation of experimental setting with the fibroblast deposited matrix in the representative photographs (picture of Coomassie stained matrix after fibroblast removal); Proliferation assay of (b) B16F0, (c) B16F1 and (d) HCmel12 cells grown on fibroblast matrix for 24 hours in 2-5 independent experiments with 4 biological replicates. Mean +/- SEM; fibroblast-deposited matrix from MMP14$^{Sf+/+}$ (mWT; control) n=3; fibroblast-deposited matrix from MMP14$^{Sf-/-}$ (mSF$^{-/-}$) n=3; ***p<0.001; ****p<0.0001.

On the contrary, apoptosis of B16F1 melanoma cells was not altered on the fibroblast matrix from both genotypes (Figure 29). Thus, loss of fibroblast-MMP14 results in the generation of a dense and a differentially modified fibroblast matrix that negatively affects melanoma cell proliferation but not apoptosis.

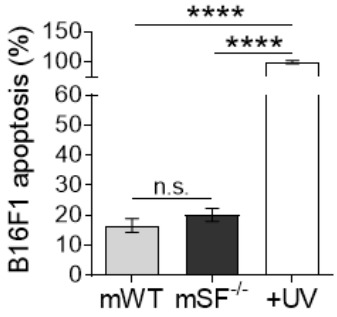

Figure 29. Analysis of B16F1 cell apoptosis on fibroblast matrix.
Apoptosis assay measuring cytoplasmatic nucleosomes in B16F1 cells, performed in two independent experiments with biological triplicates. Mean +/- SEM; fibroblast-deposited matrix from MMP14$^{Sf+/+}$ (mWT; control) n=3; fibroblast-deposited matrix from MMP14$^{Sf-/-}$ (mSF$^{-/-}$) n=3; ****p<0.0001.

3.7.1.2 MMP14$^{Sf-/-}$ fibroblast matrix does not support melanoma cells migration

The composition and mechanical properties of the extracellular matrix are crucial characteristics that affect melanoma migration [321]. To analyze how the matrix from MMP14-deleted fibroblast affects melanoma cells migration, we seeded B16F1 cells on MMP14$^{Sf-/-}$ and control fibroblast matrix and recorded cell migration for 24 hours. B16F1 cells were previously mitotically inactivated (to eliminate differences due to cell proliferation). After 4 hours, we detected a modest decrease of melanoma cell migration on the MMP14$^{Sf-/-}$ fibroblast matrix compared to the MMP14$^{Sf+/+}$ matrix (Figure 30). This delay became more pronounced after 8 hours and remained constant until 24 hours when melanoma migration on MMP14$^{Sf-/-}$ fibroblast matrix was significantly decreased compared to control. Initial migration relies on substrate recognition and adhesion. However, the most significant migration changes on the MMP14$^{Sf-/-}$ matrix were detected later, when cells could also secrete factors or matrices to support migration.

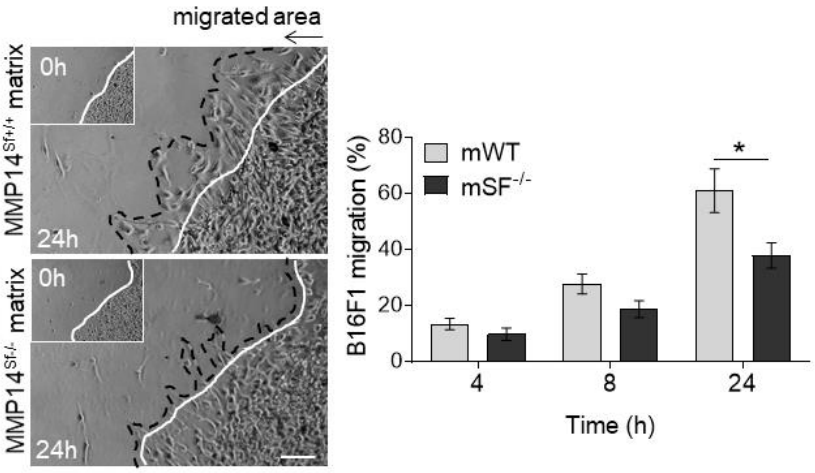

Figure 30. B16F1 migration on fibroblast deposited matrix.
Colony outgrowth assay showing representative pictures of melanoma migration after 24 hours on fibroblast matrix (left) and the relative quantification (right). Mean +/- SEM; fibroblast-deposited matrix from MMP14$^{Sf+/+}$ (mWT; control, n=3); fibroblast-deposited matrix from MMP14$^{Sf-/-}$ (mSF$^{-/-}$, n=3); continuous line: initial cell front at time 0 hours; dashed line: cell front at the indicated time-point; *p<0.05.

3.7.2 Proteome analysis of fibroblast matrix and supernatants

To investigate in more detail the deposited and soluble matrices altered in fibroblasts upon deletion of MMP14, we used an unbiased proteomic approach. For this, we analyzed fibroblast's deposited matrix, the matrices, and soluble factors secreted by MMP14$^{Sf-/-}$ and control cell isolations in culture. This would also provide information on

fibroblasts-specific contribution to the altered peritumoral environment that we detected in the analyzed dissected tissues *in vivo* (Figure 25 and Figure 26).

We cultured primary fibroblasts from three MMP14$^{Sf-/-}$ and control mice independent isolations for two weeks and allowed them to deposit their matrix. In addition, serum-free fibroblast conditioned medium (c.m.) was collected after 24 hours of culture. A proteomic approach analyzed all samples. Several differentially expressed extracellular matrix proteins were identified in samples from MMP14$^{Sf-/-}$ fibroblasts compared to control, including several laminin subunits (α-2, α-5, β-2), fibronectin and collagen types (I, III, VI, VIII, XI, XIV, XV, XVI) (Figure 31). As previously shown [233], collagen type I is increased, although here more modestly, in MMP14$^{Sf-/-}$ fibroblast lysates and conditioned medium compared to controls (Figure 31). Among additional altered proteins, only collagen type XIV was significantly increased in all three independent isolates from MMP14$^{Sf-/-}$ fibroblast matrix and conditioned medium.

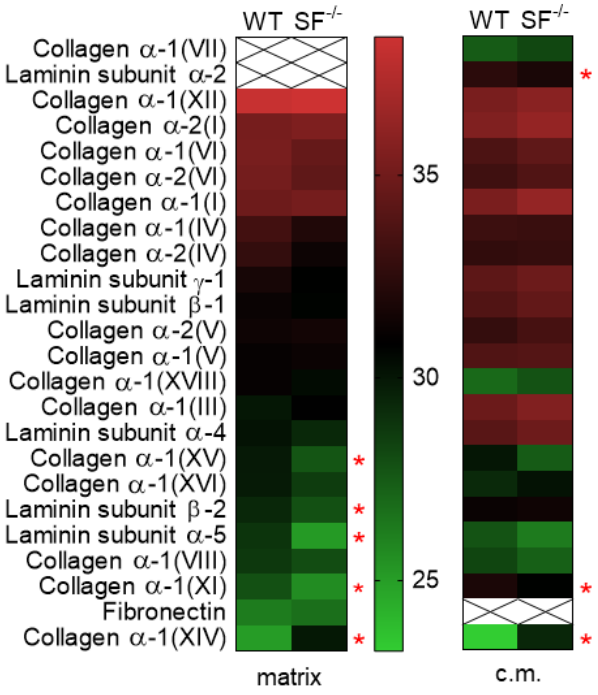

Figure 31. Proteome analysis of fibroblast deposited matrix and conditioned medium.
The heat maps show selected matrix proteins that were identified in fibroblast deposited matrix (matrix) and conditioned medium (c.m.). Significantly altered proteins ($p<0.05$) are marked with red stars. MMP14$^{Sf+/+}$ (WT; control) matrix n=3, c.m. n=3; MMP14$^{Sf-/-}$ (SF$^{-/-}$) matrix n=3, conditioned medium (c.m.) n=3.

3.7.3 Expression of collagens

Collagen types I and VI belong to the most abundant structural proteins in the skin, being part of the ECM scaffold [322]. Fibril-forming collagens as type I serve as an

anchor for FACIT types XII and XIV, often expressed in differentiated and stiff tissues [323, 324]. Immunoblot analysis of matrix and conditioned medium from MMP14$^{Sf-/-}$ and control mice fibroblasts showed increased collagen type I strongly in MMP14$^{Sf-/-}$ fibroblast matrix and more modestly in the conditioned medium as compared to control fibroblasts (Figure 32a), thus confirming the previously published data [233]. Consistent with the proteomic data, collagen type VI was modestly decreased in matrix from MMP14-deficient fibroblasts while increased in the conditioned medium compared to controls. In agreement with a net overall comparable amount of collagen type VI in both fibroblasts' genotypes, mRNA levels of this collagen were not altered (Figure 32b). Immunoblot analysis of collagen type XII showed an apparent increase in MMP14$^{Sf-/-}$ fibroblast matrix compared to control, whereas almost no protein was detected in soluble form (Figure 32a).

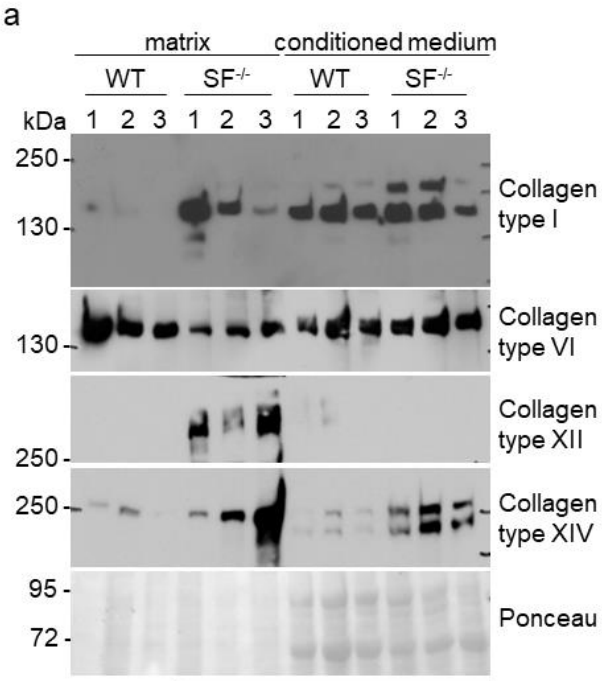

	Average ratio	
	matrix	c.m.
	SF^{KO}/SF^{WT}	SF^{KO}/SF^{WT}
collagen I	17,22	1,36
collagen VI	0,33	1,35
collagen XII	22,83*	0,43
collagen XIV	21,81	10,21*

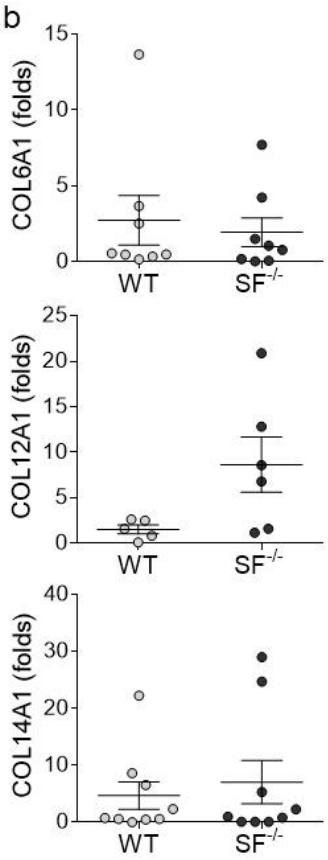

Figure 32. Analysis of selected types of collagens in fibroblast matrix and conditioned medium. (a) Immunoblot analysis of collagen type I, VI, XII, and XIV in fibroblast deposited matrix and conditioned medium (upper) and densitometry analysis (lower). (b) Transcriptional analysis of collagen type VI (COL6A1), XII (COL12A1), and XIV (COL14A1) in fibroblast lysates. Mean +/- SEM; MMP14$^{Sf+/+}$ (WT; control) n=9; MMP14$^{Sf-/-}$ (SF$^{-/-}$) n=8.

This protein increase was likely due to increased *de novo* protein synthesis (Figure 32b). Further, collagen type XIV was increased in both matrix and conditioned medium of MMP14$^{Sf-/-}$ fibroblasts compared to MMP14$^{Sf+/+}$ fibroblasts.

However, on the transcriptional level, collagen type XIV was not altered, suggesting that the changes in protein expression may result from an altered posttranslational event and being MMP14 a proteolytic enzyme, possibly by impaired protein processing.

In this context, an *in vitro* cleavage assay with recombinant MMP14 and collagen type XIV and subsequent fingerprint analysis was performed in our group (Figure 33) [325]. This analysis showed that collagen type XIV is a substrate of MMP14, which cleaves the protein generating fragments sized between 60 - 85 kDa (Figure 33, black arrows). Fingerprint analysis points at two potential cleavage sites in the N-terminal, generating the 72kDa fragment, and at the C-terminal, generating the 80kDa fragment. Since the antibody we used in the immunoblot analysis binds the N-terminal part of collagen type XIV, we expected to detect the 72kDa cleavage fragment or a fragment of 121kDa size in the control medium treated MMP14$^{Sf+/+}$ fibroblasts. However, we could not detect collagen type XIV fragments in fibroblast supernatants, possibly due to the instability of the generated pieces and, or its fast degradation. More investigations are required to clear this issue.

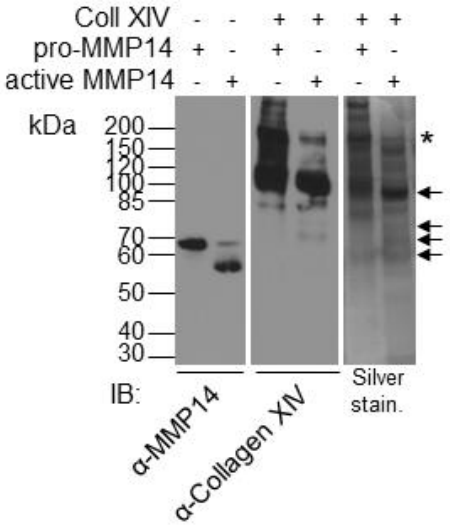

Figure 33. *In vitro* cleavage analysis of collagen type XIV by MMP14.
Processing of collagen type XIV (Coll XIV) by trypsin activated recombinant MMP14 was visualized on immunoblot and silver stained SDS PAGE (4-12% Bis-Tris gradient gel). Black asterisk indicates full length collagen type XIV; black arrows indicate collagen type XIV fragments generated by MMP14. The figure was adapted and modified from [325].

3.7.3.1 Melanoma cell proliferation on collagen type XIV

To investigate the functional biological significance of increased collagen type XIV in MMP14$^{Sf-/-}$ fibroblast-deposited matrix for melanoma cells, we first addressed its role in cell proliferation. To address that, we seeded B16F1 melanoma cells on tissue

culture plates coated with low (1µg/ml) and high (10µg/ml) concentrations of collagen type XIV and FCS as a positive control.

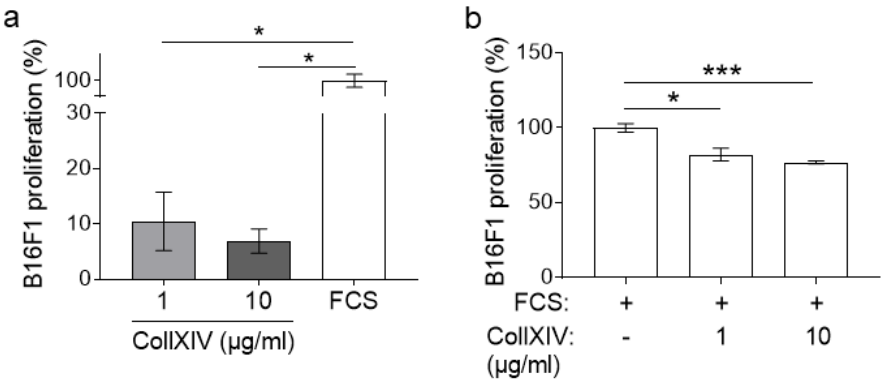

Figure 34. Analysis of B16F1 melanoma cell proliferation on collagen type XIV.
Proliferation measured upon B16F1 cell culture on (a) collagen type XIV (CollXIV) coating and (b) FCS coating in combination with collagen type XIV (1µg/ml; 10µg/ml). Culture on FCS was the positive control. Mean +/- SEM; *p<0.05; ***p<0.001.

Incorporation of BrdU in B16F1 cells after 24 hours culture was significantly diminished in both low and high collagen type XIV coating when compared to FCS control (Figure 34a). Moreover, collagen type XIV acted competitively by decreasing dose-dependently FCS-induced melanoma cell proliferation (Figure 34b).

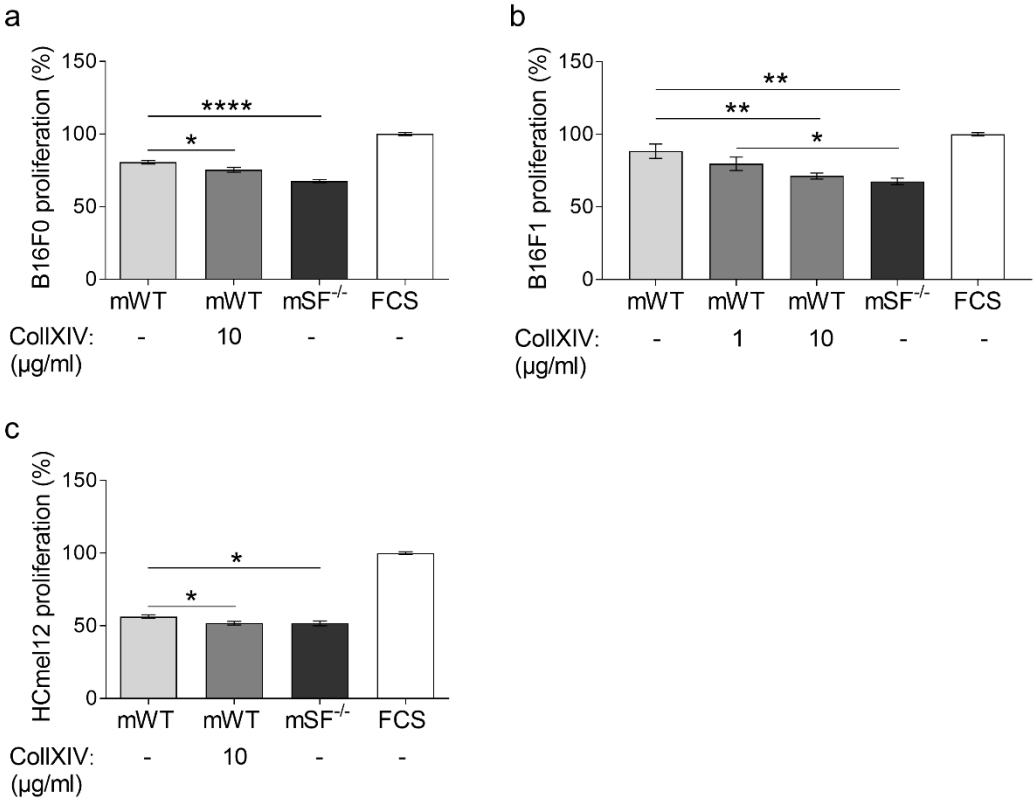

Figure 35. Analysis of melanoma cell proliferation on fibroblast matrix.

Proliferation measured by BrdU incorporation assay in (a) B16F0, (b) B16F1 and (c) HCmel12 cells cultured on fibroblast deposited matrix in combination with collagen type XIV (1µg/ml; 10µg/ml). Culture on FCS was the positive control. Mean +/- SEM; fibroblast-deposited matrix from MMP14$^{Sf+/+}$ (mWT; control) n=3; fibroblast-deposited matrix from MMP14$^{Sf-/-}$ (mSF$^{-/-}$) n=3; *p<0.05; **p<0.01; ****p<0.0001.

Comparably, the addition of type XIV collagen to the MMP14$^{Sf+/+}$ matrix led to reduced proliferation of B16F0, B16F1, and HCmel12 melanoma cells to a similar extent as observed upon culture on MMP14$^{Sf-/-}$ fibroblast matrix where this protein is enriched (Figure 35). This possibly explains the reduced melanoma cell proliferation on the MMP14$^{Sf-/-}$ fibroblast matrix. These data indicate that collagen type XIV is a matrix protein that does not support melanoma cell proliferation and can act dose-dependently as an inhibitory molecule.

3.7.3.2 Collagen type XIV is not pro-migratory for melanoma

To address whether collagen type XIV is a substrate for cell migration, we seeded mitotically inactivated B16F1 melanoma cells on low (1 µg/ml) and high concentrations (10 µg/ml) of collagen type XIV and FCS as positive control and monitored cell migration overtime.

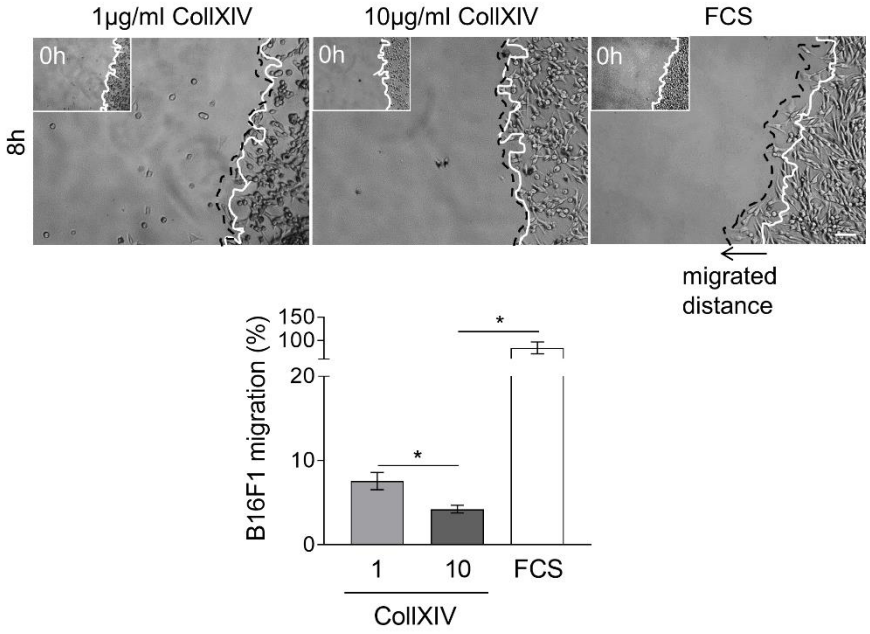

Figure 36. B16F1 migration on collagen type XIV coating.
Colony outgrowth assay showing B16F1 cell migration on collagen type XIV (CollXIV) coating after 8 hours and quantification. Mean +/- SEM; continuous line: cell front after 0 hours; dashed line: cell front after 8 hours; *p<0.05; scale: 100µm.

On both concentrations of collagen type XIV B16F1, cells barely moved, showing a significant decrease of migration when compared to FCS (Figure 36). However, after

8 hours, while melanoma cells on low concentration (1 µg/ml) moved a minimal distance, on higher, 10 µg/ml collagen type XIV, they remained at the initial front (Figure 36). This indicates that collagen type XIV is not a pro-migratory substrate for melanoma.

To investigate if reduced melanoma cell migration on MMP14$^{Sf-/-}$ fibroblast matrix (Figure 30) resulted from the matrix enrichment in collagen type XIV, we added collagen type XIV (10 µg/ml) to the pro-migratory matrix of MMP14$^{Sf+/+}$ fibroblasts and let melanoma cells migrate on it. After 4 hours, we detected a modest decrease in melanoma cell migration on the MMP14$^{Sf+/+}$ fibroblast matrix supplemented with collagen type XIV compared to the untreated control matrix (Figure 37). This difference was significant after 8 hours and remained up to 24 hours (Figure 37), indicating that the increased collagen type XIV content in the MMP14$^{Sf-/-}$ fibroblast matrix negatively affects melanoma cell migration.

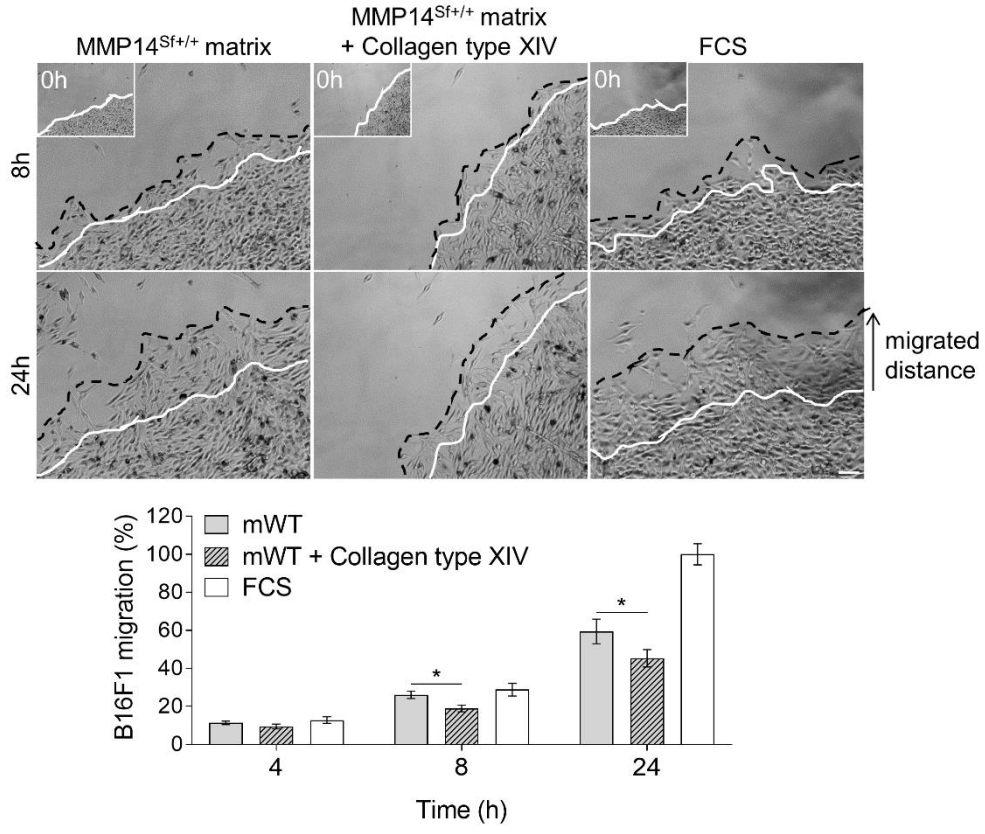

Figure 37. B16F1 migration on MMP14$^{Sf+/+}$ fibroblast matrix with collagen type XIV.
Colony outgrowth assay showing B16F1 cell migration on MMP14$^{Sf+/+}$ fibroblast matrix (mWT) alone and in combination with 10 µg/ml collagen type XIV (mWT + Collagen type XV). Representative pictures are shown. In the graph the quantification of the migrated area is displayed as mean +/- SEM (mWT; control, n=3); (mWT + Collagen type XIV, n=3). The continuous line marks the initial cell border; The dashed line marks the distance reached by the cells at the indicated time-point; *p< 0.05; scale: 100µm.

3.7.3.3 Melanoma cell adhesion is reduced by collagen type XIV

One of the reasons why cells do not migrate on a due substrate is the lack of substrate recognition which is primarily based on cellular interaction mediated by integrin receptors [326]. We used adhesion assays to address whether melanoma cells can recognize collagen type XIV. B16F1 melanoma cells were seeded on 1µg/ml and 10µg/ml collagen type XIV and fibronectin coatings; the latter was used as a positive control. Cells were allowed to adhere for two hours, then fixed and stained with crystal violet. Retained dye was solubilized and quantified by photometry. Melanoma cell adhesion was low on both concentrations of collagen type XIV and decreased dose-dependently with increasing collagen concentration compared to fibronectin control, where adhesion was very high (Figure 38a). Interestingly, when collagen type XIV was supplied to the MMP14$^{Sf+/+}$ matrix, melanoma cell adhesion was reduced almost to the level detected on the MMP14$^{Sf-/-}$ matrix (Figure 38b). Thus, increased amounts of collagen type XIV in the MMP14$^{Sf-/-}$ fibroblast matrix competes for melanoma cell adhesion and contributes to reduced cell migration (Figure 37).

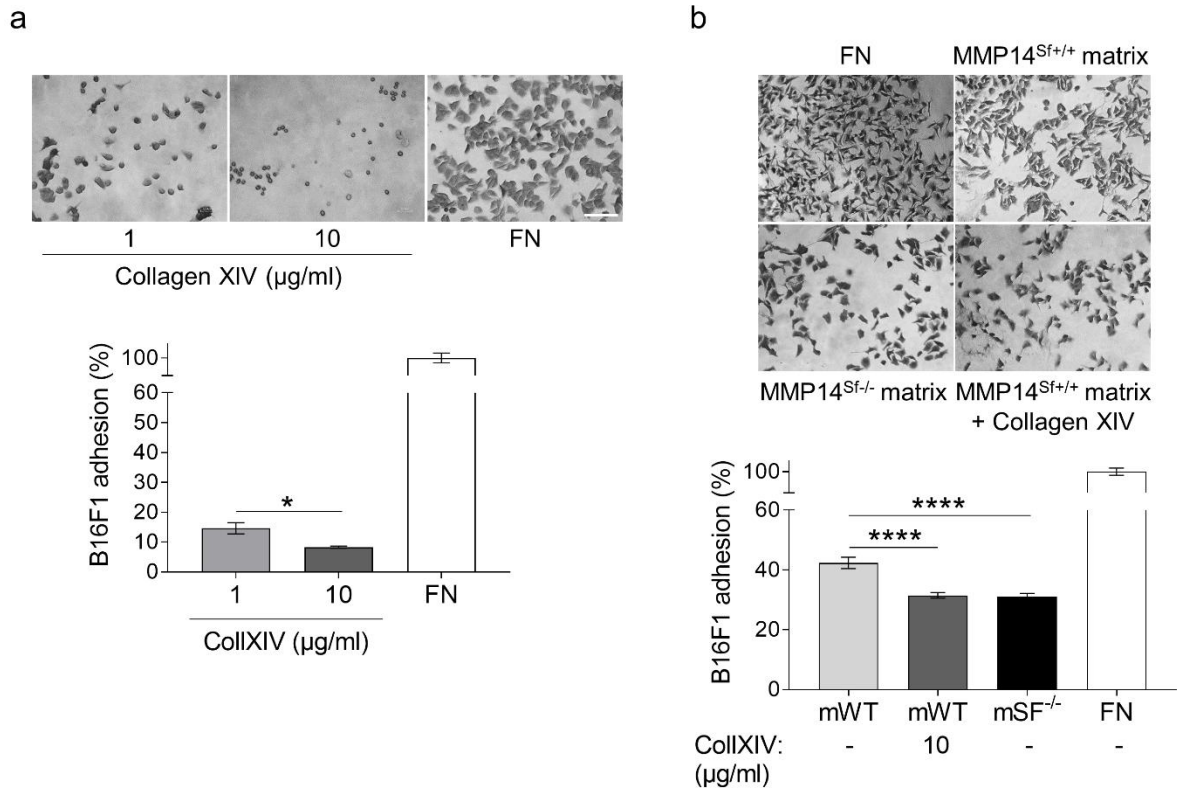

Figure 38. Adhesion assay on collagen type XIV coating and fibroblast-deposited matrix.
B16F1 cell adhesion assay on (a) collagen type XIV coating, (b) fibroblast matrix from MMP14$^{Sf+/+}$ (mWT), fibroblast matrix from MMP14$^{Sf+/+}$ in combination with collagen type XIV and on fibroblast matrix from MMP14$^{Sf-/-}$ (mSF$^{-/-}$). Representative pictures are shown. Quantification of adhered cells is displayed as mean +/- SEM; (mWT, control, n=3); (mWT + Collagen type XIV, n=3); (mSF$^{-/-}$, n=3); *p< 0.05; ****p<0.0001; scale: 100µm.

3.7.4 Fibroblast secretome

3.7.4.1 Influence of fibroblast secreted factors on melanoma proliferation and apoptosis

Besides its function in matrix-directed proteolysis, MMP14 also regulates the behavior of cells by modulating synthesis, release, and processing of soluble factors involved in the regulation of cell proliferation, survival, and inflammation [210, 327]. Thus, to address whether, in addition to the matrix, further modifications of soluble factors secreted or released from fibroblasts' cell surface contribute to modulating melanoma cell proliferation, we analyzed B16F1 cell proliferation and apoptosis after culturing them in fibroblast conditioned medium (c.m.). For this, MMP14$^{Sf-/-}$ and primary control fibroblasts were cultured for 24 hours in FCS-free media, c.m. was collected and used freshly to treat melanoma cells (Figure 39a).

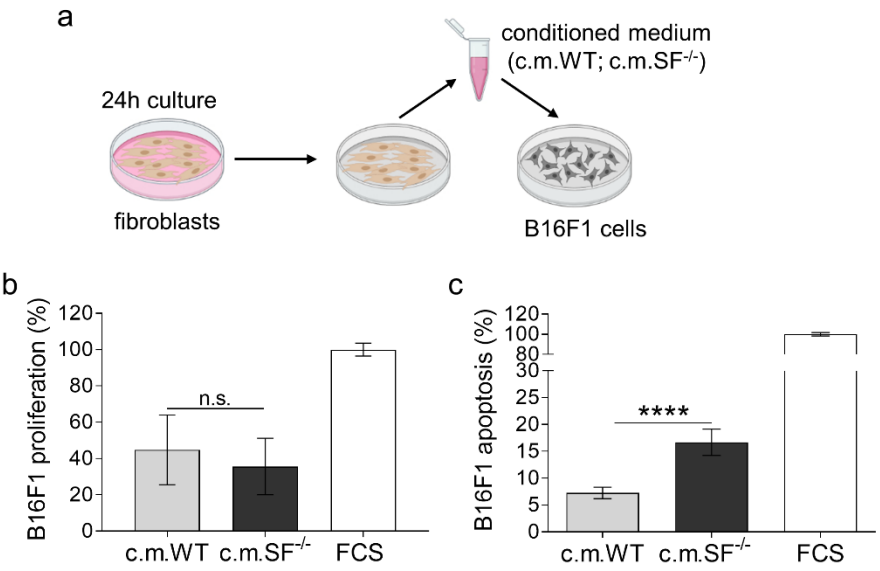

Figure 39. Analysis of melanoma cell proliferation and apoptosis in fibroblast conditioned medium.
(a) Schematic representation of experimental settings (MMP14$^{Sf+/+}$ fibroblast media, c.m. WT; MMP14$^{Sf-/-}$ fibroblast media, c.m. SF$^{-/-}$). (b) Proliferation assay and (c) apoptosis assay of B16F1 cells grown in fibroblast conditioned medium. Mean +/- SD; Experiments were performed in triplicates and repeated 5 - 7 times; ****p<0.0001.

After culture in fibroblast c.m. for 24 hours, melanoma cell proliferation was almost comparable in MMP14$^{Sf-/-}$ and control c.m. (Figure 39b). On the contrary, melanoma apoptosis was significantly increased when cultured with c.m. from MMP14-deficient fibroblasts compared to control (Figure 39c). Thus, soluble factors secreted by

fibroblasts in the absence of MMP14 induce melanoma cell death without affecting cellular proliferation.

3.7.4.2 Analysis of soluble factors in fibroblast conditioned medium

To identify factors in the fibroblast MMP14$^{Sf-/-}$ c.m. responsible for the increased cell death of melanoma cells, we investigated the data obtained from the proteome analysis of fibroblast matrix and supernatant (section 3.7.1). Several growth factors were identified, but none displayed significant alterations in fibroblast matrix or c.m. in the absence of MMP14 (Table 6). However, it is possible that by mass spectrometry, cytokines present in low quantity and of lower molecular weight compared to other proteins are not detected [328].

Table 6. Identified growth factors in proteome analysis of fibroblast matrix and conditioned medium.

	matrix			conditioned medium		
Protein	WT	SF$^{-/-}$	p-val	WT	SF$^{-/-}$	p-val
angiopioetin 2	-	-	-	27,11	0	0,01
angiopioetin 4	26,71	27,89	0,48	-	-	-
ccl11/eotaxin	-	-	-	27,24	27,35	0,95
FGF7	-	-	-	25,78	26,12	0,77
HDGF	-	-	-	29,38	29,45	0,86
HGF	26,62	26,47	0,79	29,49	30,95	0,08
IGFBP2	-	-	-	31,64	30,54	0,36
IGFBP5	27,43	25,69	0,28	30,83	30,61	0,80
IGFBP6	26,76	26,97	0,73	33,14	32,75	0,28
IGFBP7	28,90	27,33	0,12	33,03	32,49	0,49
MMP3	-	-	-	30,67	32,08	0,42
PDGF D	27,45	27,66	0,68	27,98	27,96	0,97
TGF β3	-	-	-	24,29	24,77	0,89
VEGF A	-	-	-	26,01	26,58	0,08
VEGF D	-	-	-	29,36	30,39	0,41
Wisp 1	27,35	25,41	0,09	27,85	27,25	0,28

However, using a mouse cytokine antibody array® for semi-quantitative detection of 111 mouse proteins (Figure 40a), we identified some cytokines that were altered in MMP14$^{Sf-/-}$ compared to control cell media. These include endothelial cell regulators such as angiopoietin 2, proliferin and CCL11/eotaxin (Figure 40a and b). Moreover, several proteins promoting cell survival, proliferation, and migration were decreased in MMP14$^{Sf-/-}$ c.m. compared to control such as IGFBP 5, IGFBP 6, Fetuin-A, and Wisp

1. In addition, the proinflammatory cytokines CXCL1/GROα, and MMP3, which we have shown to be increased in the skin of MMP14$^{Sf-/-}$ mice in earlier investigations (unpublished data from the laboratory), were up-regulated in MMP14$^{Sf-/-}$ as compared to control c.m. (Figure 40b).

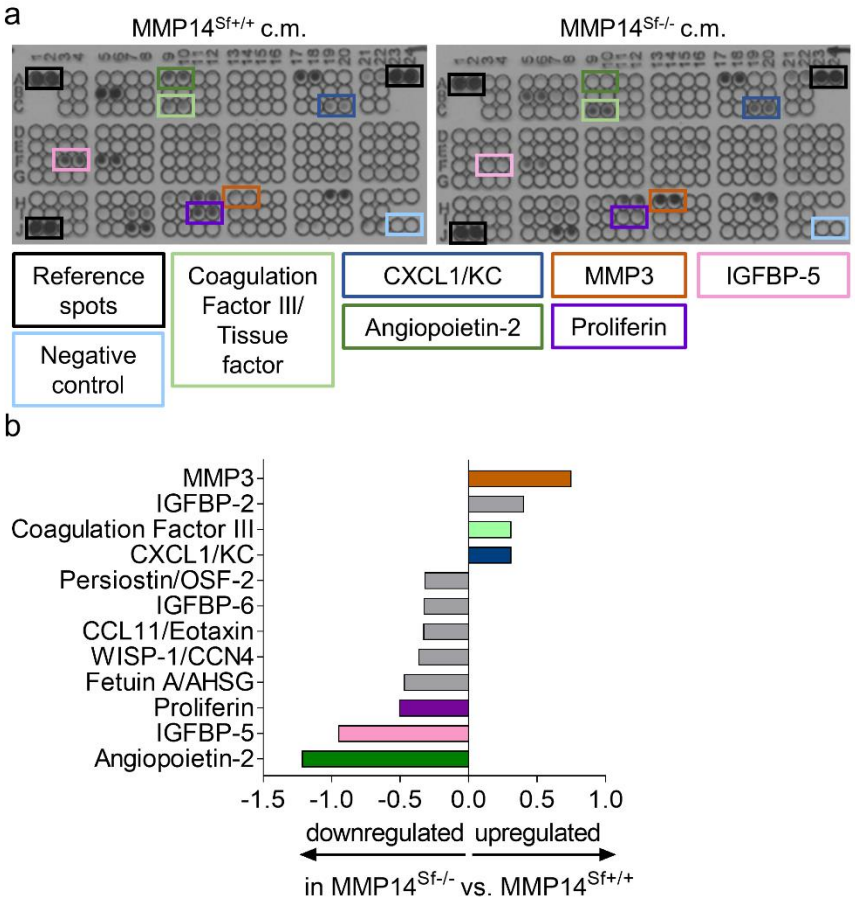

Figure 40. Cytokine antibody array.
(a) Arrangement of antibody spots on nitrocellulose membrane. Colored boxes mark highly regulated proteins on the membrane. (b) Quantified antibody signals from nitrocellulose membrane for mostly regulated proteins. Colored columns correspond to highly regulated proteins marked with colored boxes on the membrane.

3.7.4.2.1 GROα and MMP3 in melanoma apoptosis

Both proteins, GROα and MMP3, have been implicated in the regulation of apoptosis in several cell types [329-332]. Consequently, we wanted to investigate if the upregulation of those proteins, secreted by MMP14-deficient fibroblast, mediates increased melanoma cell death (Figure 39).

In preliminary investigations, we used a pharmacological approach, in which we reduced the catalytic activity of MMP3 by adding a specific cell-permeable hydroxamate-based inhibitor (MMP3i) [333] to MMP14$^{Sf-/-}$ fibroblast c.m. before B16F1

melanoma cell treatment. Melanoma cells irradiated with 0.1 J/cm^2 UV-B, thereby undergoing apoptosis [334], were used as positive controls. However, the addition of MMP3i to MMP14$^{Sf-/-}$ c.m. did not rescue the MMP14$^{Sf-/-}$ fibroblast-induced melanoma cell apoptosis (Figure 41a), indicating that increased activity of MMP3 in the c.m. from MMP14-deficient fibroblasts does not mediate this process.

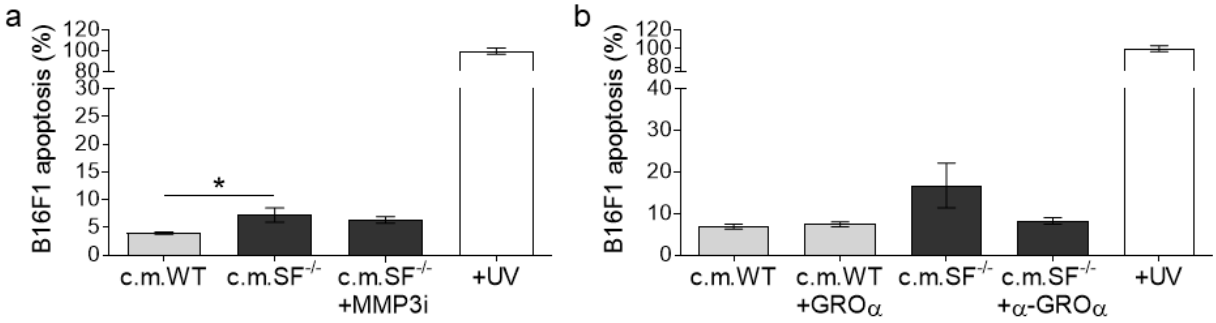

Figure 41. Apoptosis assays of B16F1 cells grown in MMP14$^{Sf-/-}$ c.m. with MMP3i and α-GROα. B16F1 cells grown in MMP14$^{Sf-/-}$ fibroblast conditioned medium (c.m. SF$^{-/-}$) with (a) an inhibitor for MMP3 (MMP3i), (b) a neutralizing antibody for GROα (α-GROα) and MMP14$^{Sf+/+}$ fibroblast conditioned medium (c.m. WT) with recombinant GROα. Mean +/- SEM. Experiments were performed in triplicates and repeated 2-3 times. *p< 0.05.

Another possible mediator of apoptosis is GROα. We used two approaches to investigate GROα implication in the pro-apoptotic effect of MMP14$^{Sf-/-}$ c.m.. We added recombinant GROα to c.m. from control fibroblasts in the first one. Secondly, we used a neutralizing antibody to GROα (α-GROα).

Neutralizing GROα activity in MMP14$^{Sf-/-}$ c.m. decreased melanoma cell death, although not significantly. Since a control isotype antibody was not included in these experiments, excluding an unspecific effect of the α-GROα antibody is impossible. Furthermore, increasing GROα levels in the MMP14$^{Sf+/+}$ c.m. did not alter cellular apoptosis (Figure 41b). These data indicate that GROα in MMP14$^{Sf+/+}$ c.m. is likely insufficient to increase melanoma apoptosis; possibly additional MMP14$^{Sf-/-}$ fibroblast-derived factors were produced (pro- or anti-apoptotic) that we have not identified herein.

3.8 Is deletion of MMP14 in fibroblasts negatively affecting the growth of epithelial tumors?

Over the last years, growth and progression of many tumors were often associated with enhanced collagen deposition, altered fiber organization, and the resulting

increased stiffness [138]. Disorganized collagen and increased tissue stiffness in breast cancer can trigger tumor transformation, leading to enhanced growth and invasiveness [126]. Moreover, the effect of collagen on tumor cell proliferation has been shown for many cancer cells of epithelial origin like prostate, pancreatic cancer, or squamous cell carcinoma [127-129]. Our experiments with melanoma showed that all these matrix changes might affect melanoma growth differently. Thus, the question arose whether the development of the epithelial type of tumors in our mouse model is also altered due to MMP14 deletion in fibroblasts, the matrix alterations in the environment, or both. To address that, we used another tumor cell type, namely murine cutaneous squamous carcinoma cells (BDVII cells [266]), and assessed the effect of stromal deletion of MMP14 and the derived dermal matrix modification on the growth of these epithelial tumor cells.

3.8.1 BDVII cell invasion in *ex vivo* skin composites

To investigate the role of differential matrix modification in MMP14$^{Sf-/-}$ mouse skin in squamous cell carcinoma cell growth, we used *ex vivo* invasion approaches with devitalized and decellularized skin biopsies, as described earlier (3.1.2.).

BDVII cells were seeded on the de-epidermized and devitalized skin biopsies (DDS) of MMP14$^{Sf-/-}$ and control mice, and incubated for three weeks. Immunofluorescence staining for keratin 6, a marker for squamous differentiation [335], shows BDVII cells on top and within the DDS (Figure 42a, left). Tumor cells could invade the DDS of both genotypes but formed tendentially larger tumor nests (white arrowhead) in MMP14$^{Sf-/-}$ compared to control biopsies (Figure 42a). However, neither proliferation (Ki67) nor cell apoptosis (cleaved caspase 3) in these tumor nests were altered in both genotypes (Figure 42b). Furthermore, proliferation and apoptosis of BDVII cells grown on the basement membrane site of the DDS composite displayed a tendential but not significant increase in MMP14$^{Sf-/-}$ compared to control composites. Therefore, the increased size of BDVII nests within the DDS of MMP14$^{Sf-/-}$ mice could result from enhanced numbers of cells invading the dermis rather than increased cell proliferation within the tumor nests. The growth of BDVII cells was further investigated using decellularized skin biopsies of MMP14$^{Sf-/-}$ and control mice to exclude the influence of cellular remains, thus focusing principally on the matrix scaffold.

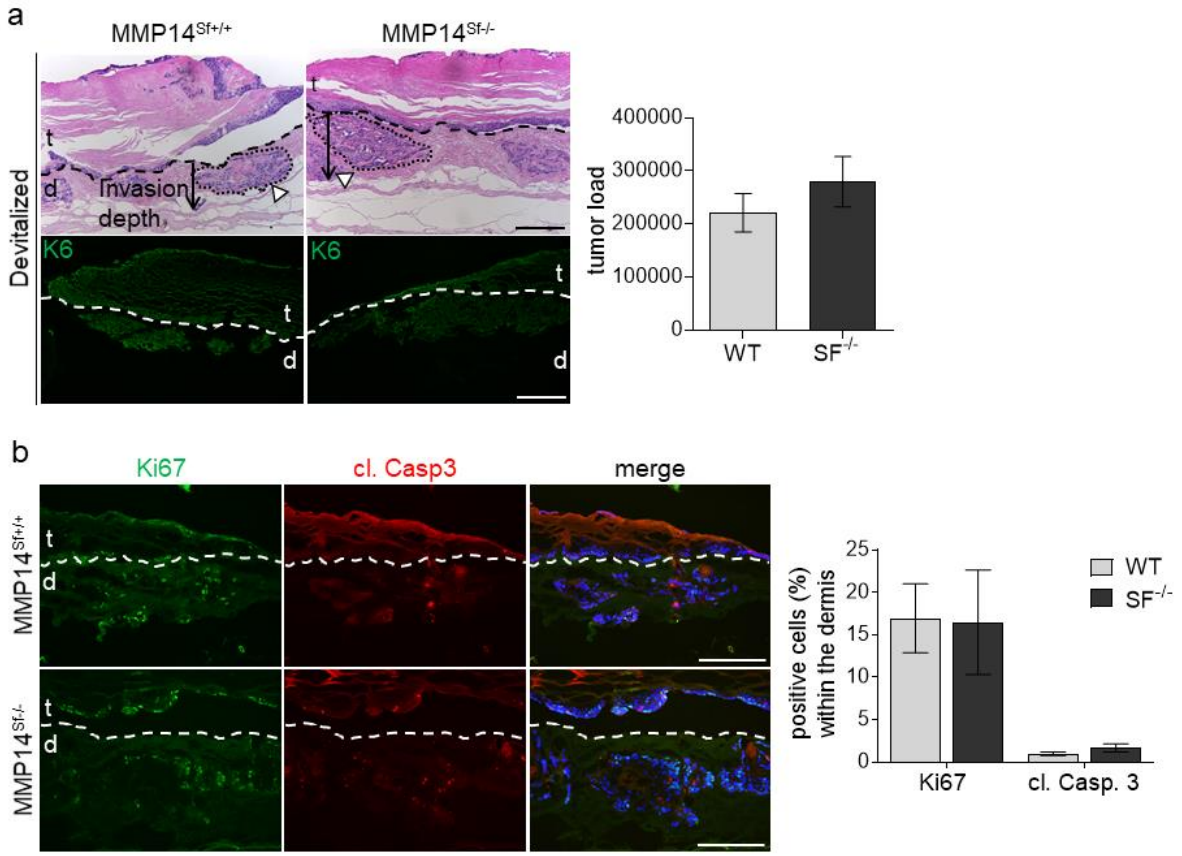

Figure 42. *Ex vivo* DDS assay with BDVII cells.
(a) H&E and Keratin 6 (K6) staining of DDS sections after three weeks of BDVII cell invasion (left). The dashed black line marks the border between BDVII cells and dermis, and grown tumor nests (white arrowhead) in the dermis are marked by a dotted line (H&E). The graph (right) depicts the quantified tumor area in µm^2 per µm^2 specimens. (b) Ki67 and cleaved (cl.) caspase 3 immunofluorescences staining of tumor-DDS sections (left). Quantification of the average ratio of positive cells (right). Mean +/- SEM; MMP14$^{Sf+/+}$ (WT; control) n=4; MMP14$^{Sf-/-}$ (SF$^{-/-}$) n=4; DDS=de-epidermized devitalized skin; t=tumor; d=dermis; scale: 200µm.

After incubation of three weeks, DDS of both genotypes were invaded by BDVII tumor cells that formed larger tumor nests in MMP14$^{Sf-/-}$ compared to control (white arrowhead; Figure 43a). Cellular proliferation (Ki67) and apoptosis (cleaved caspase 3) within the tumor nests were not altered in both genotypes (Figure 43b). Unfortunately, quantifying proliferating and apoptotic cells on top of the DDS was impossible because of technical reasons; during the processing of all specimens, cell layers of cells grown on top of the basement membrane side were washed out.
However, altogether, these data suggest that the ECM-rich skin of MMP14$^{Sf-/-}$ mice positively affects the growth of squamous carcinoma cells.

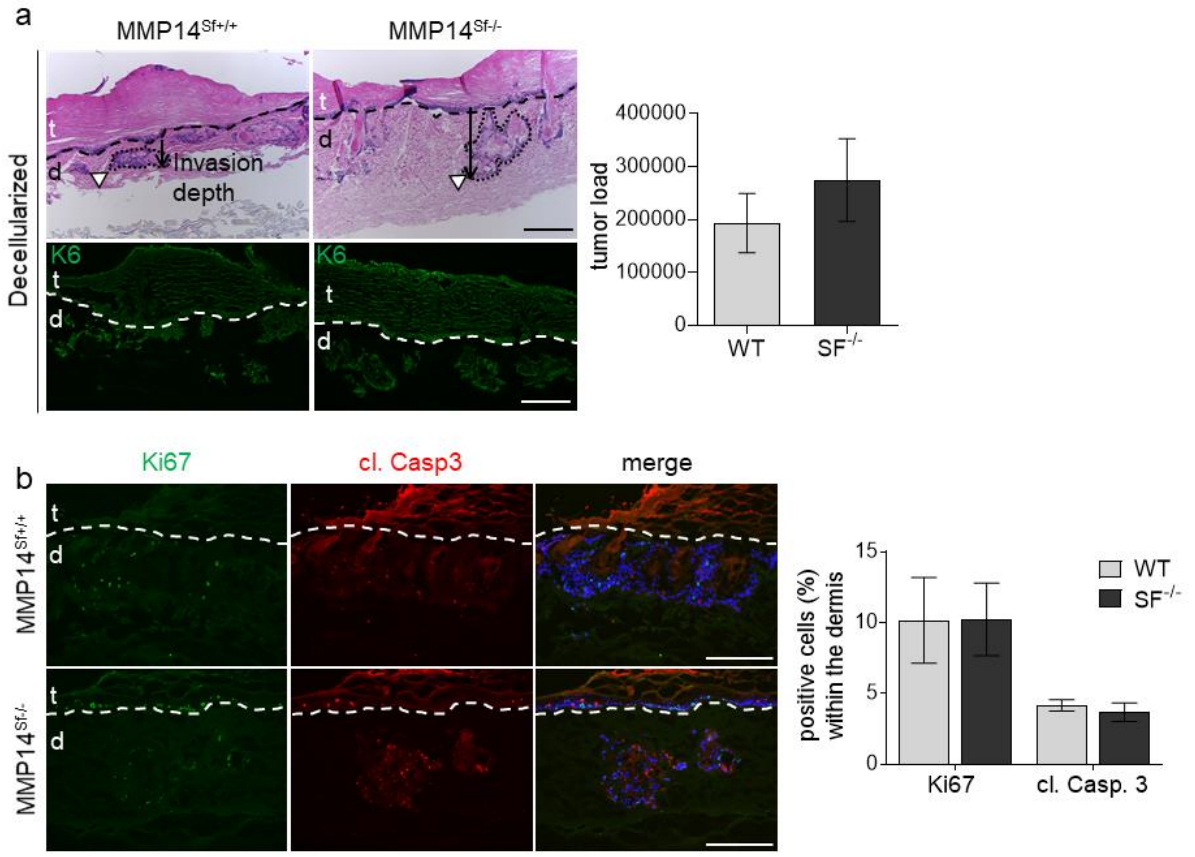

Figure 43. *Ex vivo* decellularized skin assay with BDVII cells.
(a) H&E and Keratin 6 (K6) staining of skin sections after three weeks of squamous cell carcinoma cell invasion (left). The dashed black line marks the border between BDVII cells and dermis, line and invading tumor nests (white arrowhead) in the dermis are marked by a dotted line. The graph (right) depicts the quantified tumor load in µm^2 per µm^2 skin. (b) Ki67 and cleaved (cl.) caspase 3 immunofluorescence staining of decellularized skin assay sections (left) and quantification of the average ratio of positive cells (right). Mean +/- SEM; MMP14$^{Sf+/+}$ (WT; control) n=6; MMP14$^{Sf-/-}$ (SF$^{-/-}$) n=6; t=tumor; d=dermis; scale: 200µm.

3.9 Altered ECM composition of peritumoral tissue due to deletion of ADAM9

During my doctoral work I have also contributed to the work initiated by Anna N. Abety, a former Ph.D. student of the group, investigating the ADAM9-dependent ECM modifications in the peritumoral tissue of B16F1 melanomas [336].

The A disintegrin and metalloproteinase 9 (ADAM9) has been described as up-regulated in several cancers, including melanoma, promoting their progression [337-341]. Moreover, ADAM9 is strongly expressed in the peritumoral tissue, where it modulates the expression of signal molecules and cleaves ECM proteins [268, 342, 343]. In this study, I analyzed *in vitro* in lysates and supernatants of primary fibroblasts from control and ADAM9-deficient mice the expression of ECM proteins that were found regulated around the melanomas grown in the ADAM9 deleted mice.

These ECM molecules included decorin and collagen type I and the collagenolytic proteases MMP13 and MMP14. The studies were conducted using primary fibroblasts cultured alone as a monolayer or in indirect co-culture, using conditioned medium (c.m.) from B16F1 melanoma cells.

The overall results of the entire study showed that ADAM9, modifying the peritumoral ECM composition, regulates B16F1 melanoma growth [336]. Proteome analysis of the tumor- stroma revealed 53 differentially expressed proteins, including six strongly altered ECM proteins exerting at least a two-fold altered expression in ADAM9$^{-/-}$ fibroblasts compared to control. Among these, collagen type I, collagen type V and decorin were up-regulated, while collagen type III, XIV, and fibronectin were down-regulated in ADAM9$^{-/-}$ peritumoral tissue compared to control. In healthy skin, these ECM proteins were not altered in both genotypes. *In vitro*, in supernatants from monolayer cultures of ADAM9-deficient and control fibroblasts, immunoblot analysis identified a low molecular weight form of decorin (40 kDa) that was not present in lysates. Further, collagen type I levels were increased in ADAM9$^{-/-}$ fibroblast matrix and supernatant compared to control. This enhancement was also detected in indirect co-cultures of fibroblasts and B16F1 melanoma cells c.m.. Interestingly, in supernatants of untreated control fibroblasts, we noticed a 70 kDa fragment of collagen type I that was poorly detected in ADAM9$^{-/-}$ fibroblasts. Using a recombinant approach, collagen type I was identified as an ADAM9 substrate, with ADAM9 processing collagen type I, resulting in the generation of a 70 kDa fragment, whose identity was further verified by peptide mass fingerprint analysis of tryptic fragments. However, ADAM9 did not degrade collagen type I fragments. The increased collagen type I amounts detected in ADAM9$^{-/-}$ fibroblast lysates and supernatants are most likely caused by reduced collagenolysis by other proteases such as MMP13 and -14 [344]. In support of this, in ADAM9-deficient fibroblasts, the expression of MMP13 and MMP14 was reduced compared to controls. Supplying collagen type I as soluble or immobilized form to melanoma cells stimulated proliferation when its concentration was at a maximum of 10 µg/ml. At the same time, it reduced cell proliferation continuously when supplied at higher concentrations. In summary, these data show that ADAM9 regulates melanoma growth by influencing the composition of the peritumoral ECM and thereby modulating melanoma cell proliferation. These data further support the negative role of high collagen on melanoma proliferation that I investigated in my work with the MMP14$^{Sf-/-}$ mice.

4 Discussion

4.1 Regulation of melanoma growth by fibroblast-derived MMP14 *in vivo*

Malignant melanoma is a rare but very severe form among skin cancers. It spreads rapidly and leads to most skin cancer deaths [3, 345]. Although many different therapeutic approaches have been developed and applied, they are still not sufficient to improve the poor survival prognosis of patients [346-348]. In the last years, several reports highlighted the pivotal role of the tumor microenvironment (TME) in cancer growth and progression, thus indicating that tumor growth is not a cancer cell-autonomous mechanism but results from complex interactions with stromal cells of the TME. Cancer-associated fibroblasts (CAFs) can modulate tumor growth by providing factors and remodeling the ECM. Depending on tumor type, stage and tissue, CAFs can either promote tumor growth [46, 78] or suppress it by inhibiting the growth and metastasis of tumor cells [349]. These cells are the primary producer and modifier of the extracellular matrix (ECM) in the TME, whose role in tumor progression has been emphasized over the past years [82, 84]. Increased expression and activation of MMPs by CAFs allow them to remodel the ECM to promote tumor growth [350, 351].

MMP14 is up-regulated in multiple types of cancer and was associated with tumor progression and poor patient outcomes [235, 236]. In melanoma, MMP14 is expressed in the early stages of development and increases progressively with tumor growth [257, 352]. While several studies describe the contribution of melanoma cell-derived MMP14 to cancer development [257, 261, 353], very little is known about the function of fibroblast-MMP14 in this context. Previous studies of our group showed that fibroblast-derived MMP14 is critical for adult tissue homeostasis [233]. Specific deletion of MMP14 in dermal fibroblasts ($MMP14^{Sf-/-}$) resulted in increased dermis thickness with enhanced collagen accumulation and tensile strength due to disturbed collagen degradation [233]. The present work aimed to unravel the cell-specific function of MMP14 produced by stromal cells and the structural microenvironment generated upon its loss for development, growth, and metastases formation of melanoma *in vivo* and *in vitro*. Using an *in vivo* grafting model, we could show that melanoma growth is reduced in mice's collagen-rich and stiff skin, harboring the fibroblast-specific deletion of MMP14. Although tumor growth in $MMP14^{Sf-/-}$ differed from control animals, numbers of metastases were not altered compared to control. Even though surprising, these data could be explained in light of previous studies on human melanoma patients. The authors demonstrated that melanomas start metastasizing at differing thicknesses,

depending on their growth rate rather than tumor size [354]. This would suggest that the growth rate of tumor cells within the tumors in MMP14$^{Sf-/-}$ mice would be similar to that of controls. However, this was not the case, as melanoma cell proliferation in MMP14$^{Sf-/-}$ mice was reduced. One can deduce that fibroblast-MMP14 is either compensated by the activity of additional stromal proteases or is unnecessary, and the activity of the melanoma-derived MMP14 is more relevant for metastasis. Indeed, using a metastasis model, blocking MMP14 in mice using a specific antibody resulted in reduced formation of melanoma metastases [355]. Reduced melanoma growth in MMP14$^{Sf-/-}$ mice may result from reduced vascularization of the tumor and the peritumoral tissue. Decreased intratumoral hypoxia paralleled this. Reduced melanoma proliferation observed in MMP14$^{Sf-/-}$ tumors is possibly the consequence of reduced hypoxia and vascularization. Indeed, tumor vascularization and hypoxia are processes that are associated with cancer progression and enhanced to promote tumor growth [356, 357]. Hypoxia-dependent increase of Hif 1-α induces expression of VEGF that leads to recruitment of angiogenic cells [358]. In line with those data, loss of Hif-1 causes reduced vascularisation and tumor growth [358]. In melanoma, increased tumor cell proliferation was induced by increased Hif 1-α and CD31 levels in these cells [359-361].

Also, increased matrix density, as observed in peritumoral tissue of MMP14$^{Sf-/-}$ mice, can decrease angiogenesis [362]. In addition, increased matrix stiffness independent of matrix density results in angiogenic outgrowth, invasion, and neovessel branching [362]. These data would explain why, at the late point of melanoma growth, when differences in peritumoral stiffness were comparable in both mice genotypes, we detected reduced vascularization in the peritumoral areas of MMP14$^{Sf-/-}$ mice.

Although CAFs are considered regulators of tumor angiogenesis by secreting growth factors, such as VEGF [363], they were not altered in MMP14$^{Sf-/-}$ peritumoral tissue. However, CAFs may contribute to tumor angiogenesis by degrading the tumor surrounding ECM [138] and release thereby activating growth factors embedded in the ECM, or generate bioactive matrix fragments, matrikins [148, 364], to affect melanoma proliferation and invasion. Even though we did not detect altered expression of growth factors in the proteome analysis of peritumoral areas, we cannot completely exclude the possibility that the release of bound growth factors is altered in MMP14$^{Sf-/-}$ and contribute to reducing the growth of melanoma. However, the *ex vivo* invasion experiments with decellularized or devitalized mouse skin further support the

assumption that structural changes of MMP14$^{Sf-/-}$ ECM are critical for reducing melanoma growth. The dermis of MMP14$^{Sf-/-}$ mice possibly restrains the growing melanoma nests impeding them from rearranging the adjacent ECM to overcome the resisting forces of the surrounding matrix. In peritumoral tissues, MMP14 can activate MMP2 and MMP13, two collagenases that have been associated with melanoma progression [365-367]. As deletion of MMP14 leads to diminished activity of MMP2 [233] and MMP13 [368], reduced growth and expansion of melanoma nests in MMP14$^{Sf-/-}$ mice as compared to control is probably the result of decreased local proteolysis by these enzymes.

4.2 Melanoma growth is modulated by collagen abundance and tissue stiffness

Collagen is a significant component of the TME and influences tumorigenesis on a molecular and cellular level [90, 295, 369]. In melanoma, the influence of peritumoral collagen on the tumor is still contradictory. While in some cases, high collagen amounts are found around the tumor [370], pointing to a tumor-supporting effect, in others, it seems to have a minor role [371] or has a tumor-suppressive function [122, 321, 372]. This may depend mainly on the properties of collagen, such as density and structural arrangement, caused by cross-linkage, which may modulate the stiffness of the tissue [138].

Tightly packed and aligned collagen fibers are found at the invasive front of several tumors [130, 133]. They can adopt a perpendicular orientation to the tumor, referred to as tumor-associated collagen signatures (TACS), and facilitate invasion and migration [131]. Analysis of collagen in MMP14$^{Sf-/-}$ mice peritumoral areas by second harmonics generation (SHG) showed that collagen fibers were wavy in the skin in peritumoral tissue of either genotype. They aligned parallel instead of perpendicular to the tumor. That is consistent with the fact that the number of metastases, thus cellular invasion, was not altered. Another feature of the TACS is the enhanced accumulation of collagen [131]. This feature was present in the peritumoral tissue from fibroblast MMP14-deficient mice. In these tissue areas, transcript levels of the two enzymes catalyzing collagen cross-linkage and lysyl residue hydroxylation, LOX and LH2, were not changed, which agrees that numbers and pattern of collagen cross-links were not altered in either genotype. However, the skin of MMP14$^{Sf-/-}$ mice and the peritumoral areas up to day six post tumor grafting were significantly stiffer than control [233, 280]. Besides enzyme-driven cross-linkage, sugar metabolites can modify collagen fibers,

leading to a non-enzymatic cross-linking process called glycation [373]. This modification usually occurs overtime during the aging process and in a smaller ratio than crosslinks formed by LOX [104, 373, 374]. Since we used young mice for our experiments, it is unlikely that glycation is the main reason for the increased tissue stiffness of MMP14$^{Sf-/-}$ mice, but we cannot entirely exclude its contribution. An additional alternative stimulus leading to tissue stiffening is solid stress resulting from internal forces of the growing tumor that stretching the ECM enables the tumor to expand [375, 376]. In melanoma of MMP14$^{Sf-/-}$ mice being cell proliferation and accordingly tumor expansion reduced, the tumor mass may push against the surrounding tissue with lower force. This leads to minor stretching and to reduced stiffness in the peritumoral tissue.

The reduced melanoma proliferation was detected *in vivo* and *in vitro* in 2D and 3D cultures. Of note, we did not observe the anti-proliferative effect when melanoma cells were cultured on monomeric collagen type I, but only when they were cultured on or embedded in fibrillar collagen, indicating a specific role for fibrillar collagen structure in this process. Since cell entry into the cell cycle is regulated by cell binding to the ECM [377, 378], collagen and its conformation may regulate this process differently depending on the types of cell interactions elicited. Fibrillar collagen type I has been shown to impair α2β1 integrin-mediated adhesion to the matrix [278]. Moreover, that interaction reduces cellular proliferation by up-regulating cdk2 and p27^{KIP1,} leading to arrest of the G_0/G_1 stage of the cell cycle in arterial smooth muscle, lung mesenchymal, and malignant melanoma cells [278, 379, 380]. In melanoma cells, the alternative collagen receptor, discoid domain receptor 2 (DDR2), is responsible for the induction of cell cycle arrest in the presence of fibrillar collagen. At the same time, its downregulation allowed cells to proliferate [381]. Integrin receptors also function as cellular sensors for mechanical changes in their environment. Once engaged, they lead to intracellular translocation of YAP and TAZ to the nucleus, where transcription of pro-proliferative genes is initiated [382]. Also, MMP14 by mediated degradation has been implicated in pathways involving YAP/TAZ molecules. MMP14-mediated processing of the pericellular matrix was shown to induce changes in cell shape and to activation of β1-integrin signaling leading to the nuclear localization of YAP and TAZ in the control of skeletal stem cells commitment [383]. Although we have not analyzed it, it is possible that in fibroblasts in the absence of MMP14, sensing is disturbed and leads *in vivo* to reduced expression of pro-proliferative factors.

We could envision that melanoma cells *in vitro* may have reduced expression of β1-integrins, occurring in other cells when cultured on fibrillar collagen type I [278], leading to altered YAP/TAZ translocation to the nucleus. That results in a lack of transcription of pro-proliferative genes [382] and cell cycle arrest [278], thus inhibiting melanoma cell proliferation. In addition, in the *in vivo* situation, it is possible that in control mice, proteolytic ECM fragments generated by fibroblast-MMP14 co-activate β1-integrin signaling in melanoma cells to a greater extent than in MMP14$^{Sf-/-}$ mice, resulting in reduced proliferation in MMP14$^{Sf-/-}$ mice.

The negative proliferative effect of high collagen in melanoma was substantiated further by our *in vivo* experiments showing that melanoma cell growth in induced-fibrotic skin was most significantly inhibited. The negative impact of increased tissue rigidity and collagen abundance on melanoma proliferation in mice is also supported by several observations made in patients. For instance, desmoplastic melanoma, associated with an extensive fibrous ECM, has a better prognosis than nodular melanoma exhibiting lower matrix accumulation [384]. Further, 30% of partly or entirely regressive human melanomas show lymphocyte infiltrates and leave fibrotic, “scar-like” areas. Whether these result from the regression of melanoma or contribute to it is unknown [385, 386]. It was also reported that patients with scleroderma, a fibrotic disease, have a higher risk of developing non-melanoma types of tumors, but not melanoma [387]. These data point to an antagonistic relationship between melanoma and fibrotic skin, implying that melanoma growth is not promoted in ECM and collagen-rich areas.

On the contrary, abnormal deposition and accumulation of collagen combined with increased tissue stiffness are among the main characteristics of solid tumors, mostly of epithelial origin with a bad prognosis [89, 138]. In support of this, cutaneous squamous carcinoma cells grown in collagen-rich areas of the MMP14$^{Sf-/-}$ skin displayed enhanced growth. Comparably, increased collagen stiffness showed a pro-tumor effect on the proliferation and invasion of oral squamous cell carcinoma cells [127, 388]. Although our data would suggest that accumulation of collagen in MMP14$^{Sf-/-}$ skin is the primary reason for reduced melanoma growth, we cannot exclude that the absence of MMP14 may also lead to additional, yet unidentified, alterations in cells or tissue impacting melanoma growth.

4.3 Deletion of MMP14 in fibroblast modulates their proteomic profile

4.3.1 Alterations in secreted and deposited matrix

Fibroblasts/CAFs are the primary producers of the ECM and essential regulators of the TME [46, 75], with MMP14 being a significant protease involved in the degradation and remodeling of several matrix proteins [210]. We confirmed the essential role of MMP14 as a matrix modifying protease by proteome analysis, showing that in matrix and supernatant of MMP14 deficient fibroblasts, some ECM proteins were altered. In matrix and cell supernatants of MMP14$^{Sf-/-}$ fibroblasts, laminin subunits α-2, α-5, and β-2 were significantly downregulated, but no γ chains were altered. This was contrary to our expectations, as some laminins, including laminin-1 α-1, -2/4 α-2, and -5 γ-2 [252, 389, 390], are documented substrates of MMP14. The α-2 subunit of the laminin-2/4 complex is cleaved by MMP14 in the basement membrane of skeletal muscle [390]. However, in the skin, while fibroblast-derived laminin 2 (laminin 211) is a component of the basement membrane of the skin [391], laminin 4 (laminin 221) is not, and it is not known yet, if laminin 211 singularly is processed by MMP14 as well. In addition, laminins containing the α-5 subunit are laminins 511, 521, 522, and 523 [392], which are not documented as MMP14 substrates. Further, laminin 522 is primarily expressed in bone marrow [393], and laminin 523 in the retina and the central nervous system [394]. In addition, laminin 511 and 521, although being components of the basement membrane of the skin [394, 395], are produced either by keratinocytes [391] or human embryonic stem cells [396]. These notions together explain why we did not detect macroscopic alterations in the basement membrane of the skin of the MMP14$^{Sf-/-}$ mice *in vivo*. Possibly, *in vivo,* the altered expression of those laminin subunits is compensated by other cells so that no apparent phenotype is generated. Besides laminins, additional structural proteins altered in matrices and supernatants of MMP14-deficient fibroblasts were collagens, including types I, III, VI, VIII, XI, XIV, XV, XVI.

4.3.2 Role for collagens remodeling in melanoma

Collagen type I, which we previously found increased in the MMP14$^{Sf-/-}$ animals [233], showed only modest and not significant upregulation. A comparable result was observed in the proteomic analysis of peritumoral tissue. A possible explanation for these discrepancies is the reduced solubility since several components of the ECM, and collagen type I is a significant part, are resistant to solubilizing agents such as

SDS and urea [397]. In support of this, further stepwise solubilization of the insoluble pelleted fraction with high salt buffers led to enhanced extraction of collagen type I.

Among the up-regulated collagens, we found collagen type XIV. This was increased in the deposited matrix and the soluble secreted protein fraction from MMP14$^{Sf-/-}$ fibroblasts. This collagen is fibril-associated with interrupted triple helices (FACIT) [398]. It occurs in tissues of high mechanical stress where it binds packed collagen type I fibrils and regulates collagen fiber assembly [318, 324, 399]. While, in cancer, collagen type I is considered an essential component of the ECM, still very little is known about the biological role of collagen type XIV in this context. Collagen type XIV is expressed mainly in differentiated and less proliferative tissues [400, 401], and in agreement with this, collagen type XIV deficiency leads to increased cardiomyocyte proliferation [402]. A comparable inhibitory effect on proliferation was detected towards fibroblasts, vascular smooth muscle cells, and human leukemia and fibrosarcoma cells [400, 403, 404]. In line with this, we found that collagen type XIV dose-dependently inhibited melanoma cell proliferation and antagonized the pro-proliferative effect of FCS or fibroblast-derived matrix. However, the mechanism controlling collagen type XIV's inhibitory effect towards proliferation is unknown. Besides that, we could also show that on collagen type XIV, melanoma cell migration is low, and, similarly to proliferation, it can antagonize melanoma migration on the fibroblast matrix.

One possible reason for the reduced melanoma migration on collagen XIV may be altered substrate recognition by the cell receptors rather than the availability of binding sites. In further support of that is the observation that melanoma cells' adhesion to collagen type XIV coatings was reduced. The cellular receptors for collagen type XIV are membrane-bound heparan sulfate proteoglycans (HSPGs) [405] and a chondroitin-dermatan sulfate variant of CD44, expressed mainly by fibroblasts and by hematopoietic cells [406]. These can bind collagen type XIV at its FN-III domain [407], and heparin or proteoglycans, such as decorin, can block this binding site preventing cell adhesion [400, 408]. In our approach, it is unlikely that the collagen type XIV binding site was blocked because no paralleled altered expression levels of heparin or decorin were detected in the proteome analysis of the MMP14$^{Sf-/-}$ fibroblast matrix. In addition, the adhesion of cells to recombinant collagen type XIV alone was also low. Therefore, it is likely that melanoma cells do not efficiently bind to the substrate rather than altered availability of the binding site on collagen type XIV.

Both collagen XIV receptors are expressed by melanoma cells, including in different variants of B16 cells, and can modulate cellular processes, such as proliferation, migration, adhesion, and differentiation [409-416]. It is unknown if the expression of these receptors was altered under the given conditions in the melanoma cells we used in this work, as we have not addressed this issue in this project. However, it is known that the interaction of cells with the ECM can influence the localization of HSPGs [412], as shown for corneal fibroblasts cultured on fibronectin. This interaction, and less that to collagen type I, led to more HSPGs in the nucleus [417]. Since HSPGs bind both fibronectin [418, 419] and collagen type XIV [407] through the FN-III domain, it is possible that nuclear trafficking also occurs when melanoma cells bind to collagen type XIV. Thereby, in the presence of increased collagen type XIV, as seen in the MMP14$^{Sf-/-}$ fibroblasts matrix, possibly more nuclear trafficking of HSPG is induced. This could lead to reduced expression of the receptors at the cell surface and reduced melanoma cell adhesion. In addition, several specific post-translational modifications of these receptors that occur during their syntheses, such as glycosylation, deacetylation, and sulfation, regulate their function and could result in altered tumor cell proliferation, apoptosis, or differentiation [420, 421]. However, this was not investigated and could be a perspective for future analysis.

Despite these, migration of melanoma cells into the collagen type XIV enriched skin of the MMP14$^{Sf-/-}$ mice was not altered, pointing to a compensatory effect from additional proteins present in the complex tumor microenvironment. *In vitro* in 2D-cultures, cells predominantly use the mesenchymal migration mode assuming a spindle-shaped morphology, form lamellipodia and are integrin-dependent [93]. When migrating into the dermis, cells are embedded in a three-dimensional matrix that can move by the amoeboid migration mode. This last is characterized by the formation of pseudopodia and movement independent of binding [422]; cell deformation allows them to move through even narrow spaces [423]. When using the mesenchymal migration mode, cells express proteases, such as MMPs, to proteolytically degrade the adjacent matrix, clear paths, and move through [424, 425]. This work showed that collagen type XIV could be processed by MMP14 [325], and in its absence, collagen type XIV accumulates in the MMP14$^{Sf-/-}$ fibroblast matrix. Although melanoma cells express MMP14, this may be insufficient to process the high amounts of collagen and release cells from its inhibitory effect. In addition, increased amounts of collagen type XIV in the MMP14$^{Sf-/-}$ fibroblast matrix might stabilize the co-expressed collagen type I fibrils,

impeding melanoma-MMP14 to form paths. In line with this, it has been suggested that collagen type XIV influences collagen type I deformability leading to inhibition of fibroblast migration into collagen type I gels [426].

4.3.3 Soluble factors released by fibroblasts modulate melanoma cell survival

CAFs are essential regulators in the TME that promote melanoma growth by modulating tumor cell proliferation, apoptosis, and motility by secretion of soluble factors [427-431]. Although MMP14 is known to activate a number of these factors, including cytokines, chemokines, growth factors, and other proteases [210, 213-215, 432], it is unclear how fibroblast-derived MMP14 modulates the CAF secretome to regulate melanoma growth. Besides cleavage-mediated activation of factors, MMP14 can regulate the expression of proteins through transcriptional control. Independently of its protease function, in macrophages or some cancer cells, MMP14 was shown to translocate to the nucleus and modulate the transcription of target genes that control invasion, immune response, or feedback to induce transcription [219, 221, 433].

When we treated melanoma cells with media from MMP14-deficient fibroblasts, we detected enhanced cell apoptosis, thus suggesting that, in normal conditions, either soluble factors processed by MMP14 have an anti-apoptotic effect or that MMP14 degrades factors with an apoptotic function. We identified several altered proteins with a putative role in promoting cell survival, proliferation, and migration by antibody array-based screening. Among those, two proteins, namely GROα (CXCL1) and MMP3 have functions in the context of apoptosis [329-332, 434, 435]. However, inhibiting MMP3 activity using a hydroxamic acid-based inhibitor [333] failed to rescue the apoptosis effect on melanoma cells. As a combination of proteolytic activity and nuclear translocation were shown to be required for MMP3 to induce apoptosis [329], we could also exclude a possible intracellular activity of MMP3. Although many studies attribute an apoptosis-inducing effect of MMP3 in the brain [330, 435-437] and cartilage tissue [438-440], it is possible that its activity for this function is tissue and cell-specific and does not apply to melanoma. Alternatively, increased secretion of MMP3 together with IL8 by melanoma cells has been linked to increased tumor cell invasion and metastasis [441, 442]. Since we have not found IL8 co-regulation, possibly only the combination may have an effect in these cells. However, it is unlikely that MMP3 and IL-8, when acting together, lead to apoptosis in melanoma cells, as IL-8 alone has been shown to promote melanoma growth and metastasis [443, 444].

Neutralizing of GROα in MMP14$^{Sf-/-}$ media using a neutralizing antibody could partially decrease apoptosis in melanoma cells. In support of this, it was shown that GROα could induce apoptosis in arterial chondrocytes, but this process depends on additional ECM signals [331]. In contrast, the addition of recombinant GROα into MMP14$^{Sf+/+}$ media did not affect melanoma apoptosis, indicating that GROα alone is insufficient to induce apoptosis in melanoma cells.

Further downregulated factors in the MMP14$^{Sf-/-}$ media were the insulin-like growth factor binding protein-5 (IGFBP-5) and proliferin. IGFBP-5 in myoblasts promotes cell survival by inhibiting intrinsic cell death in an IGF-dependent manner [445]. Blocking IGFBP-5 results in apoptosis induction in neuroblastoma cells [446]. Proliferin was shown to have a growth-stimulating function in smooth muscle cells and skeletal muscle [447, 448]. In addition, secreted proliferin from adipose stromal cells (ASCs) was shown to induce proliferation in human and mouse prostate cancer cell lines [449]. Therefore, reduced proliferin release by fibroblasts in the absence of MMP14 could explain the reduced proliferation observed in melanoma *in vivo* in the MMP14$^{Sf-/-}$ mice. Although I could not further investigate these molecules during my doctoral work, it would be interesting to address whether the application of the recombinant protein could reduce the potential of MMP14$^{Sf-/-}$ media to induce melanoma apoptosis. In addition, it would be essential to analyze the effect of regulating IGFBP-5 and proliferin as soluble factors on melanoma cells apoptosis and proliferation.

4.4 Therapeutic importance

The differentially modified ECM during cancer development can affect drug accessibility to the tumor and even lead to therapy resistance [450, 451]. The stiff and dense peritumoral matrix, building a physical barrier, decreases the drug supply to the tumor, which occurs mainly by diffusion [450, 451]. Collagen has been documented to protect many tumors from chemotherapy either directly by forming a shield or increasing the interstitial pressure [452, 453]. This reduces drug accessibility to cancer and results in therapy resistance [454]. Moreover, the drug's ability to reach the tumor is hampered by matrix density, reducing angiogenesis. Even though it promotes angiogenesis, matrix stiffness also leads to the contraction of existing blood vessels [362, 455]. Contrary to our expectations, fibroblast-specific deletion of MMP14 has no synergistic effect with cisplatin (platinum-based cytostatic drug) in melanoma treatment. A possible explanation for this is that cisplatin can bind to collagen fibers in

normal and tumor tissue [456], pointing to a potentially enhanced retention of cisplatin molecules by the reduced enzymatic processing of collagen accumulates in the skin of MMP14$^{Sf-/-}$ mice. However, cisplatin can also slowly be released over time, but it is unclear if it retains its biological activity [456]. Furthermore, cisplatin is a drug that binds to DNA, disturbing DNA synthesis and causing DNA damage, which results in impaired cell growth and cell death of the fastest replicating cells [315]. Thus, we cannot exclude that since tumor proliferation is reduced in MMP14$^{Sf-/-}$ mice, a reduced proliferative potential may render cells less sensitive to the treatment. In addition, it is possible that the impaired vascularization in melanomas of fibroblast MMP14-deficient mice further reduces the supply of the drug to the tumor. At last, there may be resistance to cisplatin drug treatment, which has been described for several cancers, such as ovaries, lungs, stomach, and melanoma [457, 458].

References

1. Erdmann, F., et al., International trends in the incidence of malignant melanoma 1953-2008--are recent generations at higher or lower risk? Int J Cancer, 2013. 132(2): p. 385-400.
2. Whiteman, D.C., A.C. Green, and C.M. Olsen, The Growing Burden of Invasive Melanoma: Projections of Incidence Rates and Numbers of New Cases in Six Susceptible Populations through 2031. J Invest Dermatol, 2016. 136(6): p. 1161-1171.
3. NIH, N.C.I. SEER Site Search. 2021 [cited 2021 2021]; Available from: https://seer.cancer.gov/statfacts/html/melan.html.
4. Heistein, J.B. and U. Acharya, Malignant Melanoma, in StatPearls. 2021, StatPearls Publishing Copyright © 2021, StatPearls Publishing LLC.: Treasure Island (FL).
5. Davis, E.J., et al., Melanoma: What do all the mutations mean? Cancer, 2018. 124(17): p. 3490-3499.
6. Haass, N.K. and M. Herlyn, Normal human melanocyte homeostasis as a paradigm for understanding melanoma. J Investig Dermatol Symp Proc, 2005. 10(2): p. 153-63.
7. Davies, H., et al., Mutations of the BRAF gene in human cancer. Nature, 2002. 417(6892): p. 949-54.
8. Sini, M.C., et al., Genetic alterations in main candidate genes during melanoma progression. Oncotarget, 2018. 9(9): p. 8531-8541.
9. Ellerhorst, J.A., et al., Clinical correlates of NRAS and BRAF mutations in primary human melanoma. Clin Cancer Res, 2011. 17(2): p. 229-35.
10. Colombino, M., et al., Discrepant alterations in main candidate genes among multiple primary melanomas. J Transl Med, 2014. 12: p. 117.
11. Casula, M., et al., Low Levels of Genetic Heterogeneity in Matched Lymph Node Metastases from Patients with Melanoma. J Invest Dermatol, 2016. 136(9): p. 1917-1920.
12. Kong, Y., S.M. Kumar, and X. Xu, Molecular pathogenesis of sporadic melanoma and melanoma-initiating cells. Arch Pathol Lab Med, 2010. 134(12): p. 1740-9.
13. Fedorenko, I.V., G.T. Gibney, and K.S. Smalley, NRAS mutant melanoma: biological behavior and future strategies for therapeutic management. Oncogene, 2013. 32(25): p. 3009-18.
14. Muñoz-Couselo, E., et al., NRAS-mutant melanoma: current challenges and future prospect. Onco Targets Ther, 2017. 10: p. 3941-3947.
15. Haluska, F.G., et al., Genetic alterations in signaling pathways in melanoma. Clin Cancer Res, 2006. 12(7 Pt 2): p. 2301s-2307s.
16. Eckerle Mize, D., et al., Familial Atypical Multiple Mole Melanoma Syndrome, in Cancer Syndromes, D.L. Riegert-Johnson, et al., Editors. 2009, National Center for Biotechnology Information (US) Copyright © 2009-, Douglas L Riegert-Johnson.: Bethesda (MD).
17. Goldstein, A.M., et al., High-risk melanoma susceptibility genes and pancreatic cancer, neural system tumors, and uveal melanoma across GenoMEL. Cancer Res, 2006. 66(20): p. 9818-28.
18. Zhou, X.P., et al., Epigenetic PTEN silencing in malignant melanomas without PTEN mutation. Am J Pathol, 2000. 157(4): p. 1123-8.
19. Birck, A., et al., Mutation and allelic loss of the PTEN/MMAC1 gene in primary and metastatic melanoma biopsies. J Invest Dermatol, 2000. 114(2): p. 277-80.
20. Dhawan, P., et al., Constitutive activation of Akt/protein kinase B in melanoma leads to up-regulation of nuclear factor-kappaB and tumor progression. Cancer Res, 2002. 62(24): p. 7335-42.
21. Stahl, J.M., et al., Deregulated Akt3 activity promotes development of malignant melanoma. Cancer Res, 2004. 64(19): p. 7002-10.
22. Robertson, G.P., Functional and therapeutic significance of Akt deregulation in malignant melanoma. Cancer Metastasis Rev, 2005. 24(2): p. 273-85.

23. Cully, M., et al., Beyond PTEN mutations: the PI3K pathway as an integrator of multiple inputs during tumorigenesis. Nat Rev Cancer, 2006. 6(3): p. 184-92.
24. Shain, A.H. and B.C. Bastian, From melanocytes to melanomas. Nat Rev Cancer, 2016. 16(6): p. 345-58.
25. D'Arcy, C. and C. Kiel, Cell Adhesion Molecules in Normal Skin and Melanoma. Biomolecules, 2021. 11(8).
26. Thingnes, J., et al., Understanding the melanocyte distribution in human epidermis: an agent-based computational model approach. PLoS One, 2012. 7(7): p. e40377.
27. Del Bino, S., C. Duval, and F. Bernerd, Clinical and Biological Characterization of Skin Pigmentation Diversity and Its Consequences on UV Impact. Int J Mol Sci, 2018. 19(9).
28. Fitzpatrick, T.B. and A.S. Breathnach, [THE EPIDERMAL MELANIN UNIT SYSTEM]. Dermatol Wochenschr, 1963. 147: p. 481-9.
29. Jimbow, K., et al., Some aspects of melanin biology: 1950-1975. J Invest Dermatol, 1976. 67(1): p. 72-89.
30. Tang, A., et al., E-cadherin is the major mediator of human melanocyte adhesion to keratinocytes in vitro. J Cell Sci, 1994. 107 (Pt 4): p. 983-92.
31. Gray-Schopfer, V., C. Wellbrock, and R. Marais, Melanoma biology and new targeted therapy. Nature, 2007. 445(7130): p. 851-7.
32. Cano, A., et al., The transcription factor snail controls epithelial-mesenchymal transitions by repressing E-cadherin expression. Nat Cell Biol, 2000. 2(2): p. 76-83.
33. Poser, I., et al., Loss of E-cadherin expression in melanoma cells involves up-regulation of the transcriptional repressor Snail. J Biol Chem, 2001. 276(27): p. 24661-6.
34. Jamal, S. and R.J. Schneider, UV-induction of keratinocyte endothelin-1 downregulates E-cadherin in melanocytes and melanoma cells. J Clin Invest, 2002. 110(4): p. 443-52.
35. Hsu, M.Y., et al., Shifts in cadherin profiles between human normal melanocytes and melanomas. J Investig Dermatol Symp Proc, 1996. 1(2): p. 188-94.
36. Hodorogea, A., et al., Epithelial-Mesenchymal Transition in Skin Cancers: A Review. Anal Cell Pathol (Amst), 2019. 2019: p. 3851576.
37. Eddy, K., R. Shah, and S. Chen, Decoding Melanoma Development and Progression: Identification of Therapeutic Vulnerabilities. Frontiers in Oncology, 2021. 10(3357).
38. Miller, A.J. and M.C. Mihm, Jr., Melanoma. N Engl J Med, 2006. 355(1): p. 51-65.
39. Lai, X., et al., Epithelial-Mesenchymal Transition and Metabolic Switching in Cancer: Lessons From Somatic Cell Reprogramming. Frontiers in Cell and Developmental Biology, 2020. 8(760).
40. Bockhorn, M., R.K. Jain, and L.L. Munn, Active versus passive mechanisms in metastasis: do cancer cells crawl into vessels, or are they pushed? Lancet Oncol, 2007. 8(5): p. 444-8.
41. Tsuji, T., S. Ibaragi, and G.F. Hu, Epithelial-mesenchymal transition and cell cooperativity in metastasis. Cancer Res, 2009. 69(18): p. 7135-9.
42. Joosse, S.A., T.M. Gorges, and K. Pantel, Biology, detection, and clinical implications of circulating tumor cells. EMBO Mol Med, 2015. 7(1): p. 1-11.
43. Kalluri, R. and R.A. Weinberg, The basics of epithelial-mesenchymal transition. J Clin Invest, 2009. 119(6): p. 1420-8.
44. Wang, M., et al., Role of tumor microenvironment in tumorigenesis. J Cancer, 2017. 8(5): p. 761-773.
45. Hanahan, D. and L.M. Coussens, Accessories to the crime: functions of cells recruited to the tumor microenvironment. Cancer Cell, 2012. 21(3): p. 309-22.
46. Ping, Q., et al., Cancer-associated fibroblasts: overview, progress, challenges, and directions. Cancer Gene Ther, 2021. 28(9): p. 984-999.
47. Mihm, M.C., Jr., C.G. Clemente, and N. Cascinelli, Tumor infiltrating lymphocytes in lymph node melanoma metastases: a histopathologic prognostic indicator and an expression of local immune response. Lab Invest, 1996. 74(1): p. 43-7.

48. Balkwill, F. and A. Mantovani, Inflammation and cancer: back to Virchow? Lancet, 2001. 357(9255): p. 539-45.
49. Zitvogel, L., A. Tesniere, and G. Kroemer, Cancer despite immunosurveillance: immunoselection and immunosubversion. Nat Rev Immunol, 2006. 6(10): p. 715-27.
50. Kornstein, M.J., J.S. Brooks, and D.E. Elder, Immunoperoxidase localization of lymphocyte subsets in the host response to melanoma and nevi. Cancer Res, 1983. 43(6): p. 2749-53.
51. Baxevanis, C.N., et al., Tumor specific cytolysis by tumor infiltrating lymphocytes in breast cancer. Cancer, 1994. 74(4): p. 1275-82.
52. Naito, Y., et al., CD8+ T cells infiltrated within cancer cell nests as a prognostic factor in human colorectal cancer. Cancer Res, 1998. 58(16): p. 3491-4.
53. Pagès, F., et al., Effector memory T cells, early metastasis, and survival in colorectal cancer. N Engl J Med, 2005. 353(25): p. 2654-66.
54. Galon, J., et al., Type, density, and location of immune cells within human colorectal tumors predict clinical outcome. Science, 2006. 313(5795): p. 1960-4.
55. Whiteside, T.L., The tumor microenvironment and its role in promoting tumor growth. Oncogene, 2008. 27(45): p. 5904-12.
56. Man, Y.G., et al., Tumor-infiltrating immune cells promoting tumor invasion and metastasis: existing theories. J Cancer, 2013. 4(1): p. 84-95.
57. Wyckoff, J., et al., A paracrine loop between tumor cells and macrophages is required for tumor cell migration in mammary tumors. Cancer Res, 2004. 64(19): p. 7022-9.
58. Wyckoff, J.B., et al., Direct visualization of macrophage-assisted tumor cell intravasation in mammary tumors. Cancer Res, 2007. 67(6): p. 2649-56.
59. Pollard, J.W., Macrophages define the invasive microenvironment in breast cancer. J Leukoc Biol, 2008. 84(3): p. 623-30.
60. Curiel, T.J., et al., Specific recruitment of regulatory T cells in ovarian carcinoma fosters immune privilege and predicts reduced survival. Nat Med, 2004. 10(9): p. 942-9.
61. Facciabene, A., et al., Tumour hypoxia promotes tolerance and angiogenesis via CCL28 and T(reg) cells. Nature, 2011. 475(7355): p. 226-30.
62. Hinshaw, D.C. and L.A. Shevde, The Tumor Microenvironment Innately Modulates Cancer Progression. Cancer Res, 2019. 79(18): p. 4557-4566.
63. Wu, Q., et al., Cancer-associated adipocytes: key players in breast cancer progression. J Hematol Oncol, 2019. 12(1): p. 95.
64. Labani-Motlagh, A., M. Ashja-Mahdavi, and A. Loskog, The Tumor Microenvironment: A Milieu Hindering and Obstructing Antitumor Immune Responses. Front Immunol, 2020. 11: p. 940.
65. Garnier, L., A.O. Gkountidi, and S. Hugues, Tumor-Associated Lymphatic Vessel Features and Immunomodulatory Functions. Front Immunol, 2019. 10: p. 720.
66. Baghban, R., et al., Tumor microenvironment complexity and therapeutic implications at a glance. Cell Commun Signal, 2020. 18(1): p. 59.
67. Salazar, N. and B.A. Zabel, Support of Tumor Endothelial Cells by Chemokine Receptors. Frontiers in Immunology, 2019. 10(147).
68. Jahanban-Esfahlan, R., K. Seidi, and N. Zarghami, Tumor vascular infarction: prospects and challenges. Int J Hematol, 2017. 105(3): p. 244-256.
69. Lugano, R., M. Ramachandran, and A. Dimberg, Tumor angiogenesis: causes, consequences, challenges and opportunities. Cell Mol Life Sci, 2020. 77(9): p. 1745-1770.
70. Dianat-Moghadam, H., et al., Cancer stem cells-emanated therapy resistance: Implications for liposomal drug delivery systems. J Control Release, 2018. 288: p. 62-83.
71. Dudley, A.C., Tumor endothelial cells. Cold Spring Harb Perspect Med, 2012. 2(3): p. a006536.
72. Liao, D. and R.S. Johnson, Hypoxia: a key regulator of angiogenesis in cancer. Cancer Metastasis Rev, 2007. 26(2): p. 281-90.

73. Pastorekova, S. and R.J. Gillies, The role of carbonic anhydrase IX in cancer development: links to hypoxia, acidosis, and beyond. Cancer Metastasis Rev, 2019. 38(1-2): p. 65-77.
74. Benej, M., S. Pastorekova, and J. Pastorek, Carbonic anhydrase IX: regulation and role in cancer. Subcell Biochem, 2014. 75: p. 199-219.
75. Sahai, E., et al., A framework for advancing our understanding of cancer-associated fibroblasts. Nat Rev Cancer, 2020. 20(3): p. 174-186.
76. Zhang, D., et al., Tumor-Stroma IL1β-IRAK4 Feedforward Circuitry Drives Tumor Fibrosis, Chemoresistance, and Poor Prognosis in Pancreatic Cancer. Cancer Res, 2018. 78(7): p. 1700-1712.
77. Calvo, F., et al., Mechanotransduction and YAP-dependent matrix remodelling is required for the generation and maintenance of cancer-associated fibroblasts. Nat Cell Biol, 2013. 15(6): p. 637-46.
78. Liu, T., et al., Cancer-Associated Fibroblasts Build and Secure the Tumor Microenvironment. Front Cell Dev Biol, 2019. 7: p. 60.
79. Goulet, C.R., et al., Cancer-associated fibroblasts induce epithelial-mesenchymal transition of bladder cancer cells through paracrine IL-6 signalling. BMC Cancer, 2019. 19(1): p. 137.
80. Wang, L., et al., CAFs enhance paclitaxel resistance by inducing EMT through the IL-6/JAK2/STAT3 pathway. Oncol Rep, 2018. 39(5): p. 2081-2090.
81. Ren, Y., et al., Paracrine and epigenetic control of CAF-induced metastasis: the role of HOTAIR stimulated by TGF-ß1 secretion. Mol Cancer, 2018. 17(1): p. 5.
82. Xing, F., J. Saidou, and K. Watabe, Cancer associated fibroblasts (CAFs) in tumor microenvironment. Front Biosci (Landmark Ed), 2010. 15: p. 166-79.
83. Gaggioli, C., et al., Fibroblast-led collective invasion of carcinoma cells with differing roles for RhoGTPases in leading and following cells. Nat Cell Biol, 2007. 9(12): p. 1392-400.
84. Fullár, A., et al., Remodeling of extracellular matrix by normal and tumor-associated fibroblasts promotes cervical cancer progression. BMC Cancer, 2015. 15: p. 256.
85. Mizutani, Y., et al., Meflin-Positive Cancer-Associated Fibroblasts Inhibit Pancreatic Carcinogenesis. Cancer Research, 2019. 79(20): p. 5367-5381.
86. Poltavets, V., et al., The Role of the Extracellular Matrix and Its Molecular and Cellular Regulators in Cancer Cell Plasticity. Frontiers in Oncology, 2018. 8(431).
87. Clause, K.C. and T.H. Barker, Extracellular matrix signaling in morphogenesis and repair. Curr Opin Biotechnol, 2013. 24(5): p. 830-3.
88. Frantz, C., K.M. Stewart, and V.M. Weaver, The extracellular matrix at a glance. J Cell Sci, 2010. 123(Pt 24): p. 4195-200.
89. Fang, M., et al., Collagen as a double-edged sword in tumor progression. Tumour Biol, 2014. 35(4): p. 2871-82.
90. Xu, S., et al., The role of collagen in cancer: from bench to bedside. J Transl Med, 2019. 17(1): p. 309.
91. Sorushanova, A., et al., The Collagen Suprafamily: From Biosynthesis to Advanced Biomaterial Development. Adv Mater, 2019. 31(1): p. e1801651.
92. Gordon, M.K. and R.A. Hahn, Collagens. Cell Tissue Res, 2010. 339(1): p. 247-57.
93. Ramchandran, R., et al., Antiangiogenic activity of restin, NC10 domain of human collagen XV: comparison to endostatin. Biochem Biophys Res Commun, 1999. 255(3): p. 735-9.
94. Pickering, J.G., Regulation of vascular cell behavior by collagen : form is function. Circ Res, 2001. 88(5): p. 458-9.
95. Hamano, Y., et al., Physiological levels of tumstatin, a fragment of collagen IV alpha3 chain, are generated by MMP-9 proteolysis and suppress angiogenesis via alphaV beta3 integrin. Cancer Cell, 2003. 3(6): p. 589-601.
96. Hong, J., et al., Fibrillar Type I Collagen Enhances the Differentiation and Proliferation of Myofibroblasts by Lowering α2β1 Integrin Expression in Cardiac Fibrosis. Biomed Res Int, 2017. 2017: p. 1790808.

97. Somaiah, C., et al., Collagen Promotes Higher Adhesion, Survival and Proliferation of Mesenchymal Stem Cells. PLoS One, 2015. 10(12): p. e0145068.
98. Beachley, V.Z., et al., Tissue matrix arrays for high-throughput screening and systems analysis of cell function. Nat Methods, 2015. 12(12): p. 1197-204.
99. Verzijl, N., et al., Effect of collagen turnover on the accumulation of advanced glycation end products. J Biol Chem, 2000. 275(50): p. 39027-31.
100. Rucklidge, G.J., et al., Turnover rates of different collagen types measured by isotope ratio mass spectrometry. Biochimica et Biophysica Acta (BBA) - General Subjects, 1992. 1156(1): p. 57-61.
101. Ricard-Blum, S., The collagen family. Cold Spring Harb Perspect Biol, 2011. 3(1): p. a004978.
102. Onursal, C., et al., Collagen Biosynthesis, Processing, and Maturation in Lung Ageing. Frontiers in Medicine, 2021. 8(495).
103. Gelse, K., E. Pöschl, and T. Aigner, Collagens--structure, function, and biosynthesis. Adv Drug Deliv Rev, 2003. 55(12): p. 1531-46.
104. Yamauchi, M. and M. Sricholpech, Lysine post-translational modifications of collagen. Essays Biochem, 2012. 52: p. 113-33.
105. Engel, J. and D.J. Prockop, The zipper-like folding of collagen triple helices and the effects of mutations that disrupt the zipper. Annu Rev Biophys Biophys Chem, 1991. 20: p. 137-52.
106. Stefanovic, B., L. Stefanovic, and Z. Manojlovic, Imaging of type I procollagen biosynthesis in cells reveals biogenesis in highly organized bodies; Collagenosomes. Matrix Biol Plus, 2021. 12: p. 100076.
107. Raghunath, M., P. Bruckner, and B. Steinmann, Delayed triple helix formation of mutant collagen from patients with osteogenesis imperfecta. J Mol Biol, 1994. 236(3): p. 940-9.
108. Koide, T. and K. Nagata, Collagen Biosynthesis, in Collagen: Primer in Structure, Processing and Assembly, J. Brinckmann, H. Notbohm, and P.K. Müller, Editors. 2005, Springer Berlin Heidelberg: Berlin, Heidelberg. p. 85-114.
109. Broder, C., et al., Metalloproteases meprin α and meprin β are C- and N-procollagen proteinases important for collagen assembly and tensile strength. Proc Natl Acad Sci U S A, 2013. 110(35): p. 14219-24.
110. Yamauchi, M., et al., The fibrotic tumor stroma. J Clin Invest, 2018. 128(1): p. 16-25.
111. Kahle, B., et al., The Extracellular Matrix Signature in Vein Graft Disease. Can J Cardiol, 2016. 32(8): p. 1008.e11-7.
112. Eyre, D.R., M.A. Paz, and P.M. Gallop, Cross-linking in collagen and elastin. Annu Rev Biochem, 1984. 53: p. 717-48.
113. Robins, S.P. and A. Duncan, Cross-linking of collagen. Location of pyridinoline in bovine articular cartilage at two sites of the molecule. Biochem J, 1983. 215(1): p. 175-82.
114. Ogawa, T., et al., A novel fluor in insoluble collagen: a crosslinking moiety in collagen molecule. Biochem Biophys Res Commun, 1982. 107(4): p. 1252-7.
115. Hanson, D.A. and D.R. Eyre, Molecular site specificity of pyridinoline and pyrrole cross-links in type I collagen of human bone. J Biol Chem, 1996. 271(43): p. 26508-16.
116. Kuypers, R., et al., Identification of the loci of the collagen-associated Ehrlich chromogen in type I collagen confirms its role as a trivalent cross-link. Biochem J, 1992. 283 (Pt 1)(Pt 1): p. 129-36.
117. Mechanic, G.L., et al., Locus of a histidine-based, stable trifunctional, helix to helix collagen cross-link: stereospecific collagen structure of type I skin fibrils. Biochemistry, 1987. 26(12): p. 3500-9.
118. Yamauchi, M., et al., Collagen cross-linking in sun-exposed and unexposed sites of aged human skin. J Invest Dermatol, 1991. 97(5): p. 938-41.
119. Kang, A.H., B. Faris, and C. Franzblau, Intramolecular cross-link of chick skin collagen. Biochem Biophys Res Commun, 1969. 36(3): p. 345-9.

120. Zhang, Y., et al., Quantitative and structural analysis of isotopically labelled natural crosslinks in type I skin collagen using LC-HRMS and SANS. Journal of Leather Science and Engineering, 2019. 1(1): p. 10.
121. Tanzer, M.L., et al., Structure of two histidine-containing crosslinks from collagen. J Biol Chem, 1973. 248(2): p. 393-402.
122. Lu, P., V.M. Weaver, and Z. Werb, The extracellular matrix: a dynamic niche in cancer progression. J Cell Biol, 2012. 196(4): p. 395-406.
123. Hinz, B., et al., Recent developments in myofibroblast biology: paradigms for connective tissue remodeling. Am J Pathol, 2012. 180(4): p. 1340-55.
124. Kauppila, S., et al., Aberrant type I and type III collagen gene expression in human breast cancer in vivo. J Pathol, 1998. 186(3): p. 262-8.
125. Kai, F., A.P. Drain, and V.M. Weaver, The Extracellular Matrix Modulates the Metastatic Journey. Dev Cell, 2019. 49(3): p. 332-346.
126. Cox, T.R. and J.T. Erler, Remodeling and homeostasis of the extracellular matrix: implications for fibrotic diseases and cancer. Dis Model Mech, 2011. 4(2): p. 165-78.
127. Hayashido, Y., et al., Overexpression of integrin αv facilitates proliferation and invasion of oral squamous cell carcinoma cells via MEK/ERK signaling pathway that is activated by interaction of integrin αvβ8 with type Ⅰ collagen. Int J Oncol, 2014. 45(5): p. 1875-82.
128. Kiefer, J.A. and M.C. Farach-Carson, Type I collagen-mediated proliferation of PC3 prostate carcinoma cell line: implications for enhanced growth in the bone microenvironment. Matrix Biol, 2001. 20(7): p. 429-37.
129. Armstrong, T., et al., Type I collagen promotes the malignant phenotype of pancreatic ductal adenocarcinoma. Clin Cancer Res, 2004. 10(21): p. 7427-37.
130. Paszek, M.J., et al., Tensional homeostasis and the malignant phenotype. Cancer Cell, 2005. 8(3): p. 241-54.
131. Provenzano, P.P., et al., Collagen reorganization at the tumor-stromal interface facilitates local invasion. BMC Med, 2006. 4(1): p. 38.
132. Conklin, M.W., et al., Aligned collagen is a prognostic signature for survival in human breast carcinoma. Am J Pathol, 2011. 178(3): p. 1221-32.
133. Acerbi, I., et al., Human breast cancer invasion and aggression correlates with ECM stiffening and immune cell infiltration. Integr Biol (Camb), 2015. 7(10): p. 1120-34.
134. Esposito, I., et al., Tenascin C and annexin II expression in the process of pancreatic carcinogenesis. J Pathol, 2006. 208(5): p. 673-85.
135. Whatcott, C.J., et al., Desmoplasia in Primary Tumors and Metastatic Lesions of Pancreatic Cancer. Clin Cancer Res, 2015. 21(15): p. 3561-8.
136. Karsdal, M.A., et al., Extracellular matrix remodeling: the common denominator in connective tissue diseases. Possibilities for evaluation and current understanding of the matrix as more than a passive architecture, but a key player in tissue failure. Assay Drug Dev Technol, 2013. 11(2): p. 70-92.
137. Yuzhalin, A.E., et al., Dynamic matrisome: ECM remodeling factors licensing cancer progression and metastasis. Biochim Biophys Acta Rev Cancer, 2018. 1870(2): p. 207-228.
138. Winkler, J., et al., Concepts of extracellular matrix remodelling in tumour progression and metastasis. Nat Commun, 2020. 11(1): p. 5120.
139. Bonnans, C., J. Chou, and Z. Werb, Remodelling the extracellular matrix in development and disease. Nat Rev Mol Cell Biol, 2014. 15(12): p. 786-801.
140. Ford, A.J. and P. Rajagopalan, Extracellular matrix remodeling in 3D: implications in tissue homeostasis and disease progression. Wiley Interdiscip Rev Nanomed Nanobiotechnol, 2018. 10(4): p. e1503.
141. López-Otín, C., L.H. Palavalli, and Y. Samuels, Protective roles of matrix metalloproteinases: from mouse models to human cancer. Cell Cycle, 2009. 8(22): p. 3657-62.
142. Stadlmann, S., et al., Cytokine-regulated expression of collagenase-2 (MMP-8) is involved in the progression of ovarian cancer. Eur J Cancer, 2003. 39(17): p. 2499-505.

143. Qin, G., et al., Reciprocal activation between MMP-8 and TGF-β1 stimulates EMT and malignant progression of hepatocellular carcinoma. Cancer Lett, 2016. 374(1): p. 85-95.
144. Åström, P., et al., The interplay of matrix metalloproteinase-8, transforming growth factor-β1 and vascular endothelial growth factor-C cooperatively contributes to the aggressiveness of oral tongue squamous cell carcinoma. Br J Cancer, 2017. 117(7): p. 1007-1016.
145. Wolf, K. and P. Friedl, Mapping proteolytic cancer cell-extracellular matrix interfaces. Clin Exp Metastasis, 2009. 26(4): p. 289-98.
146. Sottile, J., Regulation of angiogenesis by extracellular matrix. Biochim Biophys Acta, 2004. 1654(1): p. 13-22.
147. O'Reilly, M.S., et al., Endostatin: an endogenous inhibitor of angiogenesis and tumor growth. Cell, 1997. 88(2): p. 277-85.
148. Da Silva, J., et al., Structural characterization and in vivo pro-tumor properties of a highly conserved matrikine. Oncotarget, 2018. 9(25): p. 17839-17857.
149. Zivkovic, T.D.a.M., Overview of MMP Biology and Gene Associations in Human Diseases. IntechOpen, 2017. The Role of Matrix Metalloproteinase in Human Body Pathologies.
150. Sterchi, E.E., Special issue: metzincin metalloproteinases. Mol Aspects Med, 2008. 29(5): p. 255-7.
151. Murphy, G. and H. Nagase, Progress in matrix metalloproteinase research. Mol Aspects Med, 2008. 29(5): p. 290-308.
152. Van Wart, H.E. and H. Birkedal-Hansen, The cysteine switch: a principle of regulation of metalloproteinase activity with potential applicability to the entire matrix metalloproteinase gene family. Proc Natl Acad Sci U S A, 1990. 87(14): p. 5578-82.
153. Osenkowski, P., et al., Mutational and structural analyses of the hinge region of membrane type 1-matrix metalloproteinase and enzyme processing. J Biol Chem, 2005. 280(28): p. 26160-8.
154. Sternlicht, M.D. and Z. Werb, How matrix metalloproteinases regulate cell behavior. Annu Rev Cell Dev Biol, 2001. 17: p. 463-516.
155. Liu, J. and R.A. Khalil, Matrix Metalloproteinase Inhibitors as Investigational and Therapeutic Tools in Unrestrained Tissue Remodeling and Pathological Disorders. Prog Mol Biol Transl Sci, 2017. 148: p. 355-420.
156. Amălinei, C., I.D. Căruntu, and R.A. Bălan, Biology of metalloproteinases. Rom J Morphol Embryol, 2007. 48(4): p. 323-34.
157. Cui, N., M. Hu, and R.A. Khalil, Biochemical and Biological Attributes of Matrix Metalloproteinases. Prog Mol Biol Transl Sci, 2017. 147: p. 1-73.
158. Nagase, H., R. Visse, and G. Murphy, Structure and function of matrix metalloproteinases and TIMPs. Cardiovascular Research, 2006. 69(3): p. 562-573.
159. Springman, E.B., et al., Multiple modes of activation of latent human fibroblast collagenase: evidence for the role of a Cys73 active-site zinc complex in latency and a "cysteine switch" mechanism for activation. Proc Natl Acad Sci U S A, 1990. 87(1): p. 364-8.
160. Ra, H.J. and W.C. Parks, Control of matrix metalloproteinase catalytic activity. Matrix Biol, 2007. 26(8): p. 587-96.
161. Thomas, G., Furin at the cutting edge: from protein traffic to embryogenesis and disease. Nat Rev Mol Cell Biol, 2002. 3(10): p. 753-66.
162. Kang, T., H. Nagase, and D. Pei, Activation of membrane-type matrix metalloproteinase 3 zymogen by the proprotein convertase furin in the trans-Golgi network. Cancer Res, 2002. 62(3): p. 675-81.
163. Ito, A. and H. Nagase, Evidence that human rheumatoid synovial matrix metalloproteinase 3 is an endogenous activator of procollagenase. Arch Biochem Biophys, 1988. 267(1): p. 211-6.
164. Imai, K., et al., Matrix metalloproteinase 7 (matrilysin) from human rectal carcinoma cells. Activation of the precursor, interaction with other matrix metalloproteinases and enzymic properties. J Biol Chem, 1995. 270(12): p. 6691-7.

165. Wang, Z., R. Juttermann, and P.D. Soloway, TIMP-2 is required for efficient activation of proMMP-2 in vivo. J Biol Chem, 2000. 275(34): p. 26411-5.
166. Kurschat, P., et al., Tissue inhibitor of matrix metalloproteinase-2 regulates matrix metalloproteinase-2 activation by modulation of membrane-type 1 matrix metalloproteinase activity in high and low invasive melanoma cell lines. J Biol Chem, 1999. 274(30): p. 21056-62.
167. Han, K.Y., et al., Evidence for the Involvement of MMP14 in MMP2 Processing and Recruitment in Exosomes of Corneal Fibroblasts. Invest Ophthalmol Vis Sci, 2015. 56(9): p. 5323-9.
168. Gomez, D.E., et al., Tissue inhibitors of metalloproteinases: structure, regulation and biological functions. Eur J Cell Biol, 1997. 74(2): p. 111-22.
169. Nagase, H., Activation mechanisms of matrix metalloproteinases. Biol Chem, 1997. 378(3-4): p. 151-60.
170. Butler, G.S., et al., The TIMP2 membrane type 1 metalloproteinase "receptor" regulates the concentration and efficient activation of progelatinase A. A kinetic study. J Biol Chem, 1998. 273(2): p. 871-80.
171. Aiken, A. and R. Khokha, Unraveling metalloproteinase function in skeletal biology and disease using genetically altered mice. Biochim Biophys Acta, 2010. 1803(1): p. 121-32.
172. Holmbeck, K., et al., MT1-MMP-deficient mice develop dwarfism, osteopenia, arthritis, and connective tissue disease due to inadequate collagen turnover. Cell, 1999. 99(1): p. 81-92.
173. Oblander, S.A., et al., Distinctive functions of membrane type 1 matrix-metalloprotease (MT1-MMP or MMP-14) in lung and submandibular gland development are independent of its role in pro-MMP-2 activation. Dev Biol, 2005. 277(1): p. 255-69.
174. Itoh, T., et al., Reduced angiogenesis and tumor progression in gelatinase A-deficient mice. Cancer Res, 1998. 58(5): p. 1048-51.
175. van Hinsbergh, V.W.M. and P. Koolwijk, Endothelial sprouting and angiogenesis: matrix metalloproteinases in the lead. Cardiovascular Research, 2007. 78(2): p. 203-212.
176. Gutiérrez-Fernández, A., et al., Increased inflammation delays wound healing in mice deficient in collagenase-2 (MMP-8). The FASEB Journal, 2007. 21(10): p. 2580-2591.
177. Caley, M.P., V.L. Martins, and E.A. O'Toole, Metalloproteinases and Wound Healing. Adv Wound Care (New Rochelle), 2015. 4(4): p. 225-234.
178. Chen, P., et al., MMP7 shedding of syndecan-1 facilitates re-epithelialization by affecting alpha(2)beta(1) integrin activation. PLoS One, 2009. 4(8): p. e6565.
179. Mosig, R.A., et al., Loss of MMP-2 disrupts skeletal and craniofacial development and results in decreased bone mineralization, joint erosion and defects in osteoblast and osteoclast growth. Hum Mol Genet, 2007. 16(9): p. 1113-23.
180. Vu, T.H., et al., MMP-9/gelatinase B is a key regulator of growth plate angiogenesis and apoptosis of hypertrophic chondrocytes. Cell, 1998. 93(3): p. 411-22.
181. Stickens, D., et al., Altered endochondral bone development in matrix metalloproteinase 13-deficient mice. Development, 2004. 131(23): p. 5883-95.
182. Longo, G.M., et al., Matrix metalloproteinases 2 and 9 work in concert to produce aortic aneurysms. J Clin Invest, 2002. 110(5): p. 625-32.
183. Matsumura, S., et al., Targeted deletion or pharmacological inhibition of MMP-2 prevents cardiac rupture after myocardial infarction in mice. J Clin Invest, 2005. 115(3): p. 599-609.
184. Johnson, J.L., et al., Divergent effects of matrix metalloproteinases 3, 7, 9, and 12 on atherosclerotic plaque stability in mouse brachiocephalic arteries. Proc Natl Acad Sci U S A, 2005. 102(43): p. 15575-80.
185. Overall, C.M., Dilating the degradome: matrix metalloproteinase 2 (MMP-2) cuts to the heart of the matter. Biochem J, 2004. 383(Pt. 3): p. e5-7.
186. D'Armiento, J., Matrix metalloproteinase disruption of the extracellular matrix and cardiac dysfunction. Trends Cardiovasc Med, 2002. 12(3): p. 97-101.

187. Molloy, K.J., et al., Unstable carotid plaques exhibit raised matrix metalloproteinase-8 activity. Circulation, 2004. 110(3): p. 337-43.
188. Shah, P.K. and Z.S. Galis, Matrix metalloproteinase hypothesis of plaque rupture: players keep piling up but questions remain. Circulation, 2001. 104(16): p. 1878-80.
189. Cawston, T.E. and A.J. Wilson, Understanding the role of tissue degrading enzymes and their inhibitors in development and disease. Best Pract Res Clin Rheumatol, 2006. 20(5): p. 983-1002.
190. Egeblad, M. and Z. Werb, New functions for the matrix metalloproteinases in cancer progression. Nat Rev Cancer, 2002. 2(3): p. 161-74.
191. RYDLOVA, M., et al., Biological Activity and Clinical Implications of the Matrix Metalloproteinases. Anticancer Research, 2008. 28(2B): p. 1389-1397.
192. Minn, A.J., et al., Lung metastasis genes couple breast tumor size and metastatic spread. Proc Natl Acad Sci U S A, 2007. 104(16): p. 6740-5.
193. Vizoso, F.J., et al., Study of matrix metalloproteinases and their inhibitors in breast cancer. Br J Cancer, 2007. 96(6): p. 903-11.
194. Acuff, H.B., et al., Analysis of host- and tumor-derived proteinases using a custom dual species microarray reveals a protective role for stromal matrix metalloproteinase-12 in non-small cell lung cancer. Cancer Res, 2006. 66(16): p. 7968-75.
195. Morgia, G., et al., Matrix metalloproteinases as diagnostic (MMP-13) and prognostic (MMP-2, MMP-9) markers of prostate cancer. Urol Res, 2005. 33(1): p. 44-50.
196. Peng, W.J., et al., Prognostic value of matrix metalloproteinase 9 expression in patients with non-small cell lung cancer. Clin Chim Acta, 2012. 413(13-14): p. 1121-6.
197. Yang, B., et al., Matrix metalloproteinase-9 overexpression is closely related to poor prognosis in patients with colon cancer. World J Surg Oncol, 2014. 12: p. 24.
198. Chen, S.Z., et al., Expression levels of matrix metalloproteinase-9 in human gastric carcinoma. Oncol Lett, 2015. 9(2): p. 915-919.
199. Xu, Y., et al., The co-expression of MMP-9 and Tenascin-C is significantly associated with the progression and prognosis of pancreatic cancer. Diagn Pathol, 2015. 10: p. 211.
200. Noël, A., M. Jost, and E. Maquoi, Matrix metalloproteinases at cancer tumor-host interface. Semin Cell Dev Biol, 2008. 19(1): p. 52-60.
201. Weaver, A.M., Invadopodia: specialized cell structures for cancer invasion. Clin Exp Metastasis, 2006. 23(2): p. 97-105.
202. Gialeli, C., A.D. Theocharis, and N.K. Karamanos, Roles of matrix metalloproteinases in cancer progression and their pharmacological targeting. Febs j, 2011. 278(1): p. 16-27.
203. Balbín, M., et al., Loss of collagenase-2 confers increased skin tumor susceptibility to male mice. Nat Genet, 2003. 35(3): p. 252-7.
204. Liotta, L.A., et al., Metastatic potential correlates with enzymatic degradation of basement membrane collagen. Nature, 1980. 284(5751): p. 67-8.
205. Coussens, L.M., et al., MMP-9 supplied by bone marrow-derived cells contributes to skin carcinogenesis. Cell, 2000. 103(3): p. 481-90.
206. Sato, H., et al., Cell surface binding and activation of gelatinase A induced by expression of membrane-type-1-matrix metalloproteinase (MT1-MMP). FEBS Lett, 1996. 385(3): p. 238-40.
207. Golubkov, V.S., et al., Proteolysis of the membrane type-1 matrix metalloproteinase prodomain: implications for a two-step proteolytic processing and activation. J Biol Chem, 2007. 282(50): p. 36283-91.
208. Golubkov, V.S., et al., Internal cleavages of the autoinhibitory prodomain are required for membrane type 1 matrix metalloproteinase activation, although furin cleavage alone generates inactive proteinase. J Biol Chem, 2010. 285(36): p. 27726-36.
209. Will, H., et al., The soluble catalytic domain of membrane type 1 matrix metalloproteinase cleaves the propeptide of progelatinase A and initiates autoproteolytic activation. Regulation by TIMP-2 and TIMP-3. J Biol Chem, 1996. 271(29): p. 17119-23.

210. Itoh, Y., Membrane-type matrix metalloproteinases: Their functions and regulations. Matrix Biol, 2015. 44-46: p. 207-23.
211. Itoh, Y., et al., Homophilic complex formation of MT1-MMP facilitates proMMP-2 activation on the cell surface and promotes tumor cell invasion. Embo j, 2001. 20(17): p. 4782-93.
212. Itoh, Y., et al., Cell surface collagenolysis requires homodimerization of the membrane-bound collagenase MT1-MMP. Mol Biol Cell, 2006. 17(12): p. 5390-9.
213. Sugiyama, N., et al., EphA2 cleavage by MT1-MMP triggers single cancer cell invasion via homotypic cell repulsion. J Cell Biol, 2013. 201(3): p. 467-84.
214. McQuibban, G.A., et al., Matrix metalloproteinase activity inactivates the CXC chemokine stromal cell-derived factor-1. J Biol Chem, 2001. 276(47): p. 43503-8.
215. McQuibban, G.A., et al., Matrix metalloproteinase processing of monocyte chemoattractant proteins generates CC chemokine receptor antagonists with anti-inflammatory properties in vivo. Blood, 2002. 100(4): p. 1160-7.
216. Barbolina, M.V. and M.S. Stack, Membrane type 1-matrix metalloproteinase: substrate diversity in pericellular proteolysis. Semin Cell Dev Biol, 2008. 19(1): p. 24-33.
217. D'Alessio, S., et al., Tissue inhibitor of metalloproteinases-2 binding to membrane-type 1 matrix metalloproteinase induces MAPK activation and cell growth by a non-proteolytic mechanism. J Biol Chem, 2008. 283(1): p. 87-99.
218. Sakamoto, T. and M. Seiki, Cytoplasmic tail of MT1-MMP regulates macrophage motility independently from its protease activity. Genes Cells, 2009. 14(5): p. 617-26.
219. Shimizu-Hirota, R., et al., MT1-MMP regulates the PI3Kδ·Mi-2/NuRD-dependent control of macrophage immune function. Genes Dev, 2012. 26(4): p. 395-413.
220. Eisenach, P.A., et al., MT1-MMP regulates VEGF-A expression through a complex with VEGFR-2 and Src. J Cell Sci, 2010. 123(Pt 23): p. 4182-93.
221. Sheehy, S. and B. Annabi, A Transcriptional Regulatory Role for the Membrane Type-1 Matrix Metalloproteinase in Carcinogen-Induced Inflammasome Gene Expression. Gene Regul Syst Bio, 2017. 11: p. 1177625017713996.
222. Zhou, Z., et al., Impaired endochondral ossification and angiogenesis in mice deficient in membrane-type matrix metalloproteinase I. Proc Natl Acad Sci U S A, 2000. 97(8): p. 4052-7.
223. Gutiérrez-Fernández, A., et al., Loss of MT1-MMP causes cell senescence and nuclear defects which can be reversed by retinoic acid. Embo j, 2015. 34(14): p. 1875-88.
224. Dechat, T., et al., Nuclear lamins: major factors in the structural organization and function of the nucleus and chromatin. Genes Dev, 2008. 22(7): p. 832-53.
225. Eriksson, M., et al., Recurrent de novo point mutations in lamin A cause Hutchinson-Gilford progeria syndrome. Nature, 2003. 423(6937): p. 293-8.
226. Mori, H., et al., New insight into the role of MMP14 in metabolic balance. PeerJ, 2016. 4: p. e2142.
227. Zigrino, P., et al., Loss of epidermal MMP-14 expression interferes with angiogenesis but not with re-epithelialization. Eur J Cell Biol, 2012. 91(10): p. 748-56.
228. Wong, H.L., et al., MT1-MMP sheds LYVE-1 on lymphatic endothelial cells and suppresses VEGF-C production to inhibit lymphangiogenesis. Nat Commun, 2016. 7: p. 10824.
229. Klose, A., P. Zigrino, and C. Mauch, Monocyte/macrophage MMP-14 modulates cell infiltration and T-cell attraction in contact dermatitis but not in murine wound healing. Am J Pathol, 2013. 182(3): p. 755-64.
230. Alonso-Herranz, L., et al., Macrophages promote endothelial-to-mesenchymal transition via MT1-MMP/TGFβ1 after myocardial infarction. Elife, 2020. 9.
231. Kümper, M., et al., LOSS OF ENDOTHELIAL CELL MMP14 REDUCES MELANOMA GROWTH AND METASTASIS BY INCREASING TUMOR VESSEL STABILITY. J Invest Dermatol, 2021.
232. Taylor, S.H., et al., Matrix metalloproteinase 14 is required for fibrous tissue expansion. Elife, 2015. 4: p. e09345.

233. Zigrino, P., et al., Fibroblast-Derived MMP-14 Regulates Collagen Homeostasis in Adult Skin. J Invest Dermatol, 2016. 136(8): p. 1575-1583.
234. Placido, L., et al., Loss of MT1-MMP in Alveolar Epithelial Cells Exacerbates Pulmonary Fibrosis. Int J Mol Sci, 2021. 22(6).
235. Turunen, S.P., O. Tatti-Bugaeva, and K. Lehti, Membrane-type matrix metalloproteases as diverse effectors of cancer progression. Biochim Biophys Acta Mol Cell Res, 2017. 1864(11 Pt A): p. 1974-1988.
236. Wu, K.P., et al., MT1-MMP is not a good prognosticator of cancer survival: evidence from 11 studies. Tumour Biol, 2014. 35(12): p. 12489-95.
237. Hillebrand, L.E., et al., MMP14 empowers tumor-initiating breast cancer cells under hypoxic nutrient-depleted conditions. Faseb j, 2019. 33(3): p. 4124-4140.
238. Kasurinen, A., et al., High tissue MMP14 expression predicts worse survival in gastric cancer, particularly with a low PROX1. Cancer Med, 2019. 8(16): p. 6995-7005.
239. Jiang, W.G., et al., Expression of membrane type-1 matrix metalloproteinase, MT1-MMP in human breast cancer and its impact on invasiveness of breast cancer cells. Int J Mol Med, 2006. 17(4): p. 583-90.
240. Knapinska, A.M. and G.B. Fields, The Expanding Role of MT1-MMP in Cancer Progression. Pharmaceuticals (Basel), 2019. 12(2).
241. Hotary, K., et al., A cancer cell metalloprotease triad regulates the basement membrane transmigration program. Genes Dev, 2006. 20(19): p. 2673-86.
242. Sabeh, F., et al., Secreted versus membrane-anchored collagenases: relative roles in fibroblast-dependent collagenolysis and invasion. J Biol Chem, 2009. 284(34): p. 23001-11.
243. Fisher, K.E., et al., MT1-MMP- and Cdc42-dependent signaling co-regulate cell invasion and tunnel formation in 3D collagen matrices. J Cell Sci, 2009. 122(Pt 24): p. 4558-69.
244. Wolf, K., et al., Compensation mechanism in tumor cell migration: mesenchymal-amoeboid transition after blocking of pericellular proteolysis. J Cell Biol, 2003. 160(2): p. 267-77.
245. Poincloux, R., F. Lizárraga, and P. Chavrier, Matrix invasion by tumour cells: a focus on MT1-MMP trafficking to invadopodia. J Cell Sci, 2009. 122(Pt 17): p. 3015-24.
246. Sanz-Moreno, V., et al., Rac activation and inactivation control plasticity of tumor cell movement. Cell, 2008. 135(3): p. 510-23.
247. Packard, B.Z., et al., Direct visualization of protease activity on cells migrating in three-dimensions. Matrix Biol, 2009. 28(1): p. 3-10.
248. Takino, T., et al., Inhibition of membrane-type 1 matrix metalloproteinase at cell-matrix adhesions. Cancer Res, 2007. 67(24): p. 11621-9.
249. Szabova, L., et al., MT1-MMP is required for efficient tumor dissemination in experimental metastatic disease. Oncogene, 2008. 27(23): p. 3274-81.
250. Birukawa, N.K., et al., Activated hepatic stellate cells are dependent on self-collagen, cleaved by membrane type 1 matrix metalloproteinase for their growth. J Biol Chem, 2014. 289(29): p. 20209-21.
251. Lohi, J., Laminin-5 in the progression of carcinomas. Int J Cancer, 2001. 94(6): p. 763-7.
252. Koshikawa, N., et al., Membrane-type matrix metalloproteinase-1 (MT1-MMP) is a processing enzyme for human laminin gamma 2 chain. J Biol Chem, 2005. 280(1): p. 88-93.
253. Chung, H., et al., Keratinocyte-derived laminin-332 promotes adhesion and migration in melanocytes and melanoma. J Biol Chem, 2011. 286(15): p. 13438-47.
254. Seftor, R.E., et al., Cooperative interactions of laminin 5 gamma2 chain, matrix metalloproteinase-2, and membrane type-1-matrix/metalloproteinase are required for mimicry of embryonic vasculogenesis by aggressive melanoma. Cancer Res, 2001. 61(17): p. 6322-7.
255. Nguyen, H.L., et al., MT1-MMP Activation of TGF-β Signaling Enables Intercellular Activation of an Epithelial-mesenchymal Transition Program in Cancer. Curr Cancer Drug Targets, 2016. 16(7): p. 618-30.

256. Tatti, O., et al., MT1-MMP releases latent TGF-beta1 from endothelial cell extracellular matrix via proteolytic processing of LTBP-1. Exp Cell Res, 2008. 314(13): p. 2501-14.
257. Thakur, V. and B. Bedogni, The membrane tethered matrix metalloproteinase MT1-MMP at the forefront of melanoma cell invasion and metastasis. Pharmacol Res, 2016. 111: p. 17-22.
258. Pekkonen, P., et al., Lymphatic endothelium stimulates melanoma metastasis and invasion via MMP14-dependent Notch3 and β1-integrin activation. Elife, 2018. 7.
259. Chapman, A., et al., Heterogeneous tumor subpopulations cooperate to drive invasion. Cell Rep, 2014. 8(3): p. 688-95.
260. Bedogni, B., et al., Notch1 is an effector of Akt and hypoxia in melanoma development. J Clin Invest, 2008. 118(11): p. 3660-70.
261. Ma, J., et al., Noncanonical activation of Notch1 protein by membrane type 1 matrix metalloproteinase (MT1-MMP) controls melanoma cell proliferation. J Biol Chem, 2014. 289(12): p. 8442-9.
262. Chan, T.S., Y. Shaked, and K.K. Tsai, Targeting the Interplay Between Cancer Fibroblasts, Mesenchymal Stem Cells, and Cancer Stem Cells in Desmoplastic Cancers. Front Oncol, 2019. 9: p. 688.
263. Eroglu, Z., et al., High response rate to PD-1 blockade in desmoplastic melanomas. Nature, 2018. 553(7688): p. 347-350.
264. Fidler, I.J., Selection of successive tumour lines for metastasis. Nat New Biol, 1973. 242(118): p. 148-9.
265. Bald, T., et al., Ultraviolet-radiation-induced inflammation promotes angiotropism and metastasis in melanoma. Nature, 2014. 507(7490): p. 109-13.
266. Meides, A., et al., Effects of selective MMP-13 inhibition in squamous cell carcinoma depend on estrogen. Int J Cancer, 2014. 135(12): p. 2749-59.
267. Smalley, K.S., et al., Multiple signaling pathways must be targeted to overcome drug resistance in cell lines derived from melanoma metastases. Mol Cancer Ther, 2006. 5(5): p. 1136-44.
268. Zigrino, P., et al., Role of ADAM-9 disintegrin-cysteine-rich domains in human keratinocyte migration. J Biol Chem, 2007. 282(42): p. 30785-93.
269. Jiang, D., et al., Two succeeding fibroblastic lineages drive dermal development and the transition from regeneration to scarring. Nat Cell Biol, 2018. 20(4): p. 422-431.
270. Rao, X., et al., An improvement of the 2ˆ(-delta delta CT) method for quantitative real-time polymerase chain reaction data analysis. Biostat Bioinforma Biomath, 2013. 3(3): p. 71-85.
271. Zheng, B., et al., Ligand-dependent genetic recombination in fibroblasts : a potentially powerful technique for investigating gene function in fibrosis. Am J Pathol, 2002. 160(5): p. 1609-17.
272. Natal, R.A., et al., Collagen analysis by second-harmonic generation microscopy predicts outcome of luminal breast cancer. Tumour Biol, 2018. 40(4): p. 1010428318770953.
273. Rezakhaniha, R., et al., Experimental investigation of collagen waviness and orientation in the arterial adventitia using confocal laser scanning microscopy. Biomech Model Mechanobiol, 2012. 11(3-4): p. 461-73.
274. Seiki, M., Membrane-type matrix metalloproteinases. Apmis, 1999. 107(1): p. 137-43.
275. Iida, J., et al., Membrane type-1 matrix metalloproteinase promotes human melanoma invasion and growth. J Invest Dermatol, 2004. 122(1): p. 167-76.
276. Shimoda, M., et al., Stromal metalloproteinases: Crucial contributors to the tumor microenvironment. Pathol Int, 2021. 71(1): p. 1-14.
277. Miskolczi, Z., et al., Collagen abundance controls melanoma phenotypes through lineage-specific microenvironment sensing. Oncogene, 2018. 37(23): p. 3166-3182.
278. Henriet, P., et al., Contact with fibrillar collagen inhibits melanoma cell proliferation by up-regulating p27KIP1. Proc Natl Acad Sci U S A, 2000. 97(18): p. 10026-31.
279. Taloni, A., et al., Mechanical properties of growing melanocytic nevi and the progression to melanoma. PLoS One, 2014. 9(4): p. e94229.

280. Pach, E., et al., Fibroblast MMP14-Dependent Collagen Processing Is Necessary for Melanoma Growth. Cancers (Basel), 2021. 13(8).
281. Nishida, N., et al., Angiogenesis in cancer. Vasc Health Risk Manag, 2006. 2(3): p. 213-9.
282. Swann, J.B. and M.J. Smyth, Immune surveillance of tumors. J Clin Invest, 2007. 117(5): p. 1137-46.
283. Gonzalez, H., C. Hagerling, and Z. Werb, Roles of the immune system in cancer: from tumor initiation to metastatic progression. Genes Dev, 2018. 32(19-20): p. 1267-1284.
284. Kaur, A., et al., Remodeling of the Collagen Matrix in Aging Skin Promotes Melanoma Metastasis and Affects Immune Cell Motility. Cancer Discov, 2019. 9(1): p. 64-81.
285. Lei, X., et al., Immune cells within the tumor microenvironment: Biological functions and roles in cancer immunotherapy. Cancer Lett, 2020. 470: p. 126-133.
286. Cerwenka, A. and L.L. Lanier, Natural killer cell memory in infection, inflammation and cancer. Nat Rev Immunol, 2016. 16(2): p. 112-23.
287. Marcus, A., et al., Recognition of tumors by the innate immune system and natural killer cells. Adv Immunol, 2014. 122: p. 91-128.
288. Iannello, A., et al., p53-dependent chemokine production by senescent tumor cells supports NKG2D-dependent tumor elimination by natural killer cells. J Exp Med, 2013. 210(10): p. 2057-69.
289. Rabbani, M., N. Zakian, and N. Alimoradi, Contribution of Physical Methods in Decellularization of Animal Tissues. J Med Signals Sens, 2021. 11(1): p. 1-11.
290. Fernández-Pérez, J. and M. Ahearne, The impact of decellularization methods on extracellular matrix derived hydrogels. Sci Rep, 2019. 9(1): p. 14933.
291. Boccafoschi, F., et al., Decellularized biological matrices: an interesting approach for cardiovascular tissue repair and regeneration. J Tissue Eng Regen Med, 2017. 11(5): p. 1648-1657.
292. Lü, W.D., et al., Decellularized and photooxidatively crosslinked bovine jugular veins as potential tissue engineering scaffolds. Interact Cardiovasc Thorac Surg, 2009. 8(3): p. 301-5.
293. Sheridan, W.S., G.P. Duffy, and B.P. Murphy, Mechanical characterization of a customized decellularized scaffold for vascular tissue engineering. J Mech Behav Biomed Mater, 2012. 8: p. 58-70.
294. Le, C.C., et al., Functional Interplay Between Collagen Network and Cell Behavior Within Tumor Microenvironment in Colorectal Cancer. Frontiers in Oncology, 2020. 10(527).
295. Emon, B., et al., Biophysics of Tumor Microenvironment and Cancer Metastasis - A Mini Review. Comput Struct Biotechnol J, 2018. 16: p. 279-287.
296. Despotović, S.Z., et al., Altered organization of collagen fibers in the uninvolved human colon mucosa 10 cm and 20 cm away from the malignant tumor. Sci Rep, 2020. 10(1): p. 6359.
297. Pavithra, V., et al., Tumor-associated Collagen Signatures: An Insight. World Journal of Dentistry, 2017. 8: p. 224-230.
298. Maller, O., et al., Tumour-associated macrophages drive stromal cell-dependent collagen crosslinking and stiffening to promote breast cancer aggression. Nat Mater, 2021. 20(4): p. 548-559.
299. Lin, S. and L. Gu, Influence of Crosslink Density and Stiffness on Mechanical Properties of Type I Collagen Gel. Materials, 2015. 8(2): p. 551-560.
300. Chapman, M.A., R. Pichika, and R.L. Lieber, Collagen crosslinking does not dictate stiffness in a transgenic mouse model of skeletal muscle fibrosis. J Biomech, 2015. 48(2): p. 375-8.
301. Ungefroren, H., et al., Interaction of tumor cells with the microenvironment. Cell Commun Signal, 2011. 9: p. 18.
302. Kamińska, K., et al., The role of the cell-cell interactions in cancer progression. J Cell Mol Med, 2015. 19(2): p. 283-96.

303. Motte, S. and L.J. Kaufman, Strain stiffening in collagen I networks. Biopolymers, 2013. 99(1): p. 35-46.
304. Yamamoto, T., Intradermal Injections of Bleomycin to Model Skin Fibrosis. Methods Mol Biol, 2017. 1627: p. 43-47.
305. Ebihara, T., et al., Changes in extracellular matrix and tissue viscoelasticity in bleomycin-induced lung fibrosis. Temporal aspects. Am J Respir Crit Care Med, 2000. 162(4 Pt 1): p. 1569-76.
306. Błyszczuk, P., et al., Experimental Mouse Model of Bleomycin-Induced Skin Fibrosis. Curr Protoc Immunol, 2019. 126(1): p. e88.
307. Yamamoto, T., et al., Animal model of sclerotic skin. I: Local injections of bleomycin induce sclerotic skin mimicking scleroderma. J Invest Dermatol, 1999. 112(4): p. 456-62.
308. Moeller, A., et al., The bleomycin animal model: a useful tool to investigate treatment options for idiopathic pulmonary fibrosis? Int J Biochem Cell Biol, 2008. 40(3): p. 362-82.
309. Mack, M., Inflammation and fibrosis. Matrix Biology, 2018. 68-69: p. 106-121.
310. Hinz, B., C.A. McCulloch, and N.M. Coelho, Mechanical regulation of myofibroblast phenoconversion and collagen contraction. Experimental Cell Research, 2019. 379(1): p. 119-128.
311. Monteran, L. and N. Erez, The Dark Side of Fibroblasts: Cancer-Associated Fibroblasts as Mediators of Immunosuppression in the Tumor Microenvironment. Frontiers in Immunology, 2019. 10: p. 1835.
312. Han, C., T. Liu, and R. Yin, Biomarkers for cancer-associated fibroblasts. Biomarker Research, 2020. 8(1): p. 64.
313. Shiga, K., et al., Cancer-Associated Fibroblasts: Their Characteristics and Their Roles in Tumor Growth. Cancers (Basel), 2015. 7(4): p. 2443-58.
314. Barrett, R.L. and E. Puré, Cancer-associated fibroblasts and their influence on tumor immunity and immunotherapy. Elife, 2020. 9.
315. Dasari, S. and P.B. Tchounwou, Cisplatin in cancer therapy: molecular mechanisms of action. Eur J Pharmacol, 2014. 740: p. 364-78.
316. Herrera, C., et al., Muscle Tissue Damage Induced by the Venom of Bothrops asper: Identification of Early and Late Pathological Events through Proteomic Analysis. PLoS Negl Trop Dis, 2016. 10(4): p. e0004599.
317. Fitch, J.M., et al., Analysis of transcriptional isoforms of collagen types IX, II, and I in the developing avian cornea by competitive polymerase chain reaction. Dev Dyn, 1995. 202(1): p. 42-53.
318. Berthod, F., et al., Differential expression of collagens XII and XIV in human skin and in reconstructed skin. J Invest Dermatol, 1997. 108(5): p. 737-42.
319. Naba, A., et al., The matrisome: in silico definition and in vivo characterization by proteomics of normal and tumor extracellular matrices. Mol Cell Proteomics, 2012. 11(4): p. M111.014647.
320. Fang, C.Y., et al., Long-term growth comparison studies of FBS and FBS alternatives in six head and neck cell lines. PLoS One, 2017. 12(6): p. e0178960.
321. Li, Y., et al., Quantitative phase imaging reveals matrix stiffness-dependent growth and migration of cancer cells. Sci Rep, 2019. 9(1): p. 248.
322. Krieg, T. and M. Aumailley, The extracellular matrix of the dermis: flexible structures with dynamic functions. Exp Dermatol, 2011. 20(8): p. 689-95.
323. Ansorge, H.L., et al., Type XIV Collagen Regulates Fibrillogenesis: PREMATURE COLLAGEN FIBRIL GROWTH AND TISSUE DYSFUNCTION IN NULL MICE. J Biol Chem, 2009. 284(13): p. 8427-38.
324. Agarwal, P., et al., Collagen XII and XIV, new partners of cartilage oligomeric matrix protein in the skin extracellular matrix suprastructure. J Biol Chem, 2012. 287(27): p. 22549-59.
325. Pach, E., et al., Extracellular Matrix Remodeling by Fibroblast-MMP14 Regulates Melanoma Growth. Int J Mol Sci, 2021. 22(22).

326. Ju, R.J., S.J. Stehbens, and N.K. Haass, The Role of Melanoma Cell-Stroma Interaction in Cell Motility, Invasion, and Metastasis. Front Med (Lausanne), 2018. 5: p. 307.
327. Rodríguez, D., C.J. Morrison, and C.M. Overall, Matrix metalloproteinases: what do they not do? New substrates and biological roles identified by murine models and proteomics. Biochim Biophys Acta, 2010. 1803(1): p. 39-54.
328. Kupcova Skalnikova, H., et al., Advances in Proteomic Techniques for Cytokine Analysis: Focus on Melanoma Research. Int J Mol Sci, 2017. 18(12).
329. Si-Tayeb, K., et al., Matrix metalloproteinase 3 is present in the cell nucleus and is involved in apoptosis. Am J Pathol, 2006. 169(4): p. 1390-401.
330. Kim, E.M., et al., Matrix metalloproteinase-3 is increased and participates in neuronal apoptotic signaling downstream of caspase-12 during endoplasmic reticulum stress. J Biol Chem, 2010. 285(22): p. 16444-52.
331. Borzi, R.M., et al., Growth-related oncogene alpha induction of apoptosis in osteoarthritis chondrocytes. Arthritis Rheum, 2002. 46(12): p. 3201-11.
332. Olivotto, E., et al., Chondrocyte hypertrophy and apoptosis induced by GROalpha require three-dimensional interaction with the extracellular matrix and a co-receptor role of chondroitin sulfate and are associated with the mitochondrial splicing variant of cathepsin B. J Cell Physiol, 2007. 210(2): p. 417-27.
333. MacPherson, L.J., et al., Discovery of CGS 27023A, a non-peptidic, potent, and orally active stromelysin inhibitor that blocks cartilage degradation in rabbits. J Med Chem, 1997. 40(16): p. 2525-32.
334. Salucci, S., et al., Ultraviolet B (UVB) Irradiation-Induced Apoptosis in Various Cell Lineages in Vitro. International Journal of Molecular Sciences, 2013. 14(1): p. 532-546.
335. Cao, L., et al., Keratin 6 expression correlates to areas of squamous differentiation in multiple independent isolates of As(+3)-induced bladder cancer. J Appl Toxicol, 2010. 30(5): p. 416-30.
336. Abety, A.N., et al., Loss of ADAM9 Leads to Modifications of the Extracellular Matrix Modulating Tumor Growth. Biomolecules, 2020. 10(9).
337. Giebeler, N. and P. Zigrino, A Disintegrin and Metalloprotease (ADAM): Historical Overview of Their Functions. Toxins (Basel), 2016. 8(4): p. 122.
338. O'Shea, C., et al., Expression of ADAM-9 mRNA and protein in human breast cancer. Int J Cancer, 2003. 105(6): p. 754-61.
339. Peduto, L., et al., Critical function for ADAM9 in mouse prostate cancer. Cancer Res, 2005. 65(20): p. 9312-9.
340. Peduto, L., ADAM9 as a potential target molecule in cancer. Curr Pharm Des, 2009. 15(20): p. 2282-7.
341. Zigrino, P., et al., Adam-9 expression and regulation in human skin melanoma and melanoma cell lines. Int J Cancer, 2005. 116(6): p. 853-9.
342. Schwettmann, L. and H. Tschesche, Cloning and expression in Pichia pastoris of metalloprotease domain of ADAM 9 catalytically active against fibronectin. Protein Expr Purif, 2001. 21(1): p. 65-70.
343. Giebeler, N., et al., Deletion of ADAM-9 in HGF/CDK4 mice impairs melanoma development and metastasis. Oncogene, 2017. 36(35): p. 5058-5067.
344. Visse, R. and H. Nagase, Matrix metalloproteinases and tissue inhibitors of metalloproteinases: structure, function, and biochemistry. Circ Res, 2003. 92(8): p. 827-39.
345. Society, A.C. Key Statistics for Melanoma Skin Cancer. 2021 January 12, 2021 [cited 2021.
346. Grimaldi, A.M., et al., Novel approaches in melanoma prevention and therapy. Cancer Treat Res, 2014. 159: p. 443-55.
347. Khaddour, K., et al., Melanoma Targeted Therapies beyond BRAF-Mutant Melanoma: Potential Druggable Mutations and Novel Treatment Approaches. Cancers, 2021. 13(22): p. 5847.

348. Marcela Valko-Rokytovská, J.Š., Mária Milkovičová and Zuzana Kostecká, Possibilities for the Therapy of Melanoma: Current Knowledge and Future Directions. IntechOpen, 2017(Human Skin Cancers - Pathways, Mechanisms, Targets and Treatments).
349. Wang, Z., et al., Cancer-Associated Fibroblasts Suppress Cancer Development: The Other Side of the Coin. Frontiers in Cell and Developmental Biology, 2021. 9.
350. Gonzalez-Avila, G., et al., Matrix metalloproteinases participation in the metastatic process and their diagnostic and therapeutic applications in cancer. Critical Reviews in Oncology/Hematology, 2019. 137: p. 57-83.
351. Cao, H., et al., Synergistic metalloproteinase-based remodeling of matrix by pancreatic tumor and stromal cells. PLoS One, 2021. 16(3): p. e0248111.
352. Hofmann, U.B., et al., Expression and activation of matrix metalloproteinase-2 (MMP-2) and its co-localization with membrane-type 1 matrix metalloproteinase (MT1-MMP) correlate with melanoma progression. J Pathol, 2000. 191(3): p. 245-56.
353. Shaverdashvili, K., et al., MT1-MMP dependent repression of the tumor suppressor SPRY4 contributes to MT1-MMP driven melanoma cell motility. Oncotarget, 2015. 6(32): p. 33512-22.
354. Tejera-Vaquerizo, A., et al., Chronology of metastasis in cutaneous melanoma: growth rate model. J Invest Dermatol, 2012. 132(4): p. 1215-21.
355. Devy, L., et al., Selective Inhibition of Matrix Metalloproteinase-14 Blocks Tumor Growth, Invasion, and Angiogenesis. Cancer Research, 2009. 69(4): p. 1517-1526.
356. Muz, B., et al., The role of hypoxia in cancer progression, angiogenesis, metastasis, and resistance to therapy. Hypoxia (Auckl), 2015. 3: p. 83-92.
357. Emami Nejad, A., et al., The role of hypoxia in the tumor microenvironment and development of cancer stem cell: a novel approach to developing treatment. Cancer Cell International, 2021. 21(1): p. 62.
358. Rey, S. and G.L. Semenza, Hypoxia-inducible factor-1-dependent mechanisms of vascularization and vascular remodelling. Cardiovasc Res, 2010. 86(2): p. 236-42.
359. Mouriaux, F., et al., Increased HIF-1α expression correlates with cell proliferation and vascular markers CD31 and VEGF-A in uveal melanoma. Invest Ophthalmol Vis Sci, 2014. 55(3): p. 1277-83.
360. Yang, X., et al., MicroRNA-199a-5p inhibits tumor proliferation in melanoma by mediating HIF-1α. Mol Med Rep, 2016. 13(6): p. 5241-7.
361. Pucciarelli, D., et al., Hypoxia increases the heterogeneity of melanoma cell populations and affects the response to vemurafenib. Mol Med Rep, 2016. 13(4): p. 3281-8.
362. Bordeleau, F., et al., Matrix stiffening promotes a tumor vasculature phenotype. Proc Natl Acad Sci U S A, 2017. 114(3): p. 492-497.
363. Sewell-Loftin, M.K., et al., Cancer-associated fibroblasts support vascular growth through mechanical force. Sci Rep, 2017. 7(1): p. 12574.
364. Deryugina, E.I. and J.P. Quigley, Matrix metalloproteinases and tumor metastasis. Cancer Metastasis Rev, 2006. 25(1): p. 9-34.
365. Zigrino, P., et al., Stromal Expression of MMP-13 Is Required for Melanoma Invasion and Metastasis. Journal of Investigative Dermatology, 2009. 129(11): p. 2686-2693.
366. Meierjohann, S., et al., MMP13 mediates cell cycle progression in melanocytes and melanoma cells: in vitro studies of migration and proliferation. Mol Cancer, 2010. 9: p. 201.
367. Rotte, A., M. Martinka, and G. Li, MMP2 expression is a prognostic marker for primary melanoma patients. Cell Oncol (Dordr), 2012. 35(3): p. 207-16.
368. Schneider, F., et al., Matrix-metalloproteinase-14 deficiency in bone-marrow-derived cells promotes collagen accumulation in mouse atherosclerotic plaques. Circulation, 2008. 117(7): p. 931-9.
369. Nissen, N.I., M. Karsdal, and N. Willumsen, Collagens and Cancer associated fibroblasts in the reactive stroma and its relation to Cancer biology. J Exp Clin Cancer Res, 2019. 38(1): p. 115.

370. Huayllani, M.T., et al., Desmoplastic Melanoma: Clinical Characteristics and Survival in the US Population. Cureus, 2019. 11(6): p. e4931.
371. Piris, A. and M.C. Mihm, Jr., Progress in melanoma histopathology and diagnosis. Hematol Oncol Clin North Am, 2009. 23(3): p. 467-80, viii.
372. Liu, J., et al., Soft fibrin gels promote selection and growth of tumorigenic cells. Nat Mater, 2012. 11(8): p. 734-41.
373. Brennan, M., Changes in the cross-linking of collagen from rat tail tendons due to diabetes. J Biol Chem, 1989. 264(35): p. 20953-60.
374. Reiser, K.M., Nonenzymatic glycation of collagen in aging and diabetes. Proc Soc Exp Biol Med, 1991. 196(1): p. 17-29.
375. Storm, C., et al., Nonlinear elasticity in biological gels. Nature, 2005. 435(7039): p. 191-4.
376. Walker, C., E. Mojares, and A. Del Río Hernández, Role of Extracellular Matrix in Development and Cancer Progression. Int J Mol Sci, 2018. 19(10).
377. Bottazzi, M.E. and R.K. Assoian, The extracellular matrix and mitogenic growth factors control G1 phase cyclins and cyclin-dependent kinase inhibitors. Trends Cell Biol, 1997. 7(9): p. 348-52.
378. Aplin, A.E., A.K. Howe, and R.L. Juliano, Cell adhesion molecules, signal transduction and cell growth. Curr Opin Cell Biol, 1999. 11(6): p. 737-44.
379. Koyama, H., et al., Fibrillar collagen inhibits arterial smooth muscle proliferation through regulation of Cdk2 inhibitors. Cell, 1996. 87(6): p. 1069-78.
380. Schuliga, M.J., et al., Fibrillar collagen clamps lung mesenchymal cells in a nonproliferative and noncontractile phenotype. Am J Respir Cell Mol Biol, 2009. 41(6): p. 731-41.
381. Wall, S.J., et al., Discoidin domain receptor 2 mediates tumor cell cycle arrest induced by fibrillar collagen. J Biol Chem, 2005. 280(48): p. 40187-94.
382. Dasgupta, I. and D. McCollum, Control of cellular responses to mechanical cues through YAP/TAZ regulation. J Biol Chem, 2019. 294(46): p. 17693-17706.
383. Tang, Y., et al., MT1-MMP-dependent control of skeletal stem cell commitment via a β1-integrin/YAP/TAZ signaling axis. Dev Cell, 2013. 25(4): p. 402-16.
384. Busam, K.J., Desmoplastic melanoma. Clin Lab Med, 2011. 31(2): p. 321-30.
385. Blessing, K. and K.M. McLaren, Histological regression in primary cutaneous melanoma: recognition, prevalence and significance. Histopathology, 1992. 20(4): p. 315-22.
386. Wenzel, J., et al., Type I interferon-associated recruitment of cytotoxic lymphocytes: a common mechanism in regressive melanocytic lesions. Am J Clin Pathol, 2005. 124(1): p. 37-48.
387. Hill, C.L., et al., Risk of cancer in patients with scleroderma: a population based cohort study. Ann Rheum Dis, 2003. 62(8): p. 728-31.
388. Hui, L., et al., Matrix stiffness regulates the proliferation, stemness and chemoresistance of laryngeal squamous cancer cells. Int J Oncol, 2017. 50(4): p. 1439-1447.
389. Ohuchi, E., et al., Membrane type 1 matrix metalloproteinase digests interstitial collagens and other extracellular matrix macromolecules. J Biol Chem, 1997. 272(4): p. 2446-51.
390. Ohtake, Y., H. Tojo, and M. Seiki, Multifunctional roles of MT1-MMP in myofiber formation and morphostatic maintenance of skeletal muscle. J Cell Sci, 2006. 119(Pt 18): p. 3822-32.
391. Üstün, Y., et al., Dual role of laminin-511 in regulating melanocyte migration and differentiation. Matrix Biology, 2019. 80: p. 59-71.
392. Aumailley, M., et al., A simplified laminin nomenclature. Matrix Biology, 2005. 24(5): p. 326-332.
393. Siler, U., et al., Laminin gamma2 chain as a stromal cell marker of the human bone marrow microenvironment. Br J Haematol, 2002. 119(1): p. 212-20.
394. Durbeej, M., Laminins. Cell Tissue Res, 2010. 339(1): p. 259-68.

395. Aumailley, M. and N. Smyth, The role of laminins in basement membrane function. J Anat, 1998. 193 (Pt 1)(Pt 1): p. 1-21.
396. Pook, M., et al., Changes in Laminin Expression Pattern during Early Differentiation of Human Embryonic Stem Cells. PLoS One, 2015. 10(9): p. e0138346.
397. Naba, A., et al., The extracellular matrix: Tools and insights for the "omics" era. Matrix Biol, 2016. 49: p. 10-24.
398. Gordon, M.K., et al., Cloning of a cDNA for a new member of the class of fibril-associated collagens with interrupted triple helices. Eur J Biochem, 1991. 201(2): p. 333-8.
399. Gerecke, D.R., et al., Complete primary structure and genomic organization of the mouse Col14a1 gene. Matrix Biol, 2004. 22(7): p. 595-601.
400. Ruehl, M., et al., The elongated first fibronectin type III domain of collagen XIV is an inducer of quiescence and differentiation in fibroblasts and preadipocytes. J Biol Chem, 2005. 280(46): p. 38537-43.
401. Luo, Y., et al., The minor collagens in articular cartilage. Protein Cell, 2017. 8(8): p. 560-572.
402. Tao, G., et al., Collagen XIV is important for growth and structural integrity of the myocardium. J Mol Cell Cardiol, 2012. 53(5): p. 626-38.
403. Freise, C., V. Bobb, and U. Querfeld, Collagen XIV and a related recombinant fragment protect human vascular smooth muscle cells from calcium-/phosphate-induced osteochondrocytic transdifferentiation. Exp Cell Res, 2017. 358(2): p. 242-252.
404. Paetow, C., Collagen XIV reduces proliferation of human CD44-positive tumour cell lines. 2009.
405. Klein, G., et al., Cell binding properties of collagen type XIV for human hematopoietic cells. Matrix Biol, 1998. 16(6): p. 307-17.
406. Ehnis, T., et al., A Chondroitin/Dermatan Sulfate Form of CD44 Is a Receptor for Collagen XIV (Undulin). Experimental Cell Research, 1996. 229(2): p. 388-397.
407. Ehnis, T., et al., Localization of a cell adhesion site on collagen XIV (undulin). Exp Cell Res, 1998. 239(2): p. 477-80.
408. Imhof, M. and B. Trueb, Alternative splicing of the first F3 domain from chicken collagen XIV affects cell adhesion and heparin binding. J Biol Chem, 2001. 276(12): p. 9141-8.
409. Nikitovic, D., et al., Heparan sulfate proteoglycans and heparin regulate melanoma cell functions. Biochim Biophys Acta, 2014. 1840(8): p. 2471-81.
410. Iida, J., et al., Coordinate role for cell surface chondroitin sulfate proteoglycan and alpha 4 beta 1 integrin in mediating melanoma cell adhesion to fibronectin. J Cell Biol, 1992. 118(2): p. 431-44.
411. Dietrich, A., et al., High CD44 surface expression on primary tumours of malignant melanoma correlates with increased metastatic risk and reduced survival. Eur J Cancer, 1997. 33(6): p. 926-30.
412. Stewart, M.D. and R.D. Sanderson, Heparan sulfate in the nucleus and its control of cellular functions. Matrix Biology, 2014. 35: p. 56-59.
413. Engbring, J.A., et al., The B16F10 cell receptor for a metastasis-promoting site on laminin-1 is a heparan sulfate/chondroitin sulfate-containing proteoglycan. Cancer Res, 2002. 62(12): p. 3549-54.
414. Liu, D., et al., Tumor cell surface heparan sulfate as cryptic promoters or inhibitors of tumor growth and metastasis. Proceedings of the National Academy of Sciences, 2002. 99(2): p. 568-573.
415. Roy, M. and D. Marchetti, Cell surface heparan sulfate released by heparanase promotes melanoma cell migration and angiogenesis. J Cell Biochem, 2009. 106(2): p. 200-9.
416. Jones, A.L., M.D. Hulett, and C.R. Parish, Histidine-rich glycoprotein binds to cell-surface heparan sulfate via its N-terminal domain following Zn2+ chelation. J Biol Chem, 2004. 279(29): p. 30114-22.

417. Richardson, T.P., V. Trinkaus-Randall, and M.A. Nugent, Regulation of heparan sulfate proteoglycan nuclear localization by fibronectin. Journal of Cell Science, 2001. 114(9): p. 1613-1623.
418. Gui, L., et al., Identification of the heparin-binding determinants within fibronectin repeat III1: role in cell spreading and growth. J Biol Chem, 2006. 281(46): p. 34816-25.
419. Zhong, X., et al., The Structure in Solution of Fibronectin Type III Domain 14 Reveals Its Synergistic Heparin Binding Site. Biochemistry, 2018. 57(42): p. 6045-6049.
420. Annaval, T., et al., Heparan Sulfate Proteoglycans Biosynthesis and Post Synthesis Mechanisms Combine Few Enzymes and Few Core Proteins to Generate Extensive Structural and Functional Diversity. Molecules (Basel, Switzerland), 2020. 25(18): p. 4215.
421. Nagarajan, A., P. Malvi, and N. Wajapeyee, Heparan Sulfate and Heparan Sulfate Proteoglycans in Cancer Initiation and Progression. Frontiers in Endocrinology, 2018. 9.
422. Bonaventure, J., M.J. Domingues, and L. Larue, Cellular and molecular mechanisms controlling the migration of melanocytes and melanoma cells. Pigment Cell Melanoma Res, 2013. 26(3): p. 316-25.
423. Wolf, K., et al., Physical limits of cell migration: control by ECM space and nuclear deformation and tuning by proteolysis and traction force. J Cell Biol, 2013. 201(7): p. 1069-84.
424. Friedl, P. and K. Wolf, Proteolytic interstitial cell migration: a five-step process. Cancer Metastasis Rev, 2009. 28(1-2): p. 129-35.
425. Gobin, E., et al., A pan-cancer perspective of matrix metalloproteases (MMP) gene expression profile and their diagnostic/prognostic potential. BMC Cancer, 2019. 19(1): p. 581.
426. Akutsu, N., et al., Effect of type XII or XIV collagen NC-3 domain on the human dermal fibroblast migration into reconstituted collagen gel. Exp Dermatol, 1999. 8(1): p. 17-21.
427. Zhou, L., et al., Targeted deactivation of cancer-associated fibroblasts by β-catenin ablation suppresses melanoma growth. Tumour Biol, 2016. 37(10): p. 14235-14248.
428. Cornil, I., et al., Fibroblast cell interactions with human melanoma cells affect tumor cell growth as a function of tumor progression. Proc Natl Acad Sci U S A, 1991. 88(14): p. 6028-32.
429. Shao, H., et al., Activation of Notch1 signaling in stromal fibroblasts inhibits melanoma growth by upregulating WISP-1. Oncogene, 2011. 30(42): p. 4316-26.
430. Erdogan, B. and D.J. Webb, Cancer-associated fibroblasts modulate growth factor signaling and extracellular matrix remodeling to regulate tumor metastasis. Biochem Soc Trans, 2017. 45(1): p. 229-236.
431. Papaccio, F., et al., Profiling Cancer-Associated Fibroblasts in Melanoma. Int J Mol Sci, 2021. 22(14).
432. Deryugina, E.I., et al., MT1-MMP initiates activation of pro-MMP-2 and integrin alphavbeta3 promotes maturation of MMP-2 in breast carcinoma cells. Exp Cell Res, 2001. 263(2): p. 209-23.
433. Saeb-Parsy, K., et al., MT1-MMP regulates urothelial cell invasion via transcriptional regulation of Dickkopf-3. British Journal of Cancer, 2008. 99(4): p. 663-669.
434. Mendonca, P., et al., Pentagalloyl glucose inhibits TNF-α-activated CXCL1/GRO-α expression and induces apoptosis-related genes in triple-negative breast cancer cells. Sci Rep, 2021. 11(1): p. 5649.
435. Choi, D.H., et al., A novel intracellular role of matrix metalloproteinase-3 during apoptosis of dopaminergic cells. J Neurochem, 2008. 106(1): p. 405-15.
436. Liu, M., et al., STAT3 regulates MMP3 in heme-induced endothelial cell apoptosis. PLoS One, 2013. 8(8): p. e71366.
437. Zhao, J., et al., Mild hypothermia reduces expression of Fas/FasL and MMP-3 after cerebral ischemia-reperfusion in rats. Iran J Basic Med Sci, 2014. 17(6): p. 454-9.

438. Zwierzchowski, T.J., et al., Evidence for apoptosis, MMP-1, MMP-3 and TIMP-2 expression and their effect on the mechanical and biochemical properties of fresh viable knee medial meniscal allografts and autografts in the rabbit. Arch Med Sci, 2012. 8(4): p. 724-32.
439. Huang, W., et al., Autophagy Protects Advanced Glycation End Product-Induced Apoptosis and Expression of MMP-3 and MMP-13 in Rat Chondrocytes. BioMed Research International, 2017. 2017: p. 6341919.
440. Tang, S., et al., Bone marrow mesenchymal stem cell-derived exosomes inhibit chondrocyte apoptosis and the expression of MMPs by regulating Drp1-mediated mitophagy. Acta Histochemica, 2021. 123(8): p. 151796.
441. Shoshan, E., et al., NFAT1 Directly Regulates IL8 and MMP3 to Promote Melanoma Tumor Growth and Metastasis. Cancer Res, 2016. 76(11): p. 3145-55.
442. Keurhorst, D., et al., MMP3 activity rather than cortical stiffness determines NHE1-dependent invasiveness of melanoma cells. Cancer Cell Int, 2019. 19: p. 285.
443. Luca, M., et al., Expression of interleukin-8 by human melanoma cells up-regulates MMP-2 activity and increases tumor growth and metastasis. The American journal of pathology, 1997. 151(4): p. 1105-1113.
444. Srivastava, S.K., et al., Interleukin-8 is a key mediator of FKBP51-induced melanoma growth, angiogenesis and metastasis. British Journal of Cancer, 2015. 112(11): p. 1772-1781.
445. Cobb, L.J., et al., Partitioning of IGFBP-5 actions in myogenesis: IGF-independent anti-apoptotic function. J Cell Sci, 2004. 117(Pt 9): p. 1737-46.
446. Tanno, B., et al., Bim-dependent apoptosis follows IGFBP-5 down-regulation in neuroblastoma cells. Biochem Biophys Res Commun, 2006. 351(2): p. 547-52.
447. Hu, L., et al., PLF-1 (Proliferin-1) Modulates Smooth Muscle Cell Proliferation and Development of Experimental Intimal Hyperplasia. J Am Heart Assoc, 2019. 8(24): p. e005886.
448. Goto, H., et al., Proliferin-1 Ameliorates Cardiotoxin-Related Skeletal Muscle Repair in Mice. Stem Cells International, 2021. 2021: p. 9202990.
449. Thompson, T.C., Androgenic Regulation of White Adipose Tissue-Prostate Cancer Interactions. 2015, University of Texas MD Anderson Cancer Center Houston,Texas 77030.
450. Huang, J., et al., Extracellular matrix and its therapeutic potential for cancer treatment. Signal Transduction and Targeted Therapy, 2021. 6(1): p. 153.
451. Henke, E., R. Nandigama, and S. Ergün, Extracellular Matrix in the Tumor Microenvironment and Its Impact on Cancer Therapy. Frontiers in Molecular Biosciences, 2020. 6.
452. Gade, T.P., et al., Imaging intratumoral convection: pressure-dependent enhancement in chemotherapeutic delivery to solid tumors. Clin Cancer Res, 2009. 15(1): p. 247-55.
453. Egeblad, M., M.G. Rasch, and V.M. Weaver, Dynamic interplay between the collagen scaffold and tumor evolution. Curr Opin Cell Biol, 2010. 22(5): p. 697-706.
454. Netti, P.A., et al., Role of extracellular matrix assembly in interstitial transport in solid tumors. Cancer Res, 2000. 60(9): p. 2497-503.
455. Provenzano, P.P., et al., Enzymatic targeting of the stroma ablates physical barriers to treatment of pancreatic ductal adenocarcinoma. Cancer Cell, 2012. 21(3): p. 418-29.
456. Chang, Q., et al., Biodistribution of cisplatin revealed by imaging mass cytometry identifies extensive collagen binding in tumor and normal tissues. Sci Rep, 2016. 6: p. 36641.
457. Brown, A., S. Kumar, and P.B. Tchounwou, Cisplatin-Based Chemotherapy of Human Cancers. J Cancer Sci Ther, 2019. 11(4).
458. Ichihashi, N. and Y. Kitajima, Chemotherapy induces or increases expression of multidrug resistance-associated protein in malignant melanoma cells. Br J Dermatol, 2001. 144(4): p. 745-50.

Erklärung

Ich versichere, dass ich die von mir vorgelegte Dissertation selbständig angefertigt, die benutzten Quellen und Hilfsmittel vollständig angegeben und die Stellen der Arbeit − einschließlich Tabellen, Karten und Abbildungen −, die anderen Werken im Wortlaut oder dem Sinn nach entnommen sind, in jedem Einzelfall als Entlehnung kenntlich gemacht habe; dass diese Dissertation noch keiner anderen Fakultät oder Universität zur Prüfung vorgelegen hat; dass sie − abgesehen von unten angegebenen Teilpublikationen − noch nicht veröffentlicht worden ist, sowie, dass ich eine solche Veröffentlichung vor Abschluss des Promotionsverfahrens nicht vornehmen werde. Die Bestimmungen der Promotionsordnung sind mir bekannt. Die von mir vorgelegte Dissertation ist von Dr. rer. nat. Paola Zigrino betreut worden.

Köln, den 14.02.2022

Elke Pach

Teilpublikationen:

Pach, E., Kümper M., Fromme J. E., Zamek J., Metzen F., Koch M., Mauch C. and Zigrino P. (2021). "Extracellular Matrix Remodeling by Fibroblast-MMP14 Regulates Melanoma Growth." Int J Mol Sci 22(22):12276.

Pach, E., Brinckmann J., Rübsam M., Kümper M., Mauch C. and Zigrino P. (2021). "Fibroblast MMP14-Dependent Collagen Processing Is Necessary for Melanoma Growth." Cancers 13(8): 1984.

Abety, A. N., **Pach E.**, Giebeler N., Fromme J. E., Aramadhaka L. R., Mauch C., Fox J. W. and Zigrino P. (2020). "Loss of ADAM9 Leads to Modifications of the Extracellular Matrix Modulating Tumor Growth." Biomolecules 10(9): 1290.

Lebenslauf

Persönliche Daten

Name:	Elke Pach
Geburtsdatum:	14.08.1988
Geburtsort:	Langenfeld (Rheinland), Deutschland
Staatsangehörigkeit:	Deutsch

Ausbildung

2017	Beginn der Promotion in der Klinik und Poliklinik für Dermatologie und Venerologie, Uniklinik Köln; Universität zu Köln, Deutschland Titel der Dissertation: „Functional role of fibroblast-derived MMP-14 in tumor growth and metastasis”
09/2015	Master of Science (M. Sc.) in Biologie RWTH Aachen, Deutschland Titel der Masterarbeit: “Funktionelle Analyse der JNK-abhängigen Phosphorylierung des Tumorsuppressors Par-4“
3/2013	Bachelor of Science (B. Sc.) in Biologie Heinrich-Heine-Universität, Düsseldorf, Deutschland Titel der Bachelorarbeit: “Zur Funktion der CRINKLY 4-Rezeptorfamilie von Arabidopsis thaliana”
06/2009	Otto-Hahn-Gymnasium, Monheim am Rhein, Deutschland Abschluss: Abitur

Auszeichnungen

Posterpreis von der Deutschen Gesellschaft für Matrixbiologie e.V. 2019 (DGMB2019, Regensburg, Deutschland, 27.03 – 30.03.2019)
Titel: “Deletion of fibroblast MMP-14 in the skin leads to reduced melanoma growth”

Veröffentlichungen

Kümper, M., Hessenthaler S., Zamek J., Niland S., **Pach E.**, Mauch C. and Zigrino P. (2021). "Loss of endothelial cell MMP14 reduces melanoma growth and metastasis by increasing tumor vessel stability." J Invest Dermatol S0022-202X(21)02633-6.

Pach, E., Kümper M., Fromme J. E., Zamek J., Metzen F., Koch M., Mauch C. and Zigrino P. (2021). "Extracellular Matrix Remodeling by Fibroblast-MMP14 Regulates Melanoma Growth." Int J Mol Sci 22(22)

Pach, E., Brinckmann J., Rübsam M., Kümper M., Mauch C. and Zigrino P. (2021). "Fibroblast MMP14-Dependent Collagen Processing Is Necessary for Melanoma Growth." Cancers 13(8): 1984.

Abety, A. N., **Pach E.**, Giebeler N., Fromme J. E., Aramadhaka L. R., Mauch C., Fox J. W. and Zigrino P. (2020). "Loss of ADAM9 Leads to Modifications of the Extracellular Matrix Modulating Tumor Growth." Biomolecules 10(9): 1290.

Tobys, D., Kowalski L. M., Cziudaj E., Müller S., Zentis P., **Pach E.**, Zigrino P., Blaeske T. and Höning S. (2021). "Inhibition of clathrin-mediated endocytosis by knockdown of AP-2 leads to alterations in the plasma membrane proteome." Traffic 22(1-2): 6-22.

Luchterhand, B., Nolten J., Hafizovic S., Schlepütz T., Wewetzer S. J., **Pach E.**, Meier K., Wandrey G. and Büchs J. (2015). "Newly designed and validated impedance spectroscopy setup in microtiter plates successfully monitors viable biomass online." Biotechnol J 10(8): 1259-1268.

Veröffentlichte Meeting Abstracts

Pach, E., Brinckmann J., Rübsam M., Kümper M., Mauch C. and Zigrino P. (2021). "274 Role of fibroblast-MMP14 in melanoma growth." J Invest Dermatol 141: S195.

Kümper, M., Hessenthaler S., Zamek J., Niland S., **Pach E.**, Mauch C. and Zigrino P. (2021). "252 Loss of endothelial cell MMP14 reduces melanoma growth and metastasis by increasing tumor vessel stability." Journal of Investigative Dermatology 141(10): S192.

Pach, E., Brinckmann J., Fox J., Mauch C. and Zigrino P. (2019). "449 Deletion of fibroblast MMP-14 in the skin leads to reduced melanoma growth." J Invest Dermatol 139: S292.

Elke Pach
Köln, den 14.02.2022

Acknowledgements

First, I would like to thank Dr. rer. nat. Paola Zigrino and Prof. Dr. Dr. Cornelia Mauch for the opportunity to join the tumorbiology group and to work on this very interesting and exciting project.

Especially, I would like to express my deepest gratitude to Dr. rer. nat. Paola Zigrino for the supervision of this project. Thank you for your continuous and unfailing support, guidance and patience to help me through this work; for always encouraging me to do my best, and that your door was always open.

I would like to thank my examination committee; Prof. Dr. Matthias Hammerschmidt and Prof. Dr. Raimund Wagener, for accepting and taking the time to review my thesis and to assess my defense; and Prof. Dr. Ines Neundorf for taking over the chairmanship of the defense committee.

Many thanks to my group, AG Zigrino/Mauch; Claudia Coerper-Ochsmann, Nina Ruers, Jan Zamek, Maike Kümper and Joy Steinkamp, for their technical advice and tips, and, for the fun and enjoyable working atmosphere. Jan, thank you for patiently introducing me into mouse work, for which I had such great respect. Maike, thank you for your support and motivation, and for being in the same Ph.D. student-boat with me.

Special thanks to my office mates, Dr. Meltem Barlin, Dr. Julia E. Fromme and Dr. Sebastian Willenborg, for the breaks with cake and coffee, an always open ear and encouraging words when things were difficult. Spending most of the day and late evenings with you made this time much more enjoyable. Additional thanks to Dr. Katrin Schönborn, Michael Piekarek, Paul F. Gehle, Lukas Müller, Sabrina Satzinger and Dr. Daniel Hoffmann for supporting, motivating, encouraging, and distracting me in the evenings after work.

My deepest thanks go to my brother, Martin Pach, for his endless emotional and technical support and advice in all situations.

Ganz besonderer Dank aus tiefstem Herzen gilt meinen Eltern, Irene und Erich Pach, für ihre grenzenlose Unterstützung in all den Jahren, während meiner Schulzeit, des Studiums und bis jetzt. Ohne euch wäre vieles nicht möglich gewesen!